78/8

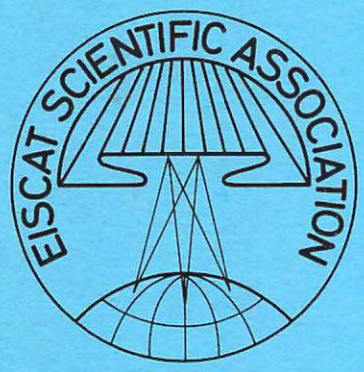

EISCAT
TECHNICAL
NOTES

FEEDER ELEMENTS FOR THE EISCAT VHF PARABOLIC CYLINDER ANTENNA

by
P.-S. Kildal

KIRUNA
Sweden

FEEDER ELEMENTS FOR THE EISCAT VHF PARABOLIC CYLINDER ANTENNA

P-S. Kildal

(Sections 3.4 and 3.5 have been prepared by E. Sørngård)

FEEDER ELEMENTS FOR THE EISCAT
VHF PARABOLIC CYLINDER ANTENNA
Report 79/8
Printed in Sweden
EISCAT Scientific Association
January 1979

EISCAT TECHNICAL NOTE No.8.
OCTOBER 1978

FEEDER ELEMENTS FOR THE EISCAT VHF PARABOLIC CYLINDER ANTENNA

P-S. Kildal

(Sections 3.4 and 3.5 have been prepared by E. Sørngård)

Summary.

The report describes results of computations and scale model measurements that have been done on the linear array feed antenna for the EISCAT VHF cylindrical reflector antenna.

The proposed feed design is a linear array of crossed dipoles that matches the radiation patterns of the longitudinal and the transverse polarization with parallel rods, referred to as beam matching rods. A method of matching the impedance for both linear polarizations is proposed, using parallel impedance matching rods.

CONTENTS

APPENDIX B. NUMERICAL RESULTS

B.1. Longitudinal Polarization with Two Rods

B.2. Transverse Polarization

Acknowledgements.

The author wish to acknowledge the benefit of several discussions with colleagues at the Division of Telecommunications at The Norwegian Institute of Technology, in particular Eddy Sørngård who has written Sec. 3.4 and 3.5 in this report. The optimization of the feed could not have been performed successfully and in time to be used by EISCAT without his excellent computer analysis of two-dimensional corner reflectors. The author is also grateful to Egil Hauger who has made impedance computations of linear array antennas of crossed dipoles.

The author is especially indepted to Tor Hagfors, Professor at The Norwegian Institute of Technology and Director of EISCAT, who has made it possible for me to participate in this interesting project. He has made a number of detailed comments which have been of great help to the author.

The author also wishes to thank Kari Øien who typed the report.

1. INTRODUCTION.

During the period September 1977 to May 1978 a study of feed designs for the EISCAT VHF parabolic cylinder antenna was carried out by the author. The purpose of the study was to synthesize a feed design which optimize its performance for EISCAT purposes. This report gives a describtion of the computations and scale model measurements that have been part of the study, and resulted in the proposed feed design using the author's idea with beam matching rods and impedance matching rods. A preliminary report was prepared and circulated in April/May 1978.

The EISCAT VHF antenna is a parabolic cylindrical reflector antenna with an offset feed. The specifications for the antenna are found on pages 4 to 11 in Ref. 1. The antenna operates at 224 MHz, e.g. with a wavelength λ = 1.34 m. The mathematical analysis is found in Appendix A. The coordinate system and the most important parameters are shown in Fig. 1.1 and 1.2.

D = aperture width (40 m)
L = aperture length (120 m)
F = focal length
E = extra offsetting of feed

The feed is a linear array antenna with 128 dual polarized elements. An element spacing of 0.7 λ yields possibilities for phase steering to 25 deg from broadside before grating lobes occur. The feed is positioned along the x-axis which is the focal line of the reflector. There are two polarizations that are excited independently of each other, the longitudinal polarization with the dipoles parallel to the focal line, and the transverse polarization with the dipoles normal to the focal line. The words transverse and cross section will refer to a cut through the antenna at right angle to the focal line, e.g. the yz plane, throughout the report.

Chapter 2 of the report is a discussion of parameters that are optimized in the feed design, such as aperture efficiency and the coincidence of the phase centers of the two polarizations.

Chapter 3 contains a description of computer programs which have

been used in the synthesis of the optimum feed. Some results of these computations for corner reflectors of different shapes are found in Chapter 4.

Some scale models of feeds have been built and measured. Results for corner reflectors are given in Chapter 5.

Chapter 6 considers the proposed optimized feed design. The beam patterns of the longitudinal and transverse polarization are matched using beam matching rods. It is also proposed to match the impedance with rods, with impedance matching rods. Measurements on a scale model with 7 crossed dipoles are presented and compared with computed beam patterns.

Finally the over all expected performance data of the EISCAT VHF cylinder antenna are listed in Chapter 8.

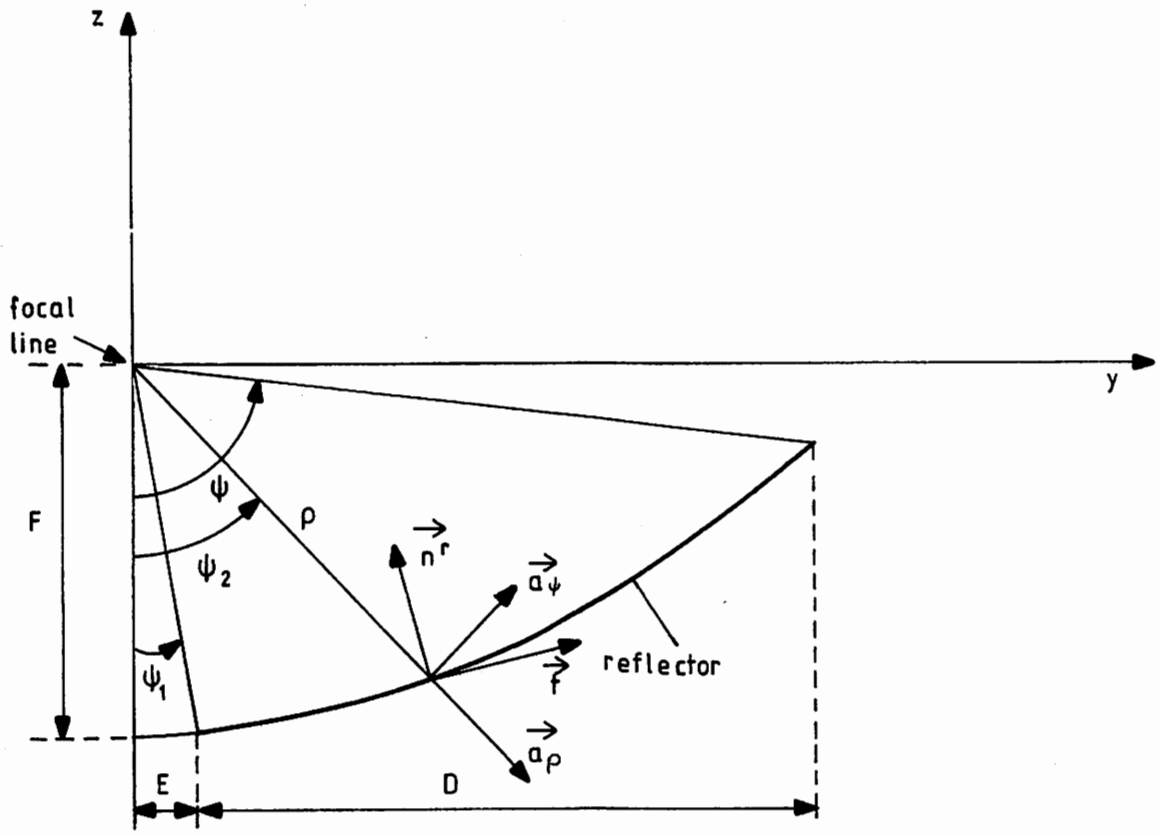

Fig. 1.2. Reflector cross section.

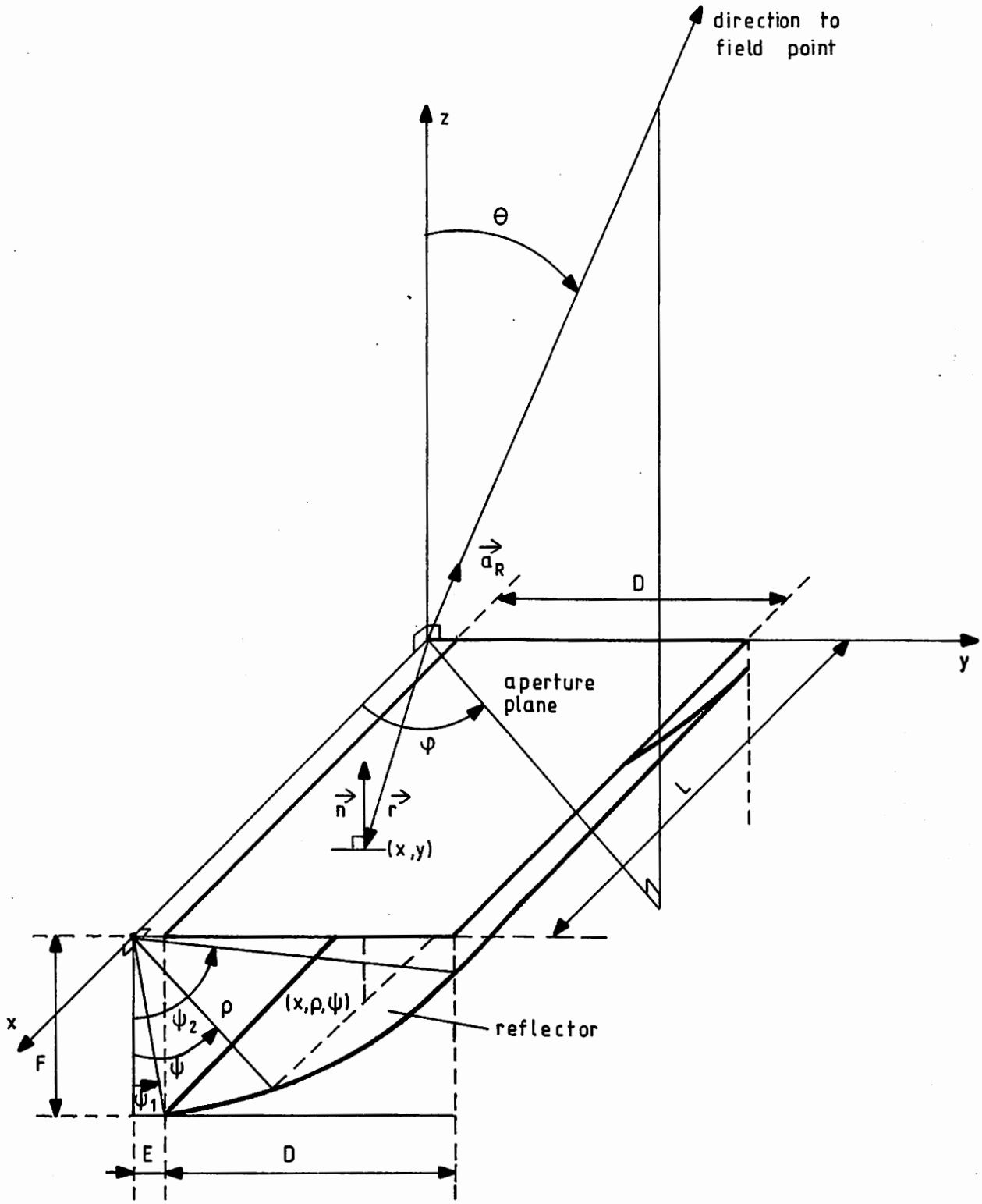

Fig. 1.1. Cylindrical reflector antenna.

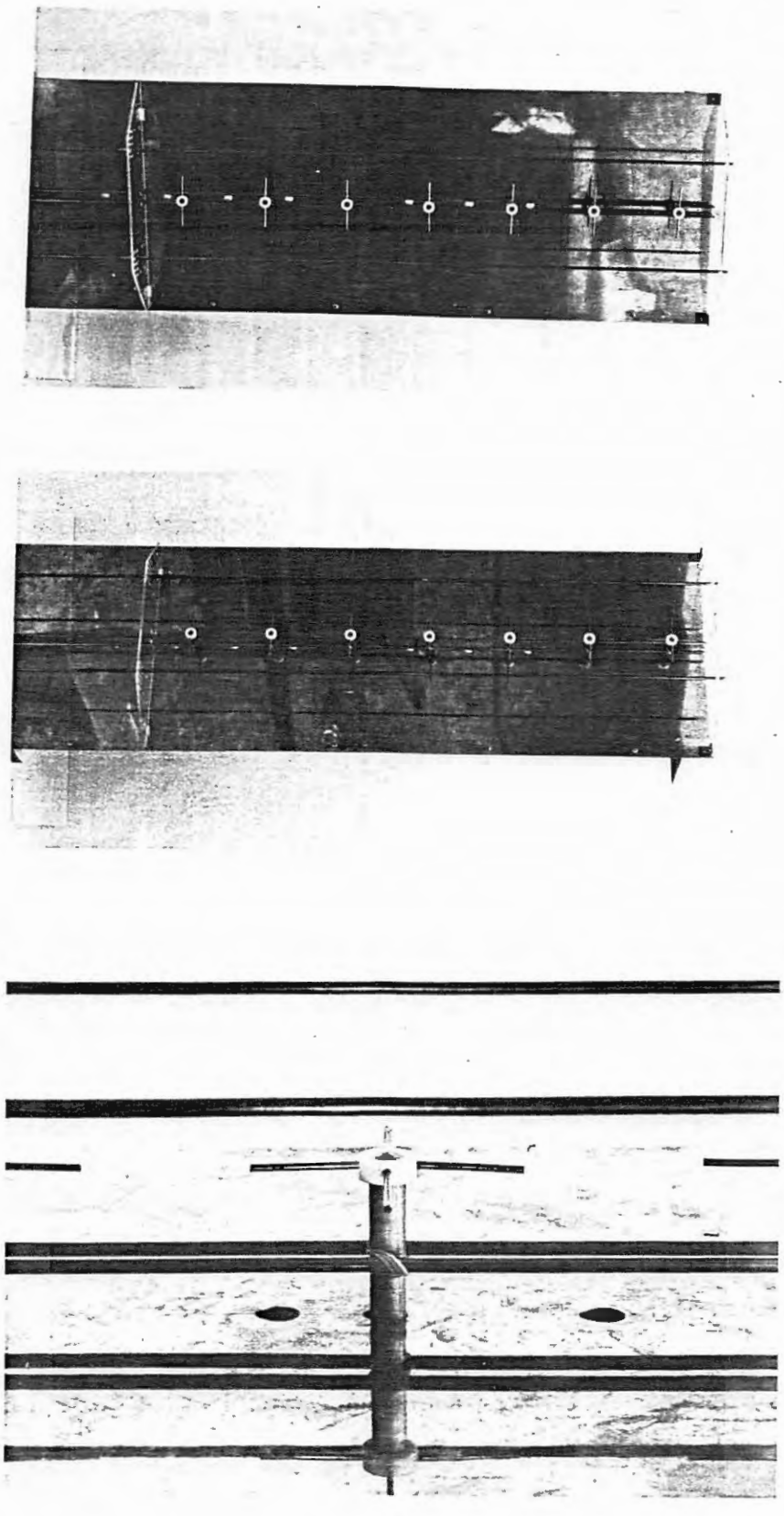

Fig. 1.3. Pictures of
scale model of proposed feed with beam
matching rods and impedance matching rods.

2. PARAMETERS FOR OPTIMIZATION.

Factors of particular importance in the feed design are aperture efficiency, cross polarization within the main beam, distance between the phase centers of the two polarizations, spillover due to direct feed radiation, and impedance variations with scan angle (when phase steered). These parameters are interrelated and cannot all be optimized simultaneously. Therefore it is important to understand the influence on the system performances of variations in the parameters. That is the subject of discussion in the present chapter.

2.1. Aperture efficiency.

The aperture efficiency for circular polarization is defined as

$$\eta^a_{circ} = \frac{\left(\sqrt{\eta^a_x} + \sqrt{\eta^a_y}\right)^2}{2} \tag{2.1}$$

where η^a_x and η^a_y are the aperture efficiencies with spillover included for the longitudinal and transverse polarization respectively. η^a_x and η^a_y may be factorized as $\eta^a_x = \eta^c_x \eta^{\ell}_x$ and $\eta^a_y = \eta^c_y \eta^{\ell}_y$, or with the abbreviated notation introduced in Appendix A

$$\eta^a_{x,y} = \eta^c_{x,y} \eta^{\ell}_{x,y} \tag{2.2}$$

$\eta^c_{x,y}$ is the <u>cross section aperture efficiency</u> (Eq.(3.6) and (3.12) of Appendix A).

$$\eta^c_{x,y} = \frac{\left| \int_E^{E+D} \frac{g_{x,\psi}(\psi)}{\sqrt{\rho}} dy \right|^2}{D \int_{-\pi}^{\pi} \left| g_{x,\psi}(\psi) \right|^2 d\psi} = \frac{F \left| \int_{\psi_1}^{\psi_2} \frac{g_{x,\psi}(\psi)}{\cos\frac{\psi}{2}} d\psi \right|^2}{D \int_{-\pi}^{\pi} \left| g_{x,\psi}(\psi) \right|^2 d\psi} \tag{2.3}$$

where $g_x(\psi)$ and $g_\psi(\psi)$ are the feed cross section beam patterns of the longitudinal and transverse polarization respectively. ρ and ψ are defined in Fig. 1.1 and 1.2.

$\eta^{\ell}_{x,y}$ is the longitudinal aperture efficiency.

$$\eta^{\ell}_{x,y} = \frac{\left| \int_0^L f_{x,\psi}(x)\,dx \right|^2}{L \int_0^L \left| f_{x,\psi}(x) \right|^2 dx} \tag{2.4}$$

where $f_x(x)$ and $f_\psi(x)$ are field distributions along the linear array feed axis for the two polarizations.

η^{a}_{circ} should be made as high as possible to extend the range of the radar. The linear array feed has a uniform excitation so that the longitudunal aperture efficiency is unity. Therefore, due to the offset feed-reflector configuration, aperture efficiencies as high as 0.90 are potentially available.

Spillover is included in Eq. (2.3). The spillover efficiency η_s may be found separately as

$$\eta^{s}_{x,y} = \frac{\int_{\psi_1}^{\psi_2} \left| g_{x,\psi}(\psi) \right|^2 d\psi}{\int_{-\pi}^{\pi} \left| g_{x,\psi}(\psi) \right|^2 d\psi}$$

Thus, the spillover, e.g. the total direct radiated power relative to the total radiated power is

$$S_{x,y} = 1 - \eta^{s}_{x,y} \tag{2.6}$$

The spillover causes spillover lobes that are evaluated in Chapter 2.4.

2.2. Cross Polarization.

The specification for the cross polarization is 20 dB (Ref. 1). That gives an axial ratio of the polarization ellipse of

$$A = \sqrt{\frac{\eta_x}{\eta_y}} \leq \frac{1+0.1}{1-0.1} = 1.22 \tag{2.7}$$

Cross polarization in all directions within the main beam has influence on the performance of the radar. Therefore, the radiation patterns of the longitudinal and transverse polarization should be kept to the required axial ratio within the main beam. These rather loose requirements for the cross polarization makes it possible to increase the aperture efficiency (Eq. (2.1)) by increasing the efficiency of one of the polarizations only, allowing some cross polarization.

2.3. Phase Center Coincidence.

Different phase centers for the two polarizations give extra phase errors across the aperture. The focal line should be placed somewhere between the phase centers to minimize the effect of the errors. The gain reduction caused by such errors will be evaluated presently.

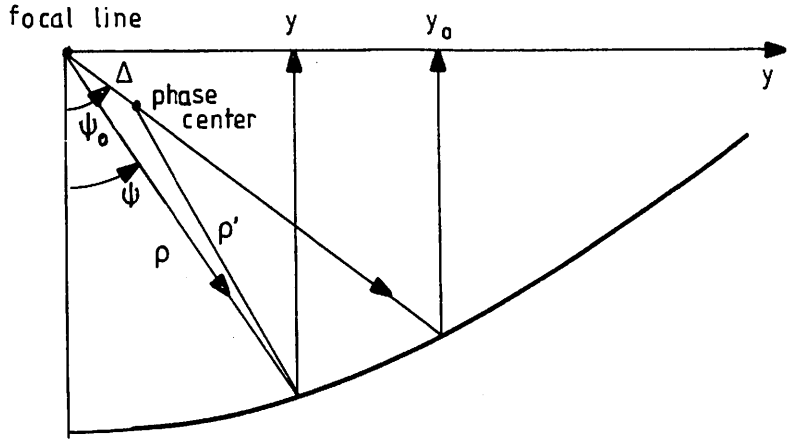

Fig. 2.1. Phase center displacement.

Let the cross section field pattern of for instance the longitudinal polarization be $g(\psi)$ $(=g_x(\psi))$. It is assumed to have a well defined phase center that is the same for all directions. Then, according to Eq. (1.5) in Appendix A, $g(\psi)$ is real when the phase center coincides with the reference axis of the phase, e.g. the x-axis. When it is displaced a distance Δ from the x-axis in the direction ψ_0, the field pattern becomes complex (See Fig. 2.1,).

$$g(\psi) = |g(\psi)|e^{j\delta} \tag{2.8}$$

$$\delta = k(\rho - \rho') \approx k\Delta\cos(\psi_0 - \psi) \quad (\Delta < \frac{1}{2}\sqrt{\frac{F\lambda}{2}}) \tag{2.9}$$

The far field in the direction normal to the aperture is found in Eq. (2.16) in Appendix A. It is (α means proporsional to)

$$E^s(0,0) \ \alpha \int_E^{E+D} \frac{g(\psi)}{\sqrt{\rho}} dy \tag{2.10}$$

The aperture distribution is

$$a(y) = \frac{g(\psi)}{\sqrt{\rho}} \tag{2.11}$$

where ψ and ρ are functions of y. Thus, the phase errors across the aperture are δ. δ may be written as a function of y. From Appendix A (Section A.4).

$$\cos\frac{\psi}{2} = \frac{1}{\sqrt{1+(\frac{y}{2F})^2}} \tag{2.12}$$

$$\sin\frac{\psi}{2} = \frac{y}{2F\sqrt{1+(\frac{y}{2F})^2}} \tag{2.13}$$

If y_0 is the aperture coordinate corresponding to ψ_0 , then

$$\begin{aligned}\delta &= k\Delta\cos(\psi_0 - \psi) = k\Delta(1-2\sin^2(\frac{\psi_0-\psi}{2})) \\ &= k\Delta(1-2(\sin\frac{\psi_0}{2}\cos\frac{\psi}{2} - \sin\frac{\psi}{2}\cos\frac{\psi_0}{2})^2) \\ &= k\Delta - \frac{2k\Delta}{(1+(\frac{y}{2F})^2(1+(\frac{y_0}{2F})^2)}(\frac{y-y_0}{2F})^2\end{aligned} \tag{2.14}$$

Thus, the phase errors vary almost quadratically over the aperture. The loss of gain because of small phase errors is given in Ref. 2 as

$$\frac{G}{G_0} = 1 - \overline{\delta^2} + (\overline{\delta})^2 = 1 - \delta_0^2 \tag{2.15}$$

where $\overline{\delta^2}$ is the mean square phase error, and $\overline{\delta}$ is the mean phase error, both weighted with the aperture distribution.

$$\overline{\delta^2} = \frac{\int_E^{E+D} |a(y)| \delta^2 dy}{\int_E^{E+D} |a(y)| dy} \tag{2.16}$$

$$\overline{\delta} = \frac{\int_E^{E+D} |a(y)| \delta dy}{\int_E^{E+D} |a(y)| dy} \tag{2.17}$$

$$\delta_0 = \sqrt{\overline{\delta^2} - (\overline{\delta})^2} \tag{2.18}$$

δ_0 is the mean square phase error calculated from the mean phase plane.

Eq. (2.16) and (2.17) are evaluated numerically for a uniform aperture distribution a(y) = 1, a pointing direction of the feed $\psi_0 = 51^\circ$, and F/D = 0.45. The result is

$$\delta_0 = 0.1k|\Delta| \quad \text{rad}$$

$$= 36.0\frac{|\Delta|}{\lambda} \quad \text{deg} \tag{2.19}$$

A phase error δ_0 = 5 deg gives a gain reduction of 0.033 dB (Eq. (2.15)). That is equivalent to a displacement (from Eq. (2.19))

$$\boxed{|\Delta| = 0.14\lambda} \tag{2.20}$$

of the phase center from the focal line of the parabolic cylinder. Thus, phase errors due to defocusing of the reflector have much smaller influence on the gain than random phase errors of the size $k\Delta$. Ref. 7 page 57 gives a similar result for a circular aperture.

Thus, the phase centers for the two linear polarizations must be closer together than 0.28λ to give extra phase errors less than 5 deg r.m.s.

2.4. Spillover Lobes.

The design goals for the far sidelobes of the total radiation pattern of the antenna are -30 dB for sidelobes more than 10 deg from the axis, and -50 dB for sidelobes more than 60 deg from the axis. (Ref. 1).

Spillover lobes due to direct feed radiation occur within the angular range of $-180 \text{ deg} < \theta < 84 \text{ deg}$ in the cross section plane with its highest value near to the boundaries $\theta = -180$ deg and $\theta = 84$ deg. A tradeoff must be made between the wanted high aperture efficiency and the low spillover lobes, because a high taper of the aperture illumination with low spillover lobes gives a low aperture efficiency. The relative size of the spillover lobes $G^S(\theta)$ is given as follows

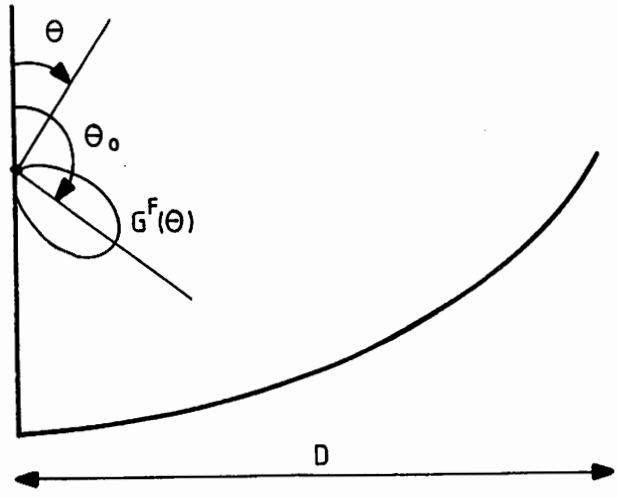

Fig. 2.2. Cross section of cylinder antenna.

$$G^S(\theta) = \frac{G^F G^F(\theta)}{G^C} \tag{2.21}$$

$G^F(\theta)$ is the cross section radiation pattern of the feed, $(G^F(\theta_0) = 1)$. G^F is the cross section directivity of the feed

in the direction θ_0 , e.g. the directivity relative to a line source that radiates isotropically in the cross section plane, but has the same field distribution as the feed along the line. It is defined in Eq. (1.11) in Appendix A as

$$G^F = \frac{2\pi}{\int_{-\pi}^{\pi} G^F(\theta)d\theta} \tag{2.22}$$

And G^C is the cross section directivity of the cylinder antenna, defined in Eq. (3.10) in Appendix A as

$$G^C = \frac{2\pi D}{\lambda}\eta^C \tag{2.23}$$

where η^C is the cross section aperture efficiency. Typical numerical values in dB are (for $D = 30\lambda$).

$$\boxed{(G^S(\theta))_{dB} = -15dB + (G^F(\theta))_{dB}} \tag{2.24}$$

Feed diagrams that illuminate the reflector properly will have a taper at the edges between -5 and -10 dB. Thus, the spillover lobes at the edges of the reflector will be 20-25 dB below the main beam level of the secondary radiation pattern. Spillover lobes below -50 dB will only be achieved in very limited angular regions within $-180 \text{ deg} < \theta < 84 \text{ deg}$.

In the feed synthesis in Chapter 4 it is assumed that it is more important to have high aperture efficiency than to achieve the design goal with regard to sidelobes.

2.5. Impedance Variations with Scan Angle.

The impedance will vary with scan angle, and the variations are different for the two linear polarizations. The impedance should preferably be matched at broadside, but in order to reduce the reflections at 25 deg beamsteering angle a match at some offset angle may be preferable. The effect of mismatch is considered here.

The 128 crossed dipoles in the linear array feed are fed from two parallel completely branched transmission line systems (Ref. 1).

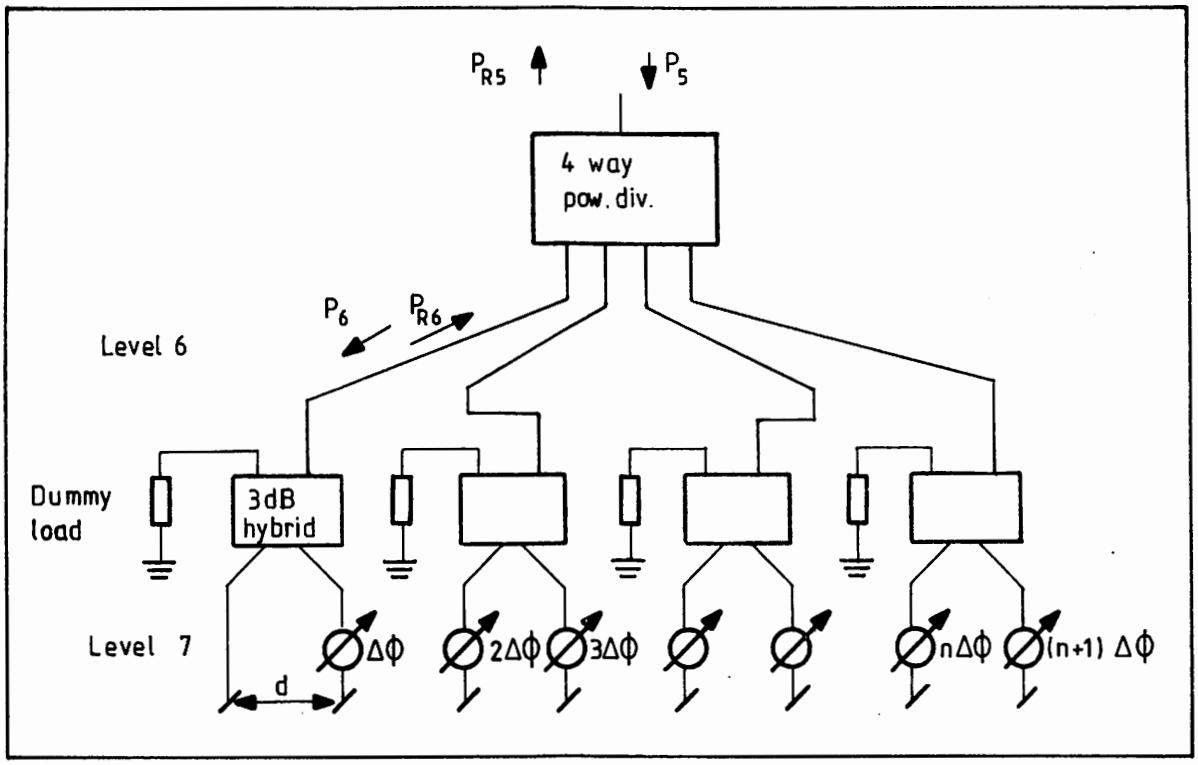

Fig. 2.3. Branched transmission line system.

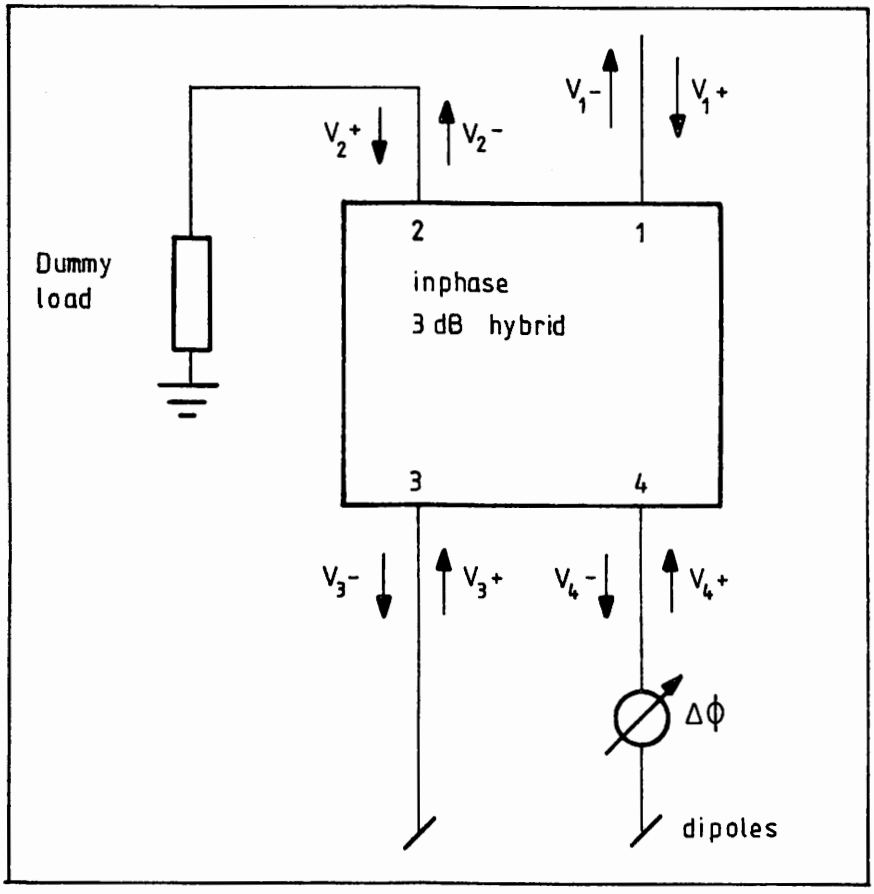

Fig. 2.4. Ideal inphase hybrid.

The two last levels (level 6 and 7), are shown in Fig. 2.3. The last power dividers are 3 dB hybrids with isolated in-phase outputs. In front of them are 4 way matched power dividers with no isolation between the outputs. All divisions in front of them are made by simple matched T-junctions. Phasing devices, for instance phase cables, give a phase progression $\Delta\phi$ along the feed. All cable lengths within one level are the same, so that when $\Delta\phi=0$, all dipoles are fed inphase. The phase progression is

$$\Delta\phi = kd\sin\theta \tag{2.25}$$

where θ is the scan angle from broadside and d the element spacing. The transmission line system is analysed at the center frequency.

If the array is assumed to be infinite, all dipole impedances are equal. The reflection coefficient is

$$\rho(\theta) = \frac{Z(\theta) - R_0}{Z(\theta) + R_0} \tag{2.26}$$

where $Z(\theta)$ is the (scan-angle dependent) dipole impedance and R_0 is the characteristic impedance of the transmission line feeding the dipoles.

The scatter matrix for the ideal inphase 3 dB hybrid in Fig. 2.4 is

$$S = \frac{1}{\sqrt{2}} \begin{bmatrix} 0 & 0 & 1 & 1 \\ 0 & 0 & -j & j \\ 1 & -j & 0 & 0 \\ 1 & j & 0 & 0 \end{bmatrix} \tag{2.27}$$

Fig. 2.4 is basis for the simple analysis that follows.

Assume $$V_1^+ = 1 \tag{2.28}$$

$$V_2^+ = 0 \tag{2.29}$$

The reflection coefficient of the dipoles are $\rho(\theta)$.

Therefore,

$$V_3^+ = \rho(\theta) V_3^- \tag{2.30}$$

$$V_4^+ = \rho(\theta) e^{j2\Delta\phi} V_4^- \tag{2.31}$$

The scatter matrix gives

$$V_3^- = \frac{1}{\sqrt{2}} \tag{2.32}$$

$$V_4^- = \frac{1}{\sqrt{2}} \tag{2.33}$$

so that

$$V_2^- = j(V_4^+ - V_3^+) = -je^{j\Delta\phi}\rho(\theta)\sin\Delta\phi \tag{2.34}$$

$$V_1^- = V_4^+ + V_3^+ = e^{j\Delta\phi}\rho(\theta)\cos\Delta\phi \tag{2.35}$$

Substituting Eq.(2.25) gives the power dissipated in the dummy load:

$$P_{dummy}(\theta) = |V_2^-|^2 P_6 = |\rho(\theta)|^2 \sin^2(kd\sin\theta) P_6 \tag{2.36}$$

where P_6 is the power at level 6. This simple analysis has neglected the coupling between the outputs of the 4 way divider, and between the outputs of the T junctions in front.

The power dissipated in the dummy load relative to the total power reflected from the two dipoles is

$$\overline{P}_{dummy}(\theta) = \frac{P_{dummy}(\theta)}{P_6|\rho(\theta)|^2} = \sin^2(kd\sin\theta) \tag{2.37}$$

This formula is shown in Fig. 7 for $d = 0.7\lambda$.

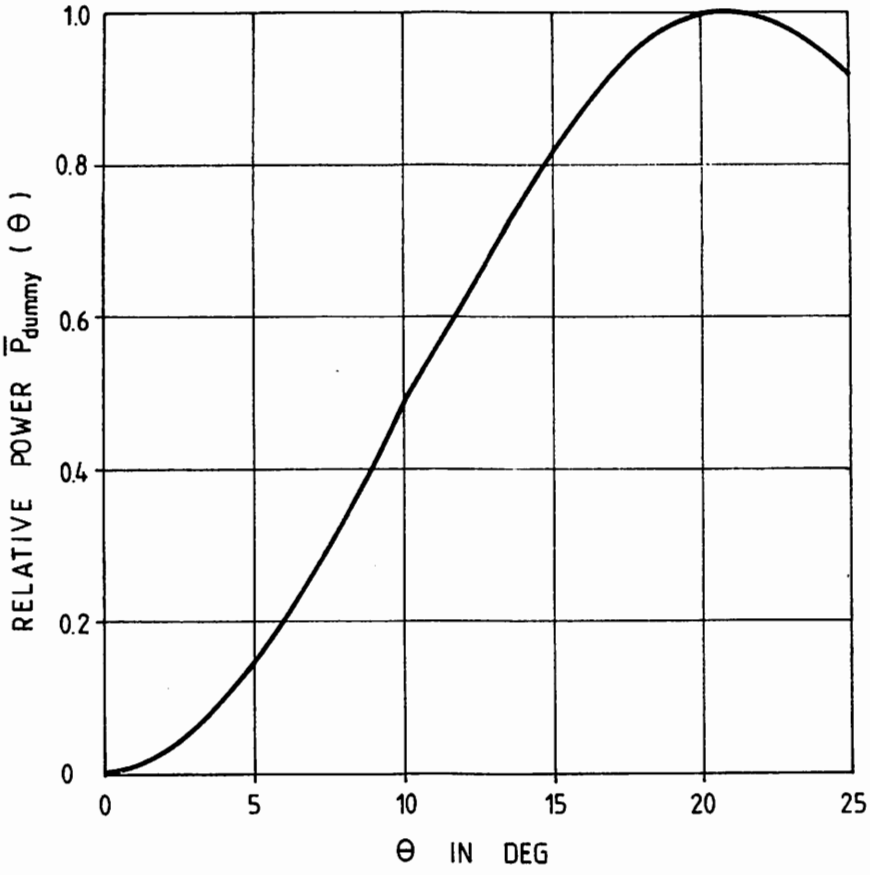

Fig. 2.5. Relative reflected power dissipated in the dummy load as a function of scan angle.

The figure shows that for scan angles around 20 deg most of the reflected power is dissipated in the dummy loads. Therefore, the dummy loads must be dimensioned to (P_6 = 6kW).

$$P_{dummy,\ max} \approx 6\left|\rho(20\ deg)\right|^2 kW \tag{2.38}$$

The reflections not dissipated in the dummy load is reflected to the outputs of the 4 way dividers. When $\theta \neq 0$ the reflections will not be in phase, and will, therefore, be coupled to the neighbouring ports of the 4 way divider. Something may also couple to the input and propagate back to the T-junctions in front where it may couple to the neighbouring output, and so on. That is because there is no isolation between the outputs. These coupled signals will cause amplitude and phase errors at the feeder elements. It is assumed that the error signal is approximately the same on all dipoles. The relative error signal is then ($\theta \neq 0$)

$$\left|\frac{V_1^-}{V_1^+}\right| \approx \left|\rho(\theta)\cos(kd\sin\theta)\right| \tag{2.39}$$

According to the specifications in Ref. 1 the amplitude error in the excitation of the dipoles must be less than 0.1. Therefore when $\theta \neq 0$

$$|\rho(\theta)\cos(kd\sin\theta)| < 0.1 \tag{2.40}$$

This gives for $\theta = 25$ deg

$$|\rho(25 \text{ deg})| < 0.35$$

or $$\boxed{\text{VSWR} < 2.1} \tag{2.41}$$

Thus, the VSWR at the dipole input must be less than 2.1 when the linear array is phase steered to 25 deg from broadside.

When $\theta = 0$ all reflections are inphase so that nothing is dissipated in the dummy loads and nothing is coupled to neighbouring outputs of the power dividers. Thus, for this ideal transmission line system at the center frequency, the VSWR will be the same on all levels when $\theta = 0$.

The conclusion is: It is important to reduce the impedance variation with scan angle in order to reduce the size of the dummy loads, reduce the error signal distributed to neighbouring dipoles when $\theta \neq 0$, and when $\theta = 0$ to reduce the VSWR seen by the transmitter.

3. COMPUTER PROGRAMS.

Some computer programs have been developed to investigate different feeder elements with regard to the design parameters given in Chapter 2.

3.1. Aperture Efficiency.

The program calculates the cross section aperture efficiency of a parabolic cylindrical reflector antenna as a function of F/D ratio and pointing direction of the feed. Adjacent parameters like spillover efficiency, the size of the spillover lobes and the taper of the aperture illumination are calculated.

Assumptions: Cylindrical wave propagating from the focal line.

Method: The aperture efficiency integral in Eq. (2.3).

Author: Per-Simon Kildal, NTH.

3.2. Phase Center.

The program calculates the phase center of a given axial symmetric radiation pattern (amplitude and phase).

Method: The phase center is determined as the phase reference point for which the root mean weighted square of the phase errors have its minimum value. The phase errors are referred to the best fit spherical wavefront propagating from the reference point of the phase. The weights in the r.m.s. computations are taken to be the amplitude of the radiation pattern. The computations follow Eq. (4.25 - 11) on page 150 in Ref. 3. (There is a misprint in the equation that should have a negative sign).

Author: Per-Simon Kildal, NTH.

3.3. Impedance of a Linear Array of Dipoles over Ground.

The program calculates the active impedance of a phase steered linear array antenna of crossed dipoles over an infinite ground plane as a function of pointing direction of the main beam for

a given number of elements, element spacing, height over ground and orientation of the dipoles.

Assumptions: All element currents have the same amplitude with an ideal linear phase progression along the array. This is a rather crude approximation for small arrays, but when the number of elements increases (>5) the approximation becomes better (except for the impedance of the edge elements). The current distribution is assumed to be sinusoidal.
Method: The emf method, Ref. 9 page 8.
A detailed description of the computations of the mutual impedances is given in Ref. 10.

Author: Egil Hauger.

3.4. Corner Reflector with Dipole Normal to the Corner Axis.

The programs calculate the cross section radiation pattern of a corner reflector with infinite length. The dipole is oriented normal to the corner axis. Variable parameters are: Corner angle (v), corner walls (a), height of dipole over corner (h), dipole length (λ), bends on the dipole arms (v_d , λ_d) in the plane normal to the corner axis.

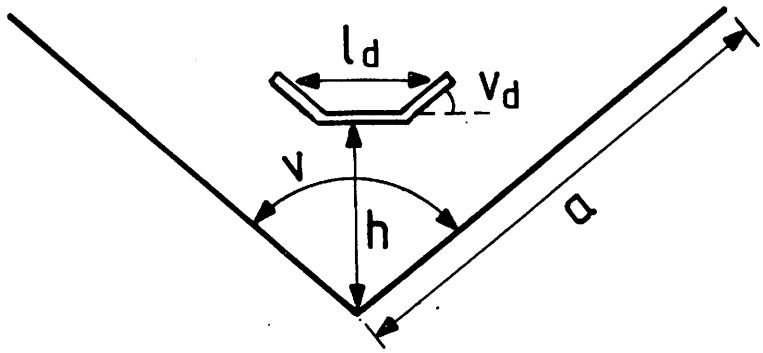

Fig. 3.1. Cross section view of corner reflector.
Transverse polarization.

Assumption: Sinusoidal current distribution on the dipole.

Method: The radiation pattern is obtained by resiprocity.
A distant current element $I\lambda_R \vec{a}_\psi$ in the cross section plane produces a plane wave in the vincinity of the reflector. The total field $\vec{E}_R$ from the current element with the corner reflector

present, is calculated. This is a two dimensional problem. If the current on the dipole is I_d , the radiation field $E_\psi \vec{a}_\psi$ from the dipole with the reflector present is now found by resiprocity (Ref. 11).

$$E_\psi(\psi) = \frac{1}{I\ell_R} \int_{\text{dipole}} \vec{E}_R \cdot I_d \vec{d}\ell$$

One way to calculate $\vec{E}_R$ is to use the geometrical theory of diffraction (GTD) (Ref. 12), which says that in addition to the geometrical optics rays we have diffracted rays emanating from the reflector edges and the corner angle.

Another approach is to use the E-field formulated integral equation for the current on the reflector induced by the instant current element. This equation is easily solved by the method of moments (MM) (Ref. 13). Once the induced current is known, the scattered field can be calculated, and $\vec{E}_R$ is the sum of the incident and the scattered field.

Programs for both methods were written, and the results were compared. The two methods gave equal results for $v = 180^o$. For other corner angles the GTD-program gave erroneous results. The reason is assumed to be that the doubly-diffracted field between the edges and the corner angle contributes a great deal to the total field in this case. Rays emanating from the edges are diffracted by the corner. The edges are to be regarded as sources for this diffraction. In this case GTD is not valid, since it is an asymtotic theory requiring a diffracted ray path of several wavelengths, while the ray path now is approximate one wavelength long.

Author: Eddy Sørngård, NTH.

3.5. Corner Reflector with Rods and Dipole Parallel to the Corner Axis.

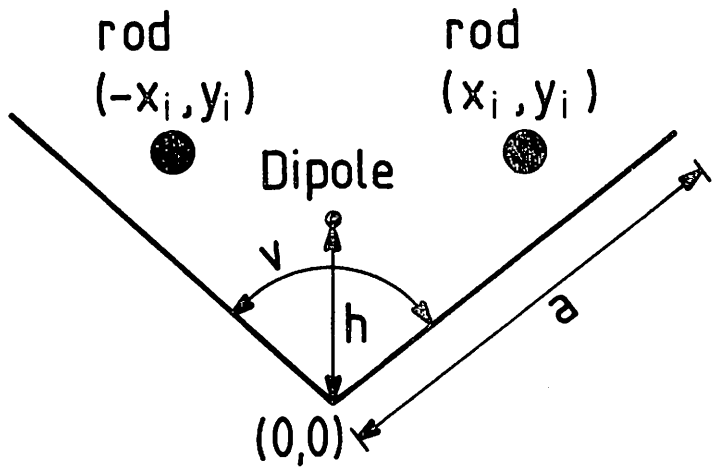

Fig. 3.2. Cross section view of corner reflector with rods. Longitudinal polarization.

The programs calculate the cross section radiation pattern of a corner reflector of infinite length with the dipole parallel to the corner axes. In one of the programs any number of infinitely long rods parallel to the dipole may be placed anywhere outside the reflector. The rods are used to obtain a wanted radiation pattern. Variable parameters are: Corner walls (a), corner angle (v), height of dipole over corner (h). If rods are to be taken account of, following additional parameters are needed: The diameter of the rods, and the coordinates (x_i, y_i) of each of the rods.

Method: The radiation pattern is again obtained by resiprocity. The distant current element is now parallel to the reflector axes, $I\ell\vec{a}_x$, and all E-fields have only a z-component. The radiation field is given by

$$E_x(\psi) = \frac{1}{I\ell} \int_{\text{dipole}} E_R I_d dz = cE_R \Big|_{\substack{\text{at} \\ \text{dipole}}}$$

where c is a constant.

Also in this case one can use an E-field formulation to get an integral equation for the current induced on the reflector and the rods, and the equation is solved by the method of moments. The

scattered field from the reflector and the rods can then be found, and E_R is the sum of the incident and the scattered field. When no rods is present, E_R can alternatively be calculated by GTD.

A computer program was written for each of the two methods, and the results were compared. For this polarization there is good agreement between the patterns calculated by the two methods for all corner angles, because the doubly-diffracted rays between the edges and the corner angle causing trouble for the other polarization, do not excist in this case.

Author: Eddy Sørngård, NTH.

4. RESULTS OF COMPUTATIONS.

The computer programs described in Chapter 3 were run a number of times to synthesize a good feed design. The variable parameters of the corner reflector were changed in order to optimize the design parameters in Chapter 2. The results given here are all for a parabolic cylindrical reflector antenna with F/D = 0.45. The feed is offset with one of the reflector edges along the vertex of the parabolic cylinder. More results, computed and measured, are given in Chapter 6 for the proposed feed design. When the aperture efficiency is mentioned in the following, spillover is always included. The phrase "little influence on the radiation pattern" means that the change in the beam illuminating the reflector is so small that the aperture efficiency does not change by more than 1-2 percent.

4.1. Dipoles Normal to the Corner Axis.

- The illumination that yields the highest aperture efficiency occur for a corner angle of 180 deg. (~ 0.887).
- For corner angles between 90 deg. and 120 deg. the r.m.s. phase error referred to the best fit phase center is significantly higher than for corner angles around 180 deg.
- The phase center for 180 deg. corner angle is slightly beneath the ground plane (~ 0.02λ). When the corner angle decreases, the phase center moves upwards so that the corner reflector acts more and more as a horn antenna with the phase center near to the aperture.
- The spillover lobes are much lower for 90 deg. corner angle than for any other corner angles.
- Bending of the dipole arms when v = 180 deg. has unfavourable influence on the radiation pattern. When the arms are bent towards the ground plane, the beam broadens, and the phase center moves slightly upwards. When the arms are bent away from the ground plane, the phase center moves farther beneath the ground plane with insignificant effect on the radiation pattern.
- For 180 deg. corner angle variations in the dipole height between 0.15λ and 0.25λ has little influence on the radiation pattern, but the spillover is slightly increasing when h increases.
- For small corner angles, for instance v = 90 deg., variations

in the dipole height effects strongly on the radiation pattern. The best diagram occur when h = 0.7λ. For this height the field normal to the corner walls is almost zero (theoretically it is zero when a → ∞ and h = 0.7λ).

- For 180 deg. corner angle variations in half the ground plane size down to a = 0.75λ has little influence on the radiation pattern, but the spillover and the spillover lobes increases somewhat. A good choice is 1.0λ < a < 1.25λ.

Some typical calculated results are shown beneath:

v	a/λ	h/λ	Δ/λ	δ_0	η_y^s	η_y^c	Spillover lobes at -180deg	Spillover lobes at 84deg
180 deg	1.0	.25	-0.028	1.32 deg	0.934	0.887	-22.5dB	-20.5dB
120 deg	1.65	.5	0.618	11.62 deg	0.748	0.719	-18.5dB	-18.0dB
90 deg	2.0	.7	0.942	9.15 deg	0.964	0.534	-33.8dB	-34.4dB

v, a and h are defined in Fig. 3.1.
Δ is the position of phase center over corner.
δ_0 is the r.m.s. of the phase errors within the subtended angle of the reflector when the phase is referred to the phase center. (Computed with the program in Sec. 3.2).
η_y^c and η_y^s are the cross section aperture efficiency (Eq. (2.3)) and the spillover efficiency (Eq. (2.5)) respectively.

4.2. Dipoles Parallel to the Corner Axis.

No rods:

- With 180 deg. corner angle the aperture efficiency is as low as 0.8 included 17% spillover.
- The aperture efficiency is increasing when the corner angle decreases from 180 deg, having a maximum of ~ 0.873 for v ≈ 140 deg, and is then decreasing down to ~ 0.80 for v = 90 deg.
- The radiation pattern is for all corner angles relatively insensitive to variations in the height h when h < 0.25 λ.
- The phase center is moving upwards with decreasing corner angle, from near the corner axis to the aperture of the corner.
- The r.m.s. phase error over the wavefront is increasing only slightly with decreasing corner angle.
- Variations of the size of the walls seems to have little influence on the radiation pattern as long as the aperture

of the corner reflector is wider than 2.0λ, e.g. $a > \frac{1.0\lambda}{\cos v}$.

- The spillover and the spillover lobes decreases with decreasing corner angle.
- The reason to the much better performance of the corner reflector when the dipole is parallel to the corner axis is assumed to be that the field at the corner walls in the cross section plane through the dipole is always zero for this polarization, causing much less diffraction from the edges than if the field was not zero, as generally is the case for the perpendicular dipole.

180 deg. corner with two rods.

- With two rods only, symmetrically placed on both sides of the dipole, the radiation diagram can be shaped very easily to give an aperture efficiency of up to 0.895.
- The size of the ground plane has little influence on the radiation pattern when $2a > 2.0\lambda$.
- The r.m.s. phase error over the wavefront within the subtended angle of the reflector referred to the phase center is less than 2.0 deg for all positions of the rods.
- The phase center is changing when the positions of the rods vary. There is a tendency of the phase center to move down when x_1 or/and y_1 is increasing. The phase center may be below the ground plane.
- To reduce spillover the height y_1 of the rods should be $y_1 < 0.5\lambda$.
- The diameter of the rods was taken to be 0.025λ.
- The highest aperture efficiency achieved was 0.896 when $x_1 = 0.45$, $y_1 = 0.45$ and $h = 0.25\lambda$.
- Small variations in the position of the rods in the area $0.45 < x_1 < 0.55$ and $0.45 < y_1 < 0.5$ yields possibilities to match radiation pattern or phase center to the results of the dipole normal to the corner axis.
- Variations in the height have little influence on the radiation pattern when $h < 0.25\lambda$, but the spillover lobes increase somewhat with increasing height.

Some typical calculated results are shown beneath:

v(deg)	a/λ	h/λ	$x_1/\lambda, y_1/\lambda$	Δ/λ	δ_0	η_x^s	η_x^c	Spillover lobes at -180deg	84deg
180	1.0	0.15	No			0.826	0.805	-19.9dB	-18.8dB
120	1.15	0.20	No	0.141	1.87deg	0.945	0.845	-24.0dB	-22.0dB
140	1.20	0.15	No	0.037	2.3 deg	0.922	0.860	-22.7dB	-20.9dB
90	2.0	0.25	No	0.434	4.11deg	0.984	0.792	-28.4dB	-25.4dB
180	1.0	0.25	0.5 , 0.5	-0.021	0.83deg	0.937	0.889	-23.6dB	-20.9dB
180	1.0	0.25	0.45,0.45	0.07	1.38deg	0.953	0.896	-23.5dB	-21.0dB

v, a, h, x_1 and y_1 are defined in Fig. 3.2.
For Δ and δ_0 see page 4.2.
For η_x^s and η_x^c see Eq. (2.5) and (2.3) respectively.

4.3. Impedance Variations.

Impedance computations were made with the program described in Chapter 3.3, for a linear array of crossed dipoles over an infinite ground plane. The computations were done mainly to have an idea of which parameters that would influence the mutual coupling. Measured results may be different, depending on the special dipole design, but the variations with the parameters should be the same. All calculations are for the center dipole in a linear array antenna of seven elements. Only the transverse polarization is applicable to the proposed feed design, and is considered here.

The element spacing (d), the height of the dipoles over ground plane (h), and the length of the dipole arms (ℓ) have influence on the impedance performance. The element spacing is for the EISCAT VHF antenna d = 0.7λ. The performance of the power reflection coefficient when the dipoles are matched at broadside is shown in Fig. 4.1 for the transverse polarization for this element spacing. The reflection coefficient clearly decreases with decreasing height. The reason is assumed to be that the mutual impedances decreases when the dipoles approach their images. The current on the dipole and on the image is out of phase causing the sum of the two field vectors on the neighbouring dipoles to decrease.

In the matching procedure of the dipoles it is convenient to know the impedance variations with height and length of arms. That is shown in Fig. 4.2 for the transverse polarization.

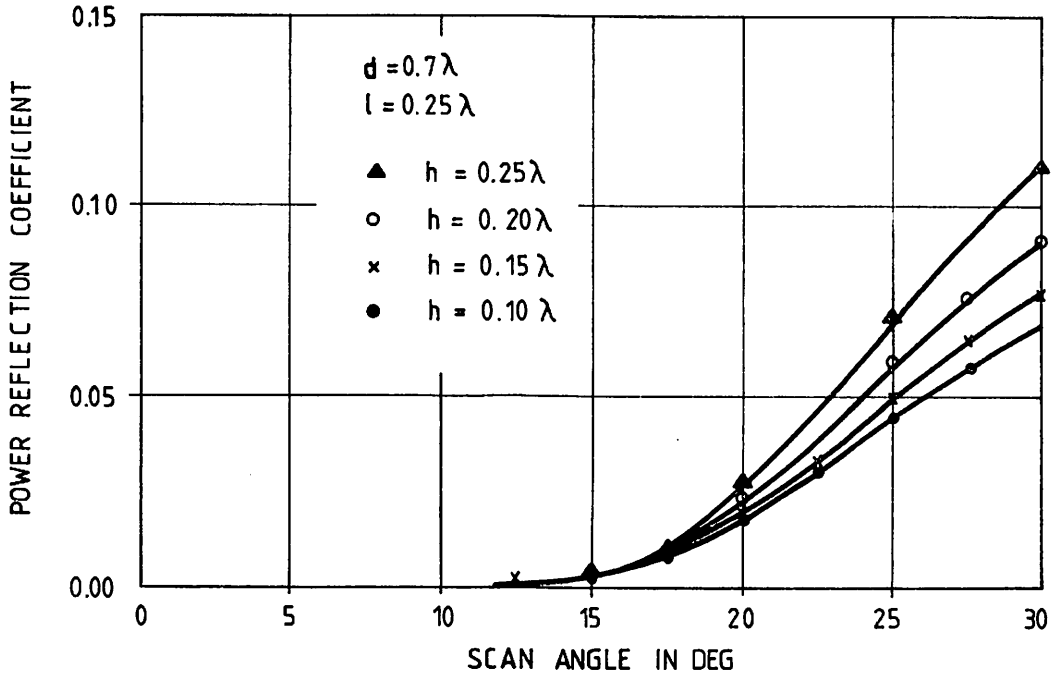

Fig. 4.1. Power reflection coefficient versus scan angle when dipoles are matched at broadside. Transverse polarization.

The calculated impedances are transformed through the lossless network mentioned in Chapter 5.1, to take account of the special balun design. Note that the actual length of the dipole arms to be used in the program is the length of one arm (in Fig. 51) plus half the diameter of the arm. That is to take account of the thickness of the dipole arm.

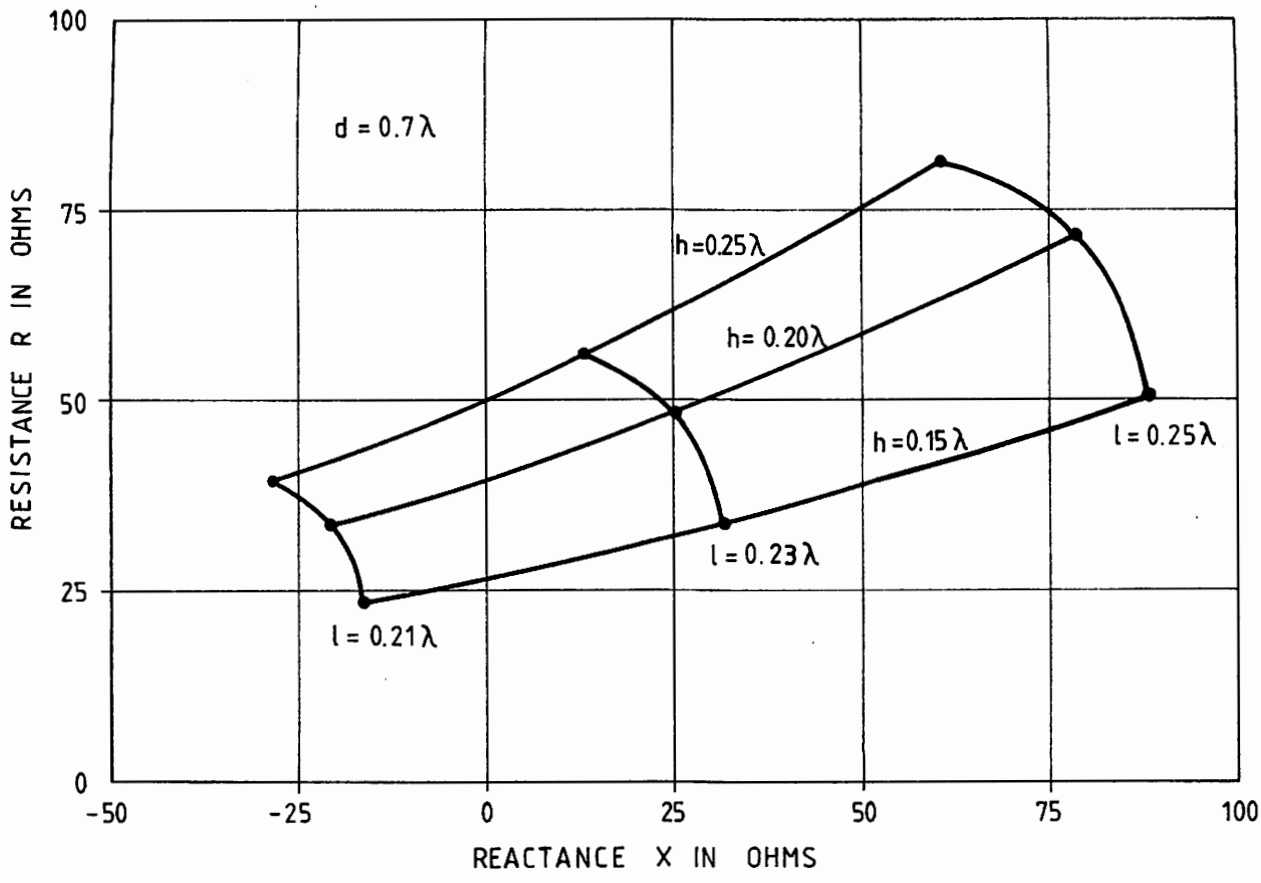

Fig. 4.2. Dipole impedance (R + jX) as a function of dipole height (h) and length of dipole arms (ℓ). Transverse polarization. Center dipole in a linear array of 7 dipoles with spacing 0.7λ. All dipoles are excited with the same amplitude and phase.

One way to compensate for the mutual coupling is to place baffles between the dipoles (Ref. 15). According to the reference baffles compensate the impedance variations of the colinear dipoles, e.g. the longitudinal dipoles, when the spacing is 0.5λ. Calculations by the periodic structure approach (Ref. 14 page 216 and 247) are more difficult to carry out for other element spacings, because then grating lobes must be considered. Baffles also turned out to have high influence on the cross section radiation pattern of the transverse dipoles (see Chapter 5.2). Therefore, it was not put more effort in considerations of baffles.

5. SCALE MODEL MEASUREMENTS.

To verify the computed radiation patterns and to measure impedances, scale models were built at 1.5 GHz (λ = 200 mm), e.g. a reduction in scale at 1:6.63. The design of the models, and some of the measurements, are given below. For the proposed feed design, however, the complete measurement results may be found in Chapter 6.

5.1. Dipole Design.

The dipoles were made with a shielded balun to allow adjustment of height above the ground plane (for matching purposes). The design is shown in Fig. 5.1. The two cables feeding the two orthogonal dipoles in one crossed dipole unit are 50 ohms SR-2 cables with teflon dielectric from Suhner. The attenuation of this cable is 0.9 dB/m, which is calibrated out by referring the impedance measurements to point A on Fig. 5.1 by using a shorted SR-2 cable of length 138.7 mm, e.g. equal to the length of the SR-2 cable in the dipole. 7 dipoles were made. The free space impedance was measured when the length of one dipole arm plus half the diamenter (ℓ in Fig. 5.1) equaled 0.25λ. The resistance R_d and reactance X_d were for all 14 inputs within

$$R_d = (105 \pm 2.5)\,\text{ohms}$$

(except for one crossed dipole where R_d = 115ohms and 112.5 ohms).

$$X_d = (53 \pm 5.5)\,\text{ohms}$$

The free space impedance may be calculated in several ways, but will not be equal to the measured ones unless the special feed gap configuration in Fig. 5.1 is taken into considerations. In Ref. 10 the free space impedance is calculated using Hallén's integral equation, extended boundary conditions and a series expansion of the current distribution in terms of trigonometric functions. The impedance of a half-wave dipole with diameter 2.5 mm (e.g. 0.0125λ) was found to be (92 + j42)ohms. The computations should be very accurate. In order to explain the discrepancy with the measured impedances, an equivalent circuit was made for the

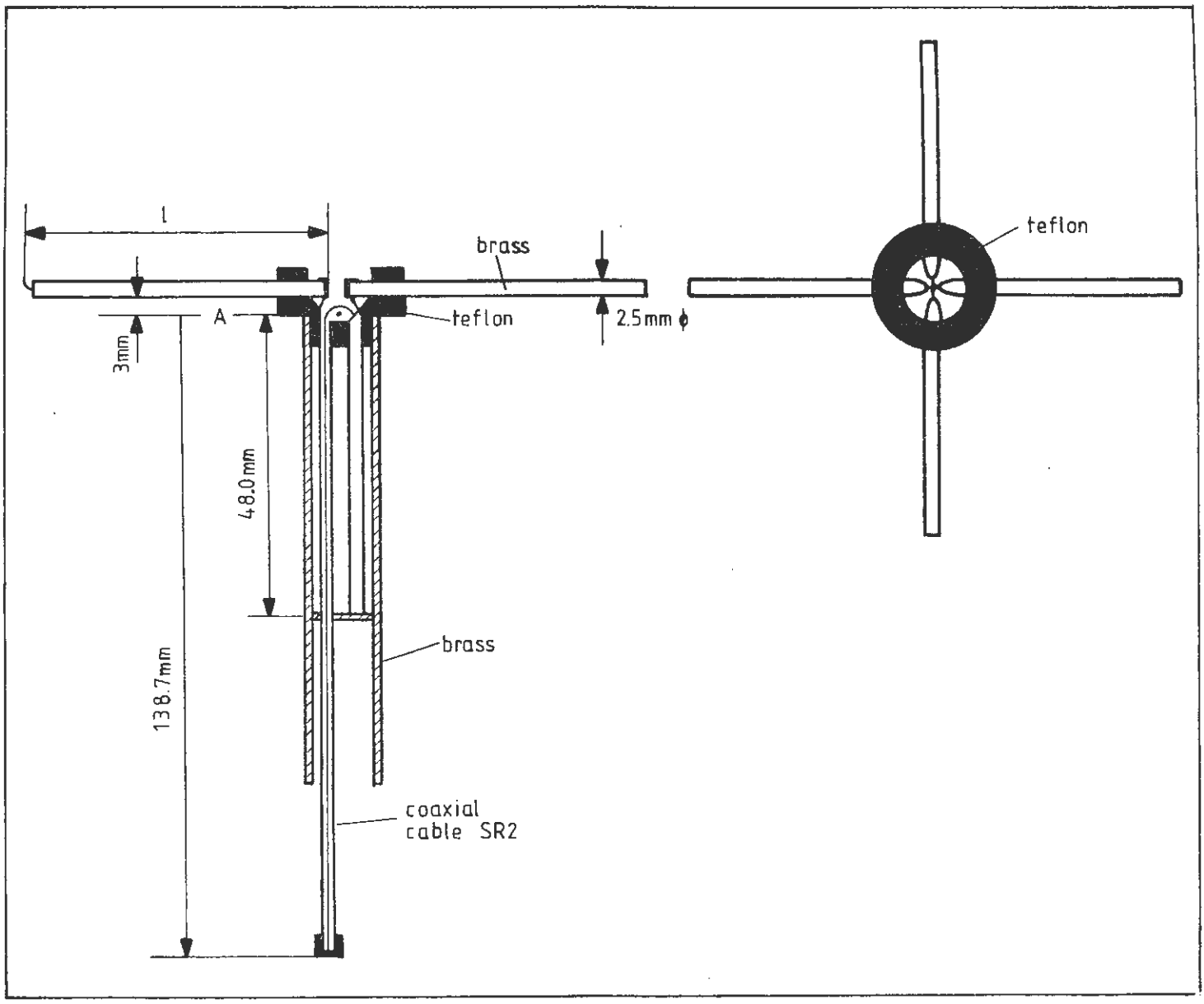

Fig. 5.1. Design of crossed dipoles.

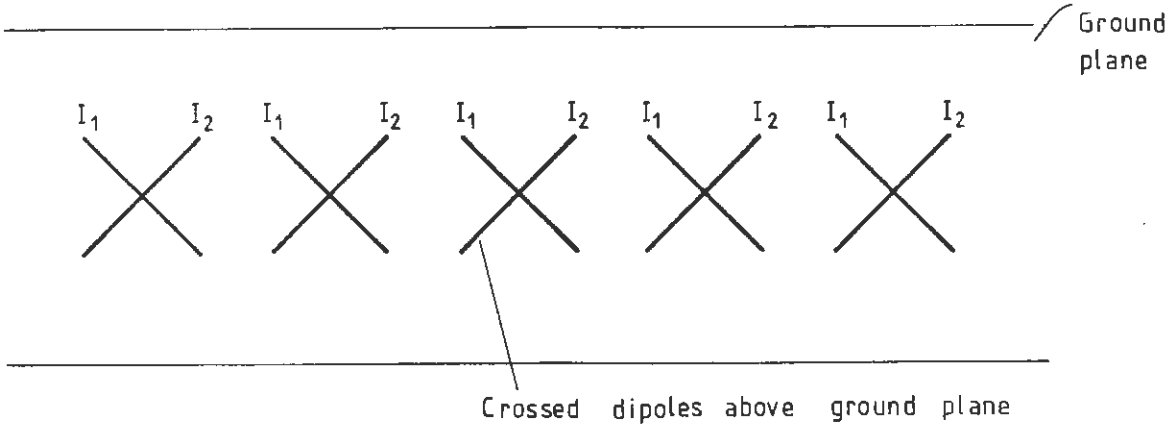

Fig. 5.2. Original idea with dipoles making a 45 deg angle with the array axis.

feed gap, using the dimensions of the physical structure between the impedance reference plane A and the feed points (Ref. 10). With this circuit, the calculated and measured impedances matched quite well. Here a transmission line equivalent will be used, a lossless transmission line with characteristic impedance 125 ohms and length 0.0278λ. When the computed free space impedance is transformed through this network, it becomes (105 + j54) ohms. A physical explanation of the equivalent circuit will not be given. It may be considered as an equivalent circuit that is "fitted" to the problem to equalize calculated and measured impedances. It is, however, believed to give a good representation of the feed gap because the free space impedance of (92 + j42)ohms is computed very accurately. Anyway, the equivalent circuit is lossless and will have only a small effect on principal impedance variations. Only the principal behaviour of the impedance variations is of interest in this report.

The program described in Sec. 3.3 computes the active impedance of a linear array of crossed dipoles. It is a simple program, assuming sinusoidal current distribution and equal current amplitude (but progressive phase) on all dipoles that have the same orientation to the linear array axis. A finite diameter of the dipoles is not considered, and must be accounted for approximately by adding half the diameter to the length of the arms (Fig. 5.1). This is to extend the current distribution around the edge at the end of the dipole arm to be zero on the axis at the end of the dipole rather than on the edge. The free space impedance computed with this program is (73 + j40)ohms. Transformed through the transmission line equivalent of the feed gap it equals (83 + j57) ohms. This is far from the measured value of (105 + j53)ohms. The discrepancy is caused by the simple analysis using a pure sinusoidal current distribution. But the program gives a good representation of the principal behaviour of the impedance, as is seen by comparing Fig. 6.12a and 6.13a with Fig. 6.14a and 6.15a respectively. The computed impedances in Fig. 6.14, 6.15 and Fig. 4.2 are all transformed through the equivalent circuit of the feed gap.

The first proposal for a linear array feed for the EISCAT cylindrical antenna was to use crossed dipoles above a ground plane, placed with a 45 deg angle to the linear array axis (Fig. 5.2). The two polarizations were fed individually from two transmitters with

equal amplitude excitation of each dipole of the same polarization (I_1 and I_2 in Fig. 5.2). Then it was possible to steer the amplitude of the longitudinal and transverse polarized field by phasing the two transmitters only (but transmitting full power in both, $I_1 = I_2$), so that circular polarization could be obtained in the main beam although the longitudinal and transverse polarization illuminates the reflector differently. The active impedance of such an array was measured as shown in Fig. 5.4, but with all 14 inputs of the 7 dipoles excited. An extra adjustable phase shifter was used to provide a phase difference between the currents I_1 and I_2 in Fig. 5.2. The impedance with the array transmitting left circular polarization turned out to be different from the impedance when the array transmitted right circular polarization. There exists coupling between one dipole excited with current I_1 and all neighbouring dipoles, both those excited with I_1 and with I_2 . The only dipole which does not couple is the orthogonal dipole in the same crossed dipole unit. Thus, the impedance of a dipole excited with I_1 is sensitive to the phase of I_2 , and is, therefore, different for right and left circular excitation. This unwanted coupling between orthogonal dipoles could cause problems with matching and polarization control. It is also more difficult to compute beam patters and to find methods of forming the beam patterns to optimize the illumination of the reflector. Therefore, longitudinal and transverse dipoles were chosen rather than the orientation in Fig. 5.2. The sensitivity of the impedance to the transmitted polarization was also computed (with the program in Sec. 3.3).

5.2. Radiation Patterns of Corner Reflectors.

Measurements were made on a 3 element array with the dipoles of Sec. 5.1 placed in a 90 deg corner reflector, a 120 deg corner reflector, and over a flat ground plane. In all cases there were baffles between the dipoles that had a spacing of 0.7λ. The cross section radiation patterns with all 3 dipoles excited were measured, and the aperture efficiences computed (from the measured patterns) with the program of Sec. 3.1. Phase measurements were not made. The baffles had no significant effect on the radiation patterns when the dipoles were parallel to the corner axis, causing the measured patterns to be equal to the patterns computed with the

program in Sec. 3.4. However, when the dipoles were normal to the corner axis, the baffles had a severe effect on the radiation patterns. Therefore, the patterns were very different from the patterns computed for the case without baffles with the program of Sec. 3.3.

Polarization	(See Fig. 3.1 and 3.2) v	a/λ	h/λ	Baffle height	Eq. 2.3 η^c	Cross section pattern (0-20dB)	Comments
Par. to Corn.	180 deg	1.0	0.15	0.3λ	0.803		Compare page 4.4
Norm.to Corn.	180 deg	1.0	0.15	0.3λ	0.835		High infl. of baffles
Par. to Corn.	120 deg	1.65	0.45	0.83λ	0.866		Compare page 4.4
Norm.to Corn.	120 deg	1.65	0.45	0.83λ	0.909		High infl. of baffles
Par. to Corn.	90 deg	2.0	0.4	1.4λ	0.780		Compare page 4.4
Norm.to Corn.	90 deg	2.0	0.4	1.4λ	0.814		High infl. of baffles

The 120 deg corner seems to be a good solution even if the shapes of the radiation patterns are slightly different. However, the use of baffles was given up because of the difficulties associated with the computation of the patterns in the cross section plane.

5.3. A linear Array of Seven Dipoles over Ground Plane with Parallel Rods.

180 deg. Corner with Rods: Based on the computations in Sec. 4.1 and 4.2 a ground plane was made, 2λ wide and with possibility to place parallel rods in different positions over the ground plane. The design is shown in Fig. 5.3 together with the numbering of the dipoles along the array. The diameter of the rods was 0.025λ.

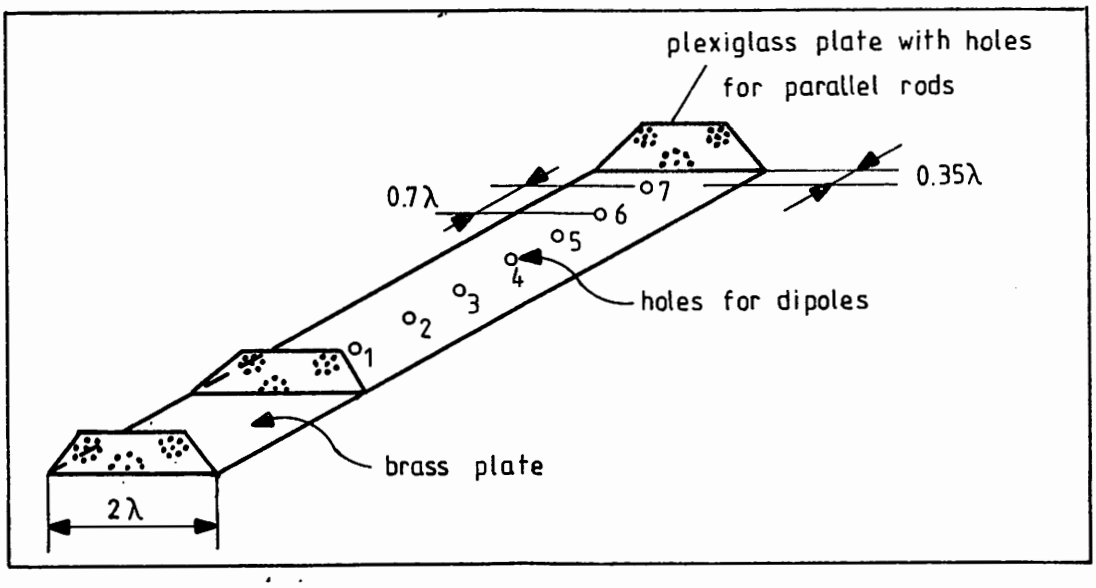

Fig. 5.3. Plane reflector with rods.

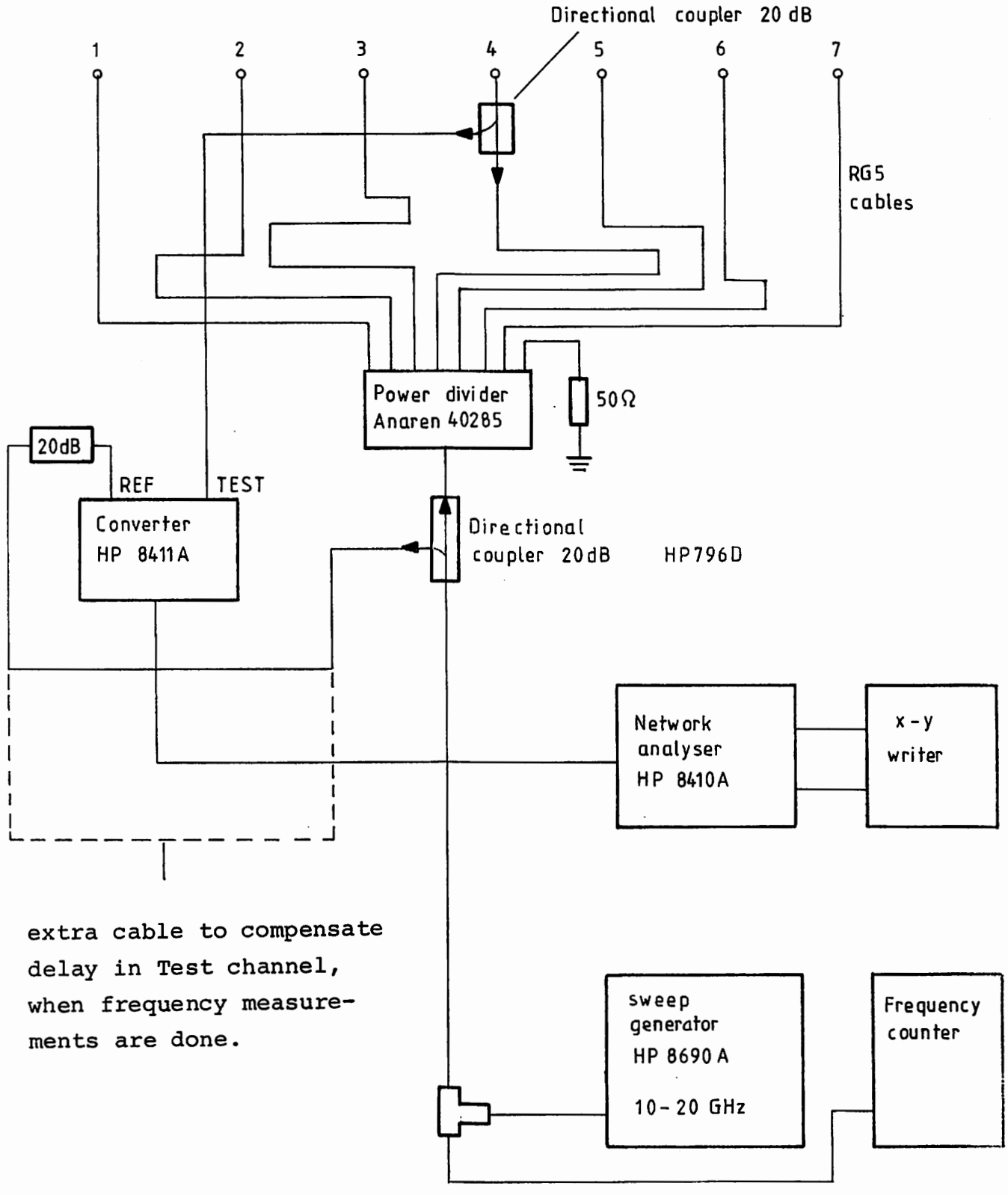

Fig. 5.4. Circuit for impedance measurements.

Impedance Measurements: The impedances were measured with all dipoles excited as shown in Fig. 5.4. The reference point of all measurements is the feed gap in the dipole, as explained in Sec. 5.1. The flexible cables (RG 5) used to connect the dipoles to the 8 way power divider were all cut to the same electrical length (±5 deg), one of them, however, was cut to the same length as the others with the directional coupler included. The accuracy of the measurements depends on the isolation of the directional coupler which was measured to -53 dB. This gives an error signal of -33 dB when the coupling is 20 dB. Thus, the impedance can be measured with an error in the power reflection coefficient of 0.022, e.g. SVWR 1.044. Reflections from connectors and cables (SR2 and SR3 with $Z_k = 50 \pm 1$ ohms, RG 5 with $Z_k = 50 \pm 2$ ohm) yield additional errors.

Phase Cables: To phase the linear array antenna, 16 cables (SR3) were cut in lengths

$$18/17\lambda,\ 19/17\lambda,\ 20/17\lambda,\ 21/17\lambda,\ 5/17\lambda,\ 6/17\lambda,\ \ldots\ldots,\ 16/17\lambda$$

to an accuracy of ±3 deg. A proper arrangement of these 16 cables provides possibilities to measure at the following scan angles (See Ref. 18).

$$\theta_n = \arcsin\left(\frac{n\lambda}{17d}\right) \qquad n = 1,\ 2,\ 3,\ 4,\ 5$$

e.g. at $\theta \approx 5$ deg, 10 deg, 15 deg, 20 deg and 25 deg. Results of measurements of the active impedance for these scan angles are shown in Sec. 6.3.

Radiation patterns: The measurements are shown in Sec. 6.3. The measured and computed patterns does not coincide well for directions outside the main beam. The reason is mainly measurement errors because of reflections from unwanted objects near to the antenna. The pattern of main interest, however, is the beam illuminating the reflector, e.g. within ±50 deg from the main direction.

6. OPTIMIZED FEED DESIGN USING BEAM MATCHING RODS.

Reference is made to the computer analysis in Chapter 4. Crossed dipoles over ground plane give a highly efficient illumination of the reflector for the transverse polarization. The longitudinal polarization, however, has too broad a beam pattern in the yz plane. But it is possible to form this pattern to give a very high aperture efficiency, using two beam matching rods. The proposed positions of the rods are shown in Fig. 6.1.

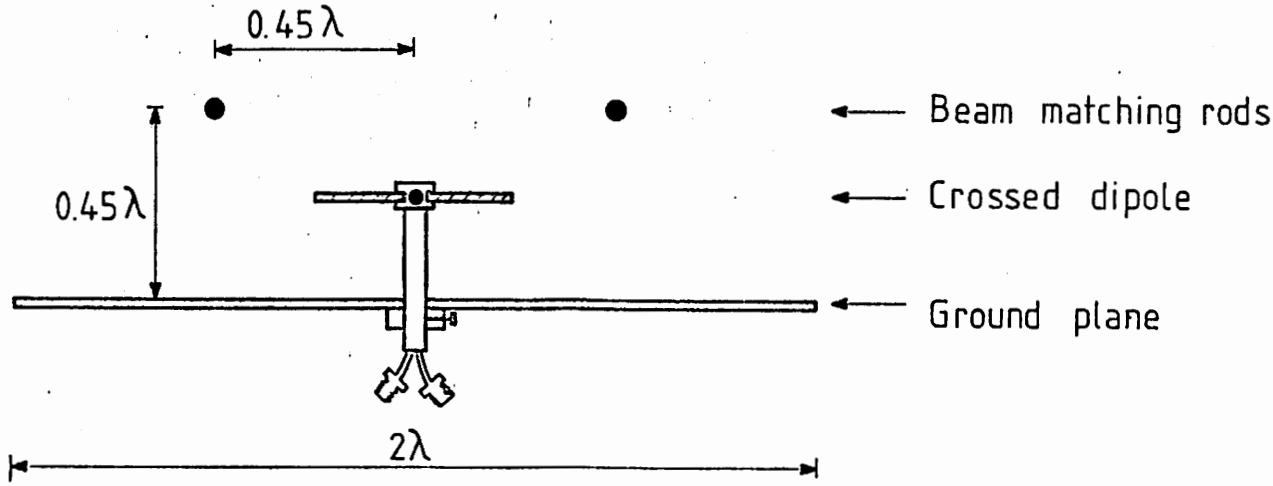

Fig. 6.1. Cross section view of proposed feed design.

Fig. 6.2 shows how the computed beam pattern in the cross section plane is formed to be almost equal to the pattern of the transverse polarization, which is not influenced by the rods. The patterns may have been matched even better with a slightly different position of the rods. But in order to maximize the aperture efficiency for circular polarization, the positions of rods yielding the highest aperture efficiency were used, although there is a small cross polar component. The aperture efficiency for circular polarization, defined by Eq. (2.1), and the cross polarization are shown in Fig. 6.3 and 6.4 respectively, both with and without beam matching rods. The pointing direction of the feed is chosen as the one that maximizes the aperture efficiency. See Fig. 6.5. The aperture efficiency has increased from 0.823 to 0.89, e.g. with more than 8%, when beam matching rods are used and F/D = 0.45.

The computations in Chapter 4 show that a corner reflector (with corner angle less than 180 deg) cannot give the same high aperture efficiency, mainly because of the "bad" radiation pattern of the

transverse polarization. Therefore, the proposed feed design in Fig. 6.1 is the one of the evaluated designs (e.g. general corner reflectors and using two beam matching rods), that yields the highest aperture efficiency for circular polarization. The two beam matching rods act in a way like a polarization sensitive corner reflector.

The height of the dipoles over ground is taken to be h = 0.25λ, to allow a common balun design with no shielding tube around it. Although the impedance variations with scan angle may be smaller with a lower height. (See Sec. 4.3).

The aperture efficiency has a maximum for F/D = 0.45. The best choice from mechanical considerations may be slightly greater, because the longer the focal length, the more effective use is made of the reflector area. The reason is that the length S of the parabolic curve in the cross section plane becomes more equal to the aperture width D when F increases. A cross section reflector illumination efficiency η^r_{circ} may be defined as the cross section aperture efficiency η^c_{circ} divided by the curve length relative to the aperture width, S/D. Thus

$$\eta^r_{circ} = \frac{\eta^c_{circ} D}{S}$$

This efficiency has its maximum for a higher F/D than η^c_{circ}. It gives the optimum F/D ratio for a given reflector area, while the maximum of η^c_{circ} gives the optimum F/D ratio for a given aperture area. η^r_{circ} is shown in Fig. 6.6 for circular polarization, with and without beam matching rods. The best choice of F/D ratio is a question of price balance between the reflector and reflector backing structure and the feeder bridge support towers. The spillover increases, and the near sidelobes increase because of more uniform aperture illumination, when F/D increases. For the EISCAT VHF cylinder antenna it was more natural to regard the aperture width as a fixed parameter rather than the reflector curve length at the time when the feed design was completed. Therefore, F/D = 0.45 was chosen. An extra offsetting E = 1.5 m of the feed will reduce the geometrical feed blockage of the aperture to zero.

The proposed parameters of the feed and the reflector, believed to be very close to the optimum choice, are summarized below.

Feed:	Width of ground plane	$2a = 2.00\lambda$
	Height of dipoles	$h = 0.25\lambda$
	Height of beam matching rods	$y_1 = 0.45\lambda$
	Spacing between beam matching rods	$2x_1 = 0.9\ \lambda$
	Diameter of beam matching rods	0.025λ
Reflector:	Aperture width	$D = 40.0$ m
	Focal length	$F = 18.0$ m
	Extra offsetting of feed	$E = 1.5$ m
	Pointing direction of feed*	$\psi_0 = 54$ deg
	Subtended angle	$\psi_2 - \psi_1 = 91.4$ deg

* The optimum pointing direction of the feed is measured from the negative z-axis (Fig. 1.2). It is greater than given in Fig. 6.5 because of the extra offset E. The offset E = 1.5 m gives $\psi_1 = 4.7$ deg.

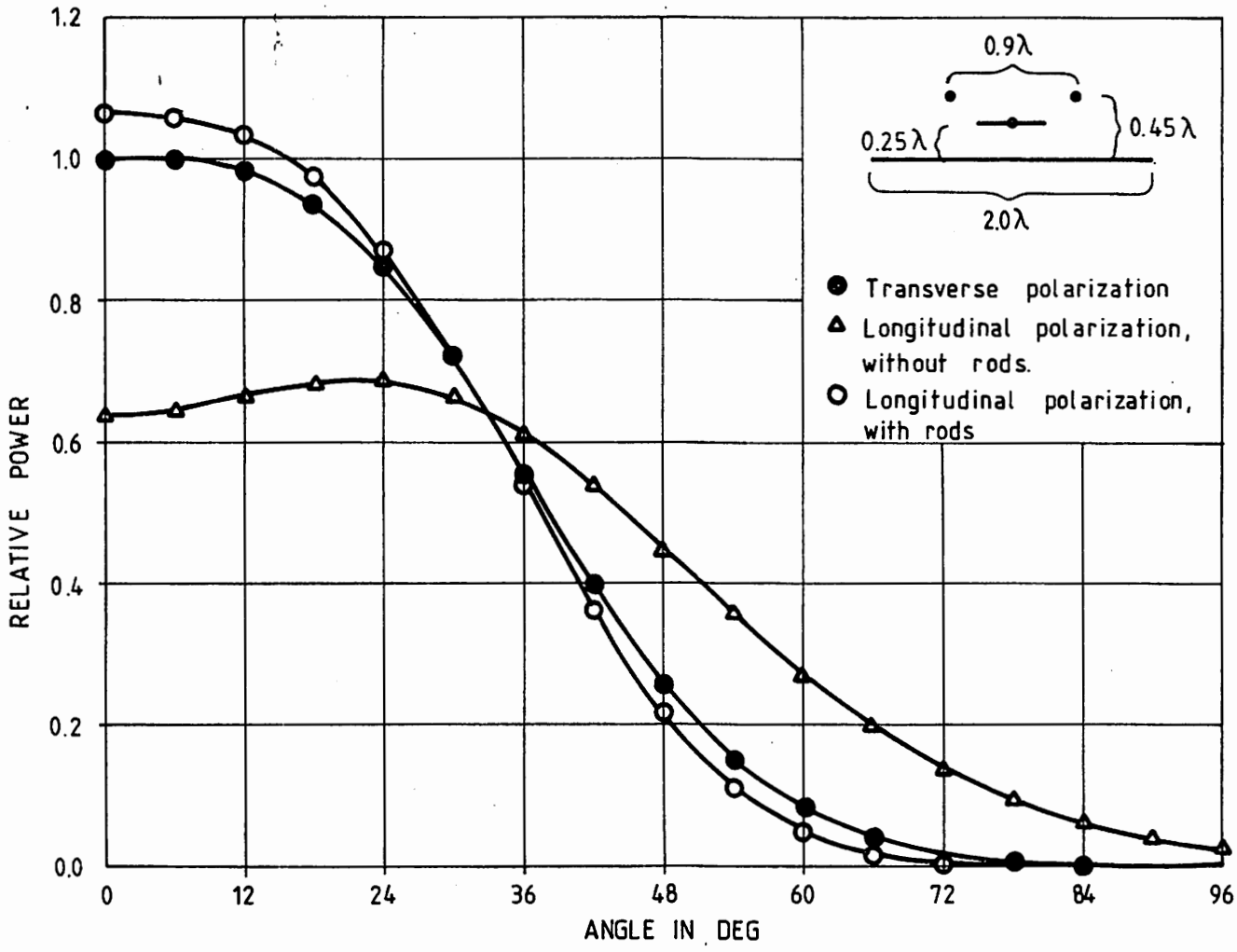

Fig. 6.2. Computed beam patterns in the cross section plane.
All patterns are normalized to a cross section directivity of 6.64 dB.
The transverse polarization is computed with GTD without rods.
The longitudinal polarization without rods is computed with GTD.
The longitudinal polarization with rods is computed with moment methods.

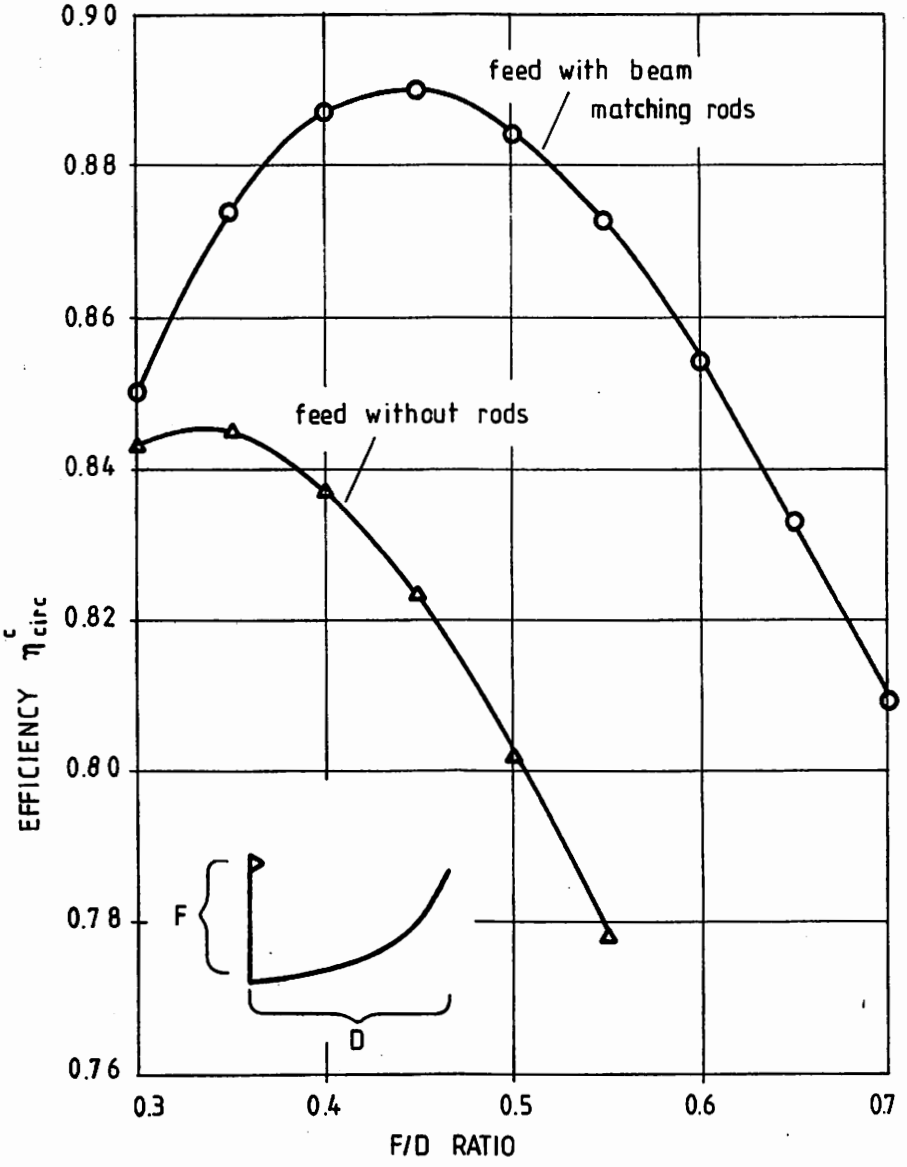

Fig. 6.3. Cross section aperture efficiency for circular polarization η^c_{circ}, based on the beam patterns in Fig. 6.2.

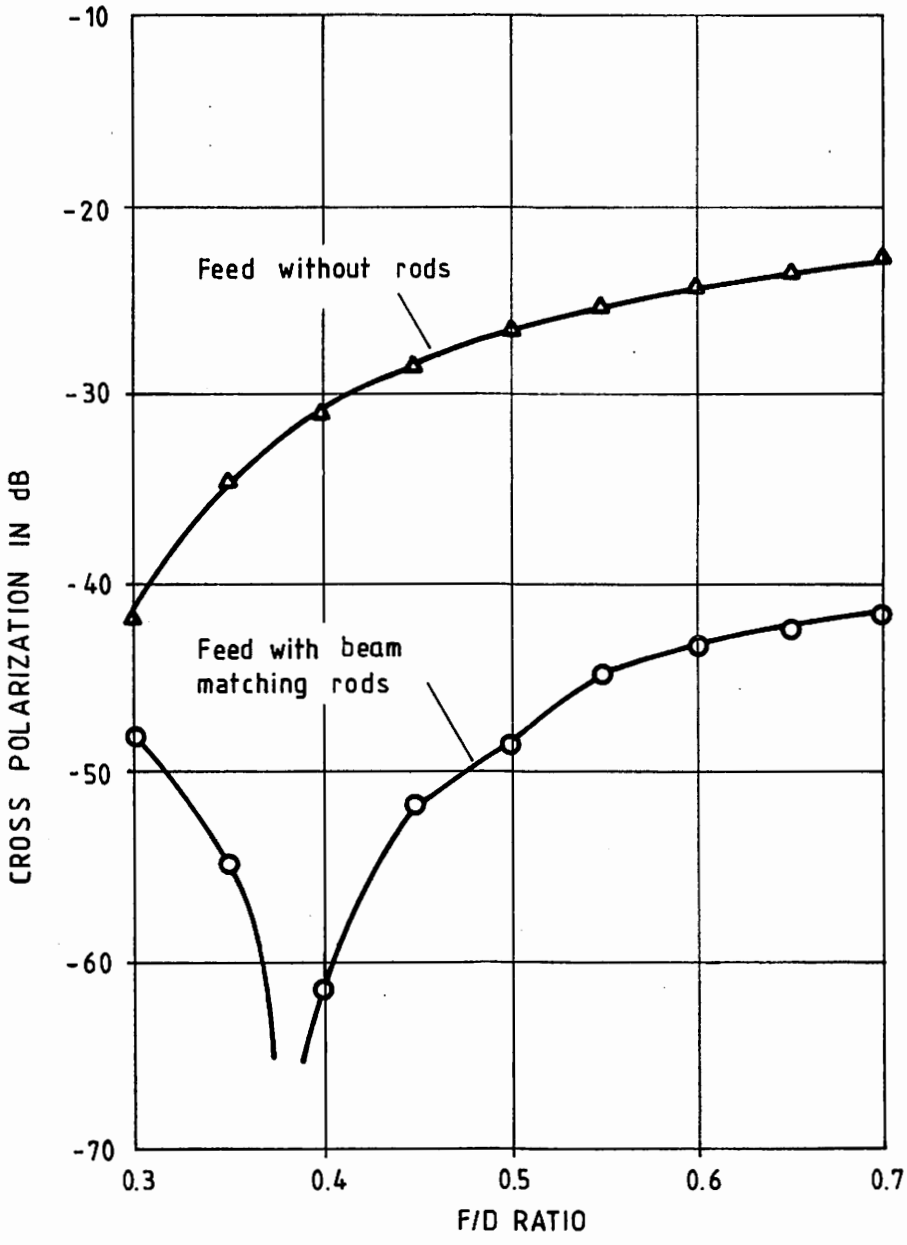

Fig. 6.4. Cross polarization on axis relative to the wanted circular polarization based on the beam patterns in Fig. 6.2.

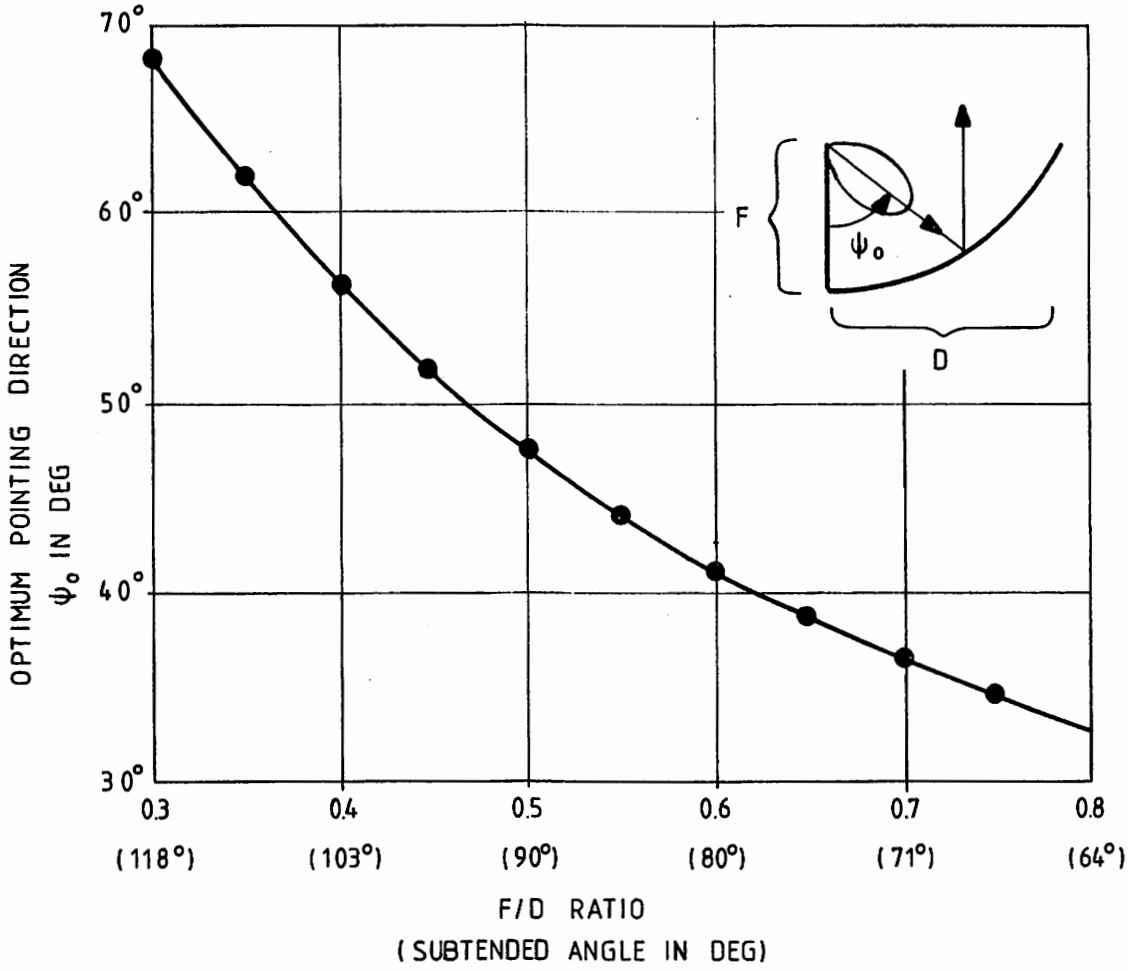

Fig. 6.5. The pointing direction ψ_0 of the feed, that maximizes the aperture efficiency. The feed is the proposed feed design with beam matching rods.

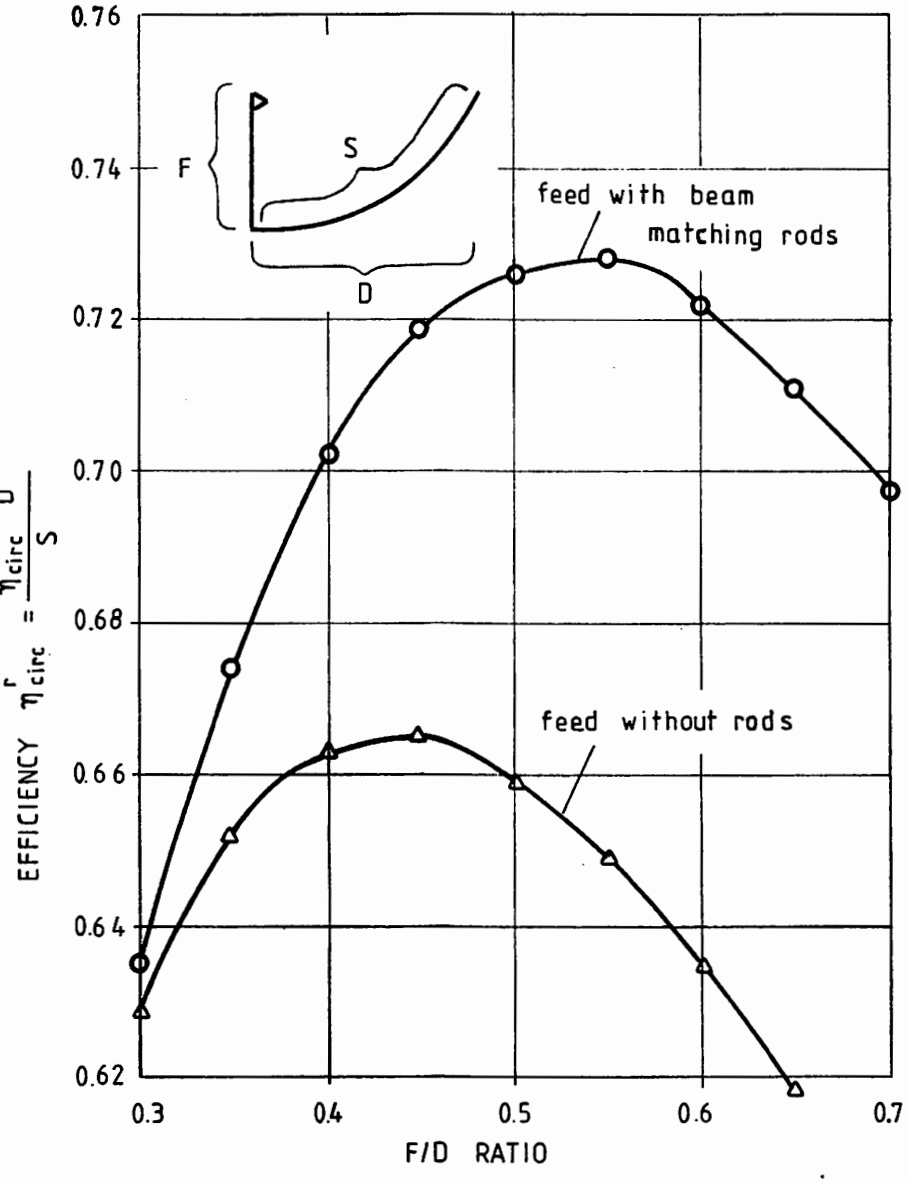

Fig. 6.6. Cross section reflector illumination efficiency η^r_{circ} for circular polarization, based on the beam patterns in Fig. 6.2.

6.1. Additional Impedance Matching Rods.

The impedance of the longitudinal and transverse dipoles will be different, due to the different mutual impedances between colinear and parallel dipoles. Therefore, separate matching of each polarization is necessary. One method is to use internal matching such as impedance transformers in the cable feeding the dipole. Here I propose another technique, using impedance matching rods.

The scale model in Fig. 5.1 and 5.2 did not allow internal matching of the two polarization. It was, however, possible to match both polarizations properly by using two extra rods parallel to the linear array axis in metallic contact with the shielding tube around the balun, as shown in Fig. 6.7. The rods act as a displaced ground plane for the longitudinal polarization, whereas they have no influence on the impedance and beam pattern of the transverse polarization. They have also insignificant influence on the beam pattern of the longitudinal polarization, as shown in Fig. 6.8. Comparison with Fig. 6.2 shows that it becomes in fact slightly more equal to the pattern of the transverse polarization.

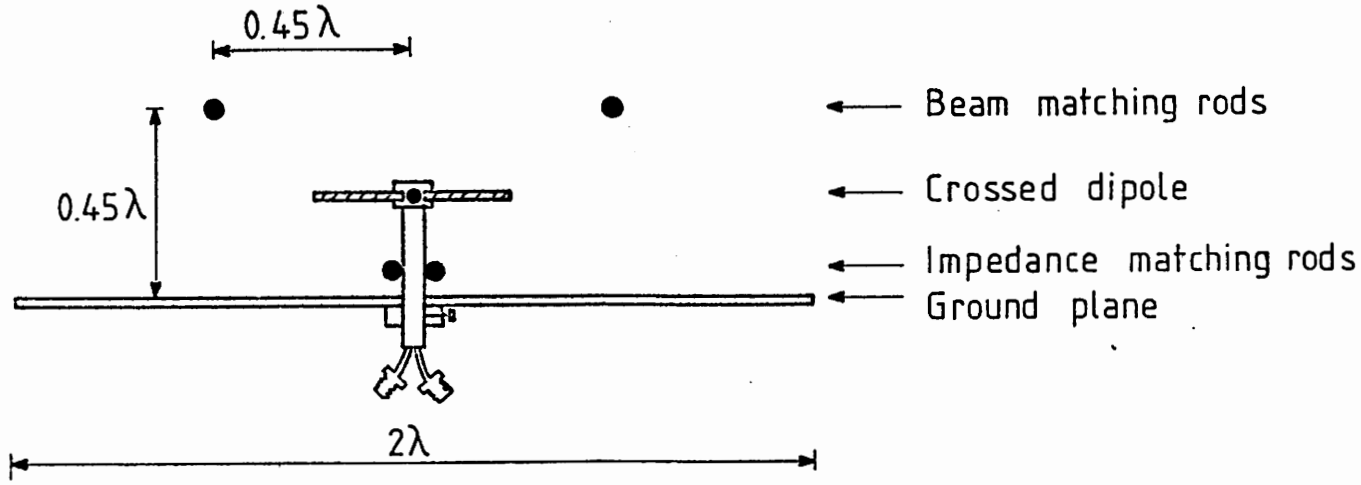

Fig. 6.7. Cross section view of feed with additional impedance matching rods.

The position of the phase center changes, but is still within the limits discussed in Sec. 2.3.

The matching procedure in the scale model was as follows. The transverse dipoles were matched by adjusting the height over ground plane and the length of the dipole arms. (See Fig. 4.3). Then the longitudinal dipoles were matched by adjusting the height of the impedance matching rods and the length of the dipole arms. A match at some offset scan angle was preferred, according to the discussion in Sec. 2.5. The parameters for properly matched dipoles in the scale model were:

Transverse polarization:	Length of dipole arms	$\ell = 0.214\lambda$
	Height of dipole over ground	$h = 0.25\lambda$
Longitudinal polarization:	Length of dipole arms	$\ell = 0.215\lambda$
	Height of extra rods	$y_2 = 0.1\lambda$

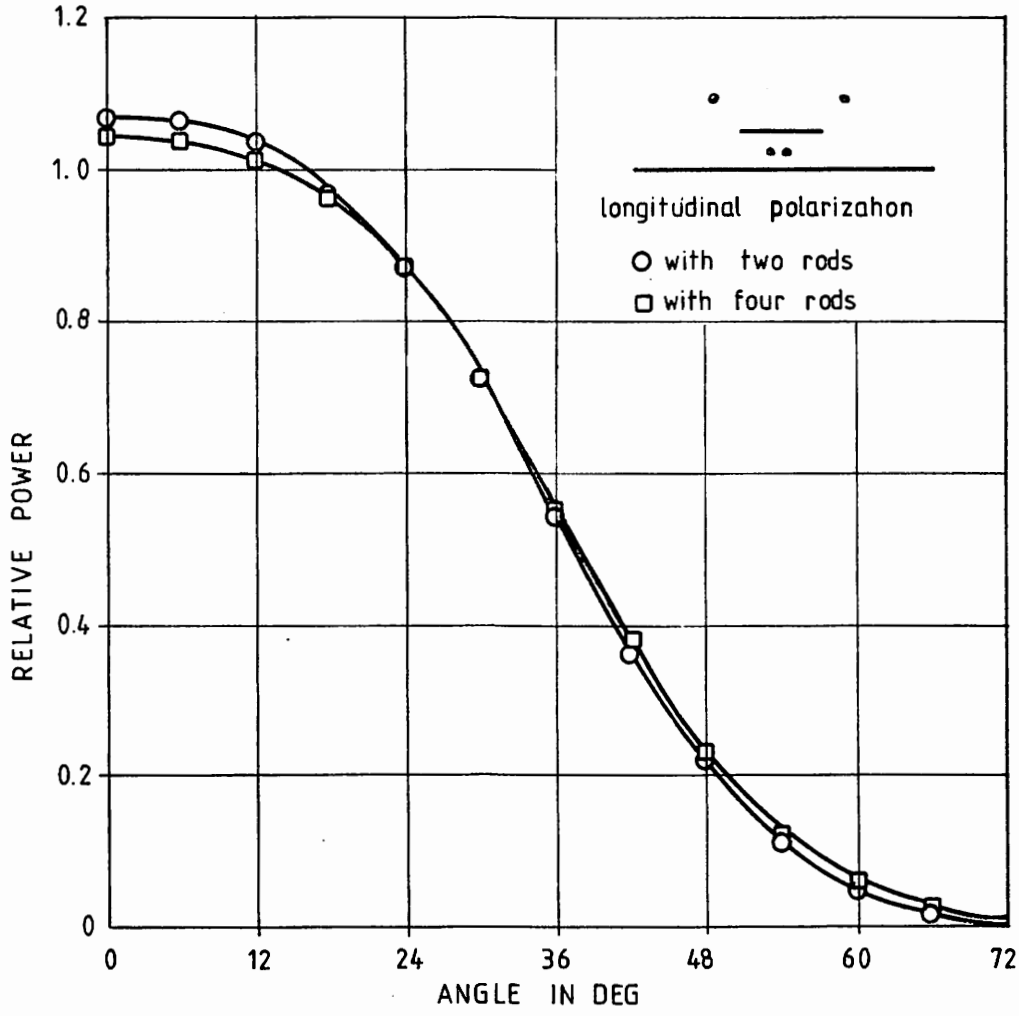

Fig. 6.8. Comparison between computed beam patterns without and with impedance matching rods. The patterns are normalized to a cross section directivity of 6.64 dB.

6.2. Scale Model Measurements.

The results of measurements on the scale model in Fig. 5.2 are presented here. All pattern measurements and impedance measurements in the figures below are done with beam matching rods and impedance matching rods, placed as shown in Fig. 6.7.

The measured beam patterns of the transverse polarization were not influenced by the beam matching rods and impedance matching rods, except for a filling out of the deep nulls in the pattern (-45 dB). The measured and computed patterns for the transverse polarization are compared in Fig. 6.9. The computations made with GTD and moment methods were almost equal (see Sec. 3.4), in fact they differed by less than 0.1 dB within ±78 deg from axis for a sufficient number of subdivisions of the ground plane in the moment method program. The measured and computed patterns coincide well within the main beam, except for some small shoulders in the measured pattern. The reason for their existance is believed to be the finite length of the scale model, causing diffraction from the ground plane edges at both ends of the dipole array. This diffraction is much greater for the transverse polarization than for the longitudinal polarization because the transverse dipoles are parallel to these edges.

The measured and computed patterns (using moment methods) of the longitudinal polarization are shown in Fig. 6.10. They agree remarkably well within the main beam. The same agreement is also present without the impedance matching rods, but the diagram is slightly narrower, see Fig. 6.8.

Neither the patterns in Fig. 6.9 nor in Fig. 6.10 coincide well outside the main beam, e.g. more than 90 deg from axis. That is caused by measurement errors due to reflections from nearby objects. It is seen how the measured pattern oscillates about the computed pattern, typical for reflections. The difference is also due to the mounting tower and feeder cables on the rear side of the scale model.

The measured patterns in the cross section plane are compared in Fig. 6.11. They correspond to the comparison of the computed patterns in Fig. 6.2.

Impedances measured on the scale model are shown in Fig. 6.12 and 6.13. They are active impedances, measured with all dipoles excited with the same input power (see Fig. 5.3), and may be compared with the computed impedances shown in Fig. 6.14 and 6.15. The computations were made with the program described in Sec. 3.3 for a linear array of 7 crossed dipoles over an infinite ground plane, without any beam matching or impedance matching rods. The rods have no influence on the impedance of the transverse dipoles. The impedances along the line is for this polarization computed with the same height and length that the actual dipoles have, see Sec. 6.1, and transformed through a lossless network that simulates the balun design, see Sec. 5.1. Compare Fig. 6.12a with Fig. 6.14a and Fig. 6.13a with Fig. 6.15a, and see that the principal behaviour is very similar. The disagreement is due to the measurement accuracy (see Sec. 5.3) and the mechanical accuracy in the construction of the dipole (see Fig. 5.1). These errors give typical measured impedances as in Fig. 6.12a where the impdances of dipole 1 and 7 (2 and 6, and 3 and 5) should have been equal. Other reasons are the finite size of the ground plane, but that has only small influence on the impedance, and the approximation that is used in the computer program described in Sec. 3.3. This approximation has the greatest effect on the end dipoles. The measured impedance on the transverse end dipole differs therefore more from the computed impedance than the impedance on the center dipole do.

The measured results for the longitudinal polarization is also shown in Fig. 6.12 and 6.13. They are not directly comparable to the computed results because the rods greatly influences the impedance. The computed results are, therefore, done for a dipole length $\ell = 0.213$ and height $h = 0.19\lambda$ which turned out to give an impedance near to 50 ohm. The computations were only done to see whether the main variations were the same with and without rods. It is seen from a comparison of Fig. 6.13b and 6.15b that the impedance variations with scan angle is less with rods (measured) than without rods (computed). Thus, the beam matching rods had a beneficial influence on the mutual coupling. Impedance as a function of frequency is shown in Fig. 6.16.

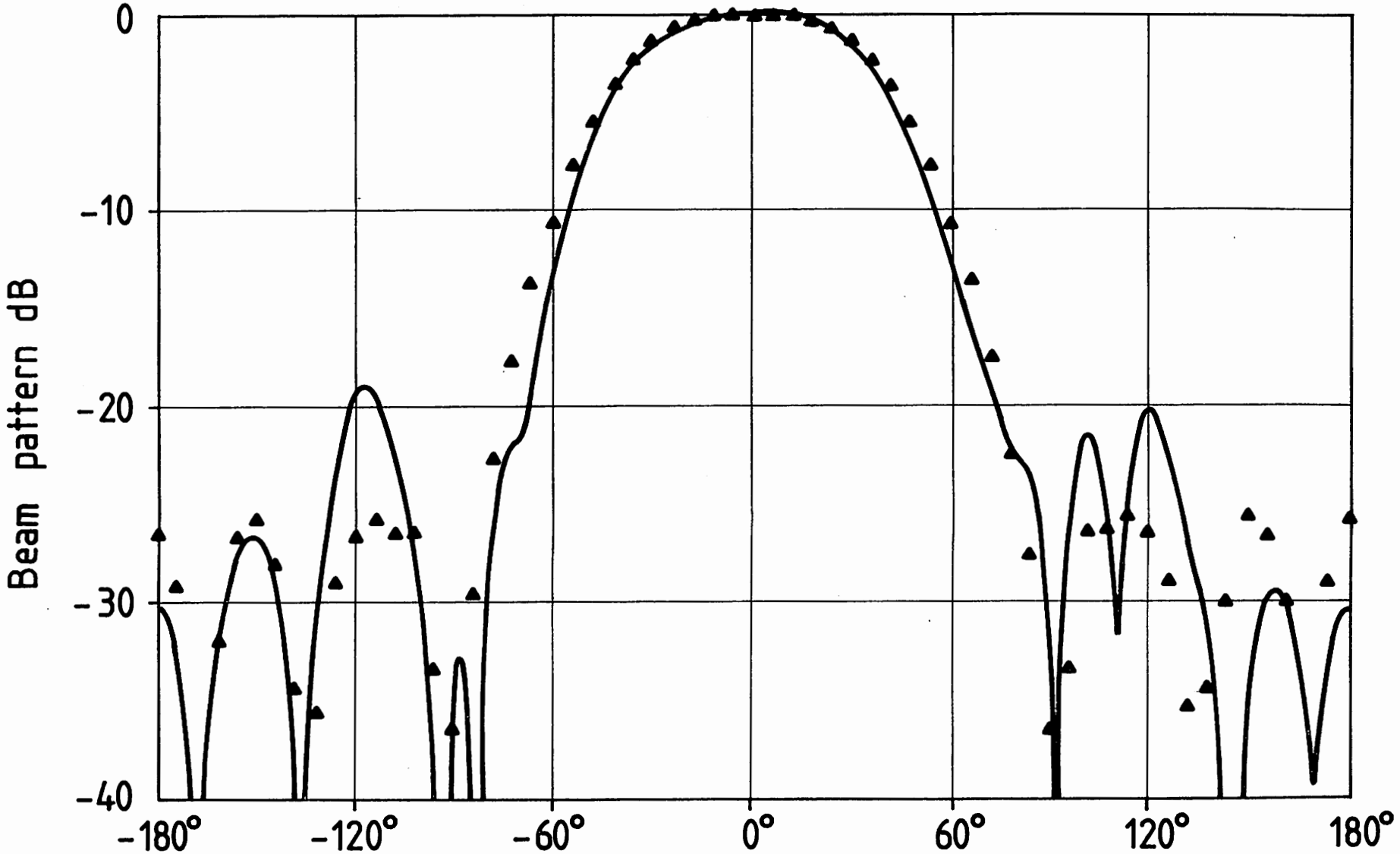

Fig. 6.9. Measured cross section beam pattern (with rods) of proposed feed compared with computed pattern (without rods). Transverse polarization.
See also Fig. 6.9a (next page) which shows the same pattern down to -10dB only.
—— Measured ▲ Computed with GTD

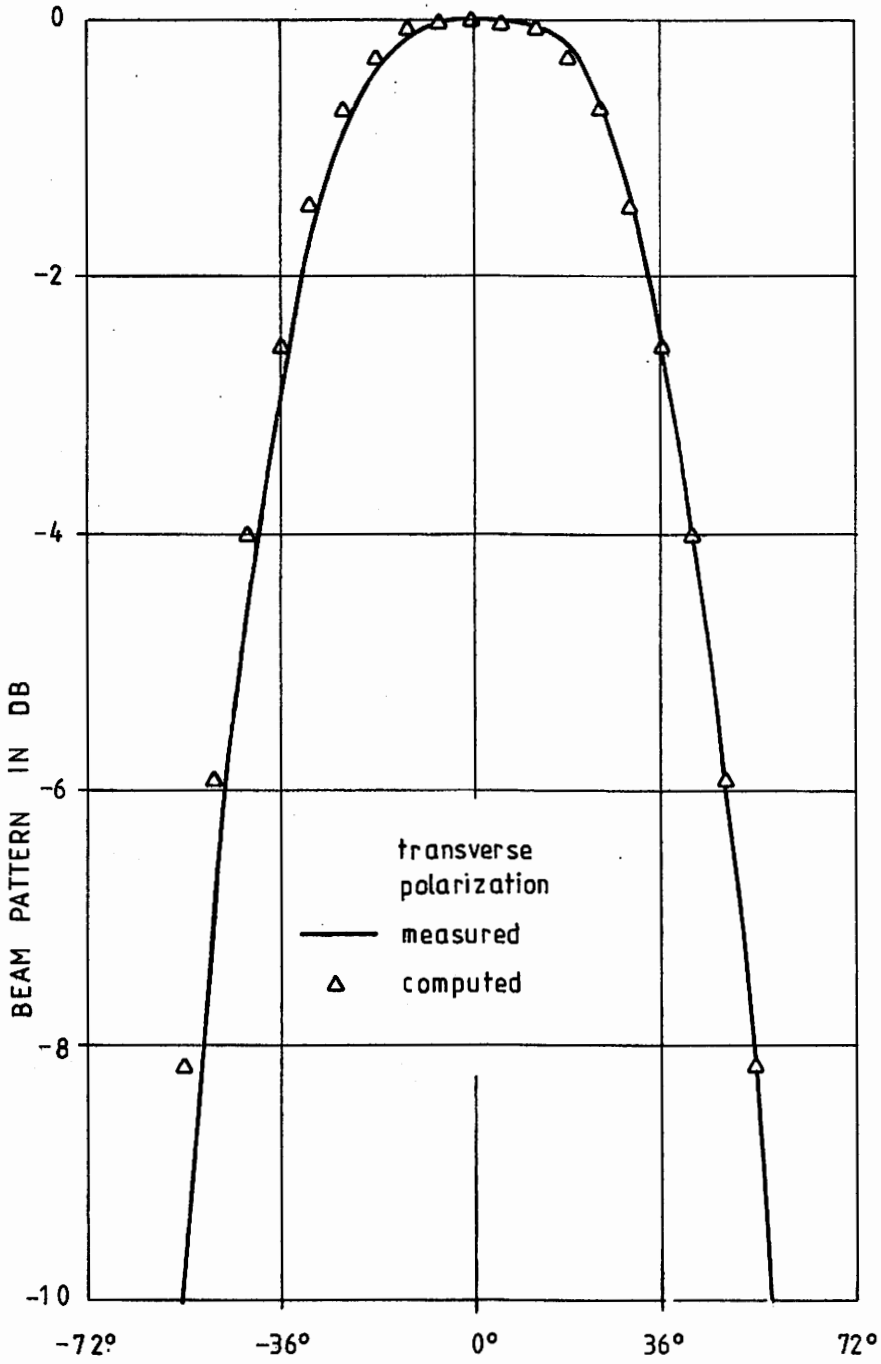
0
-2
-4
-6
-8
-10
BEAM PATTERN IN DB
-72°
-36°
0°
36°
72°
transverse
polarization
measured
computed

Fig. 6.9a.

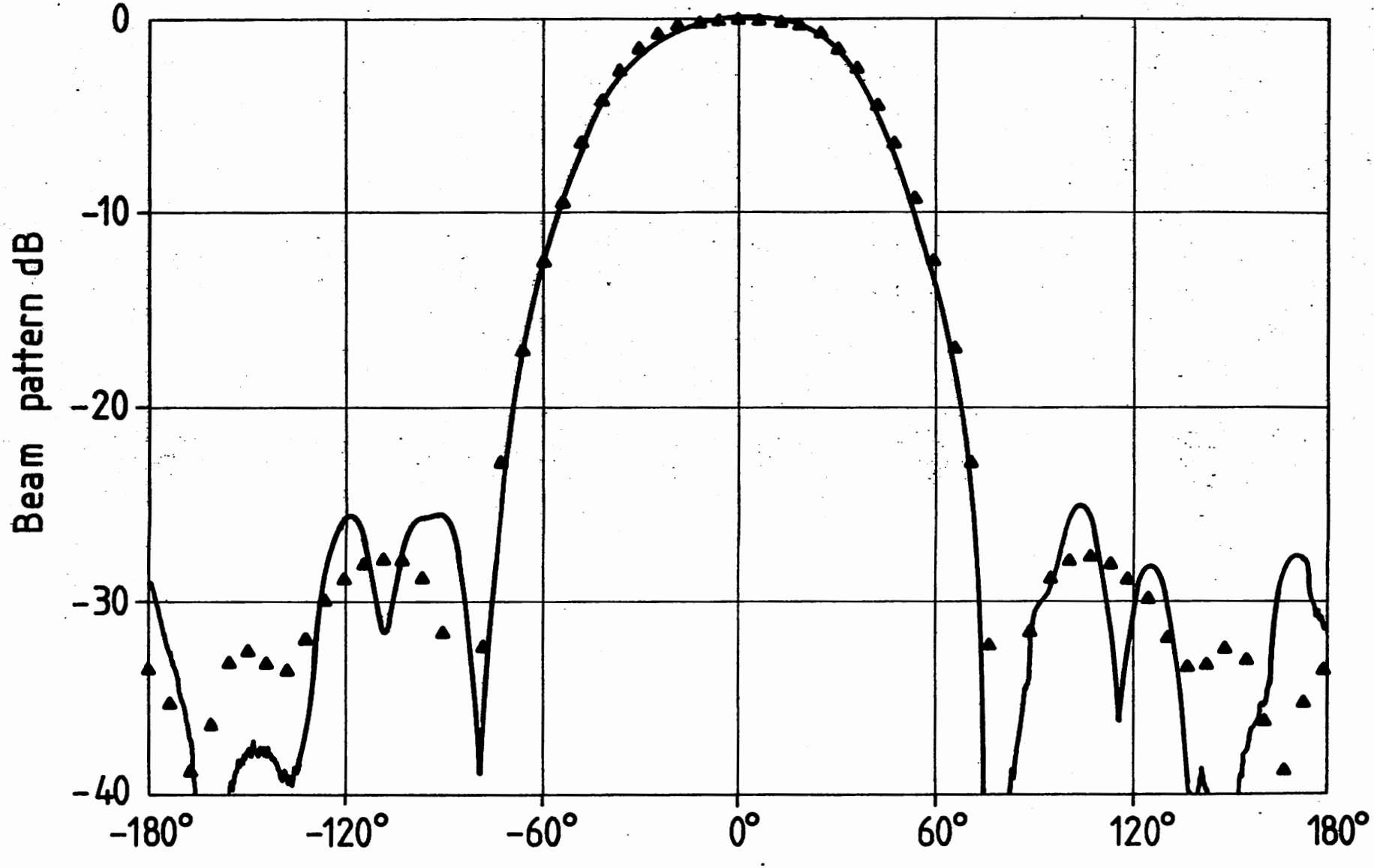

Fig. 6.10. Cross section beam patterns of proposed feed with beam matching rods and impedance matching rods. Longitudinal polarization.

See also Fig. 6.10a (next page) which shows the same pattern down to -10 dB.

——— Measured ▲ Computed with moment methods.

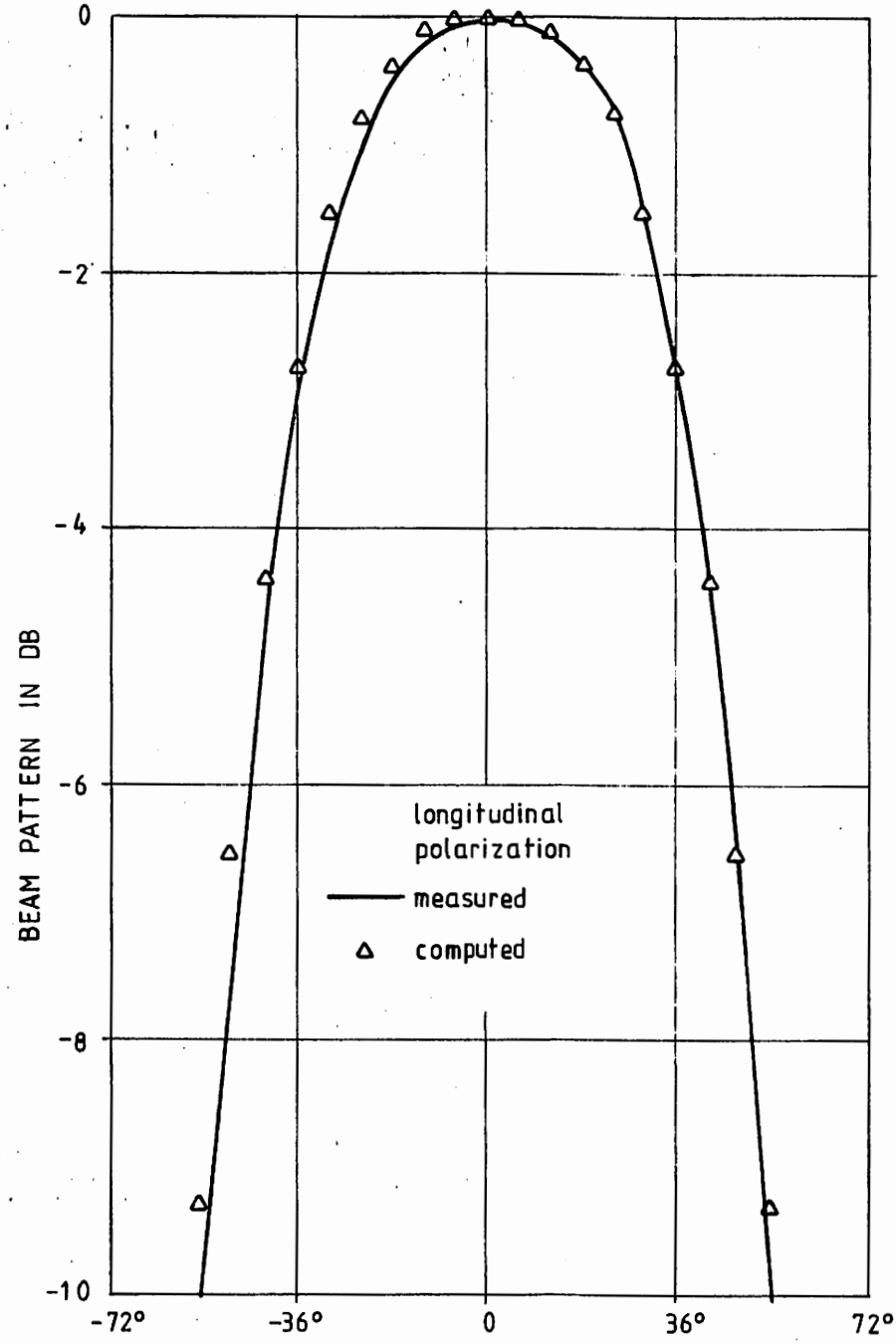
0
-2
-4
-6
-8
-10
BEAM PATTERN IN DB
-72°
-36°
0
36°
72°
longitudinal
polarization
measured
computed

Fig. 6.10a.

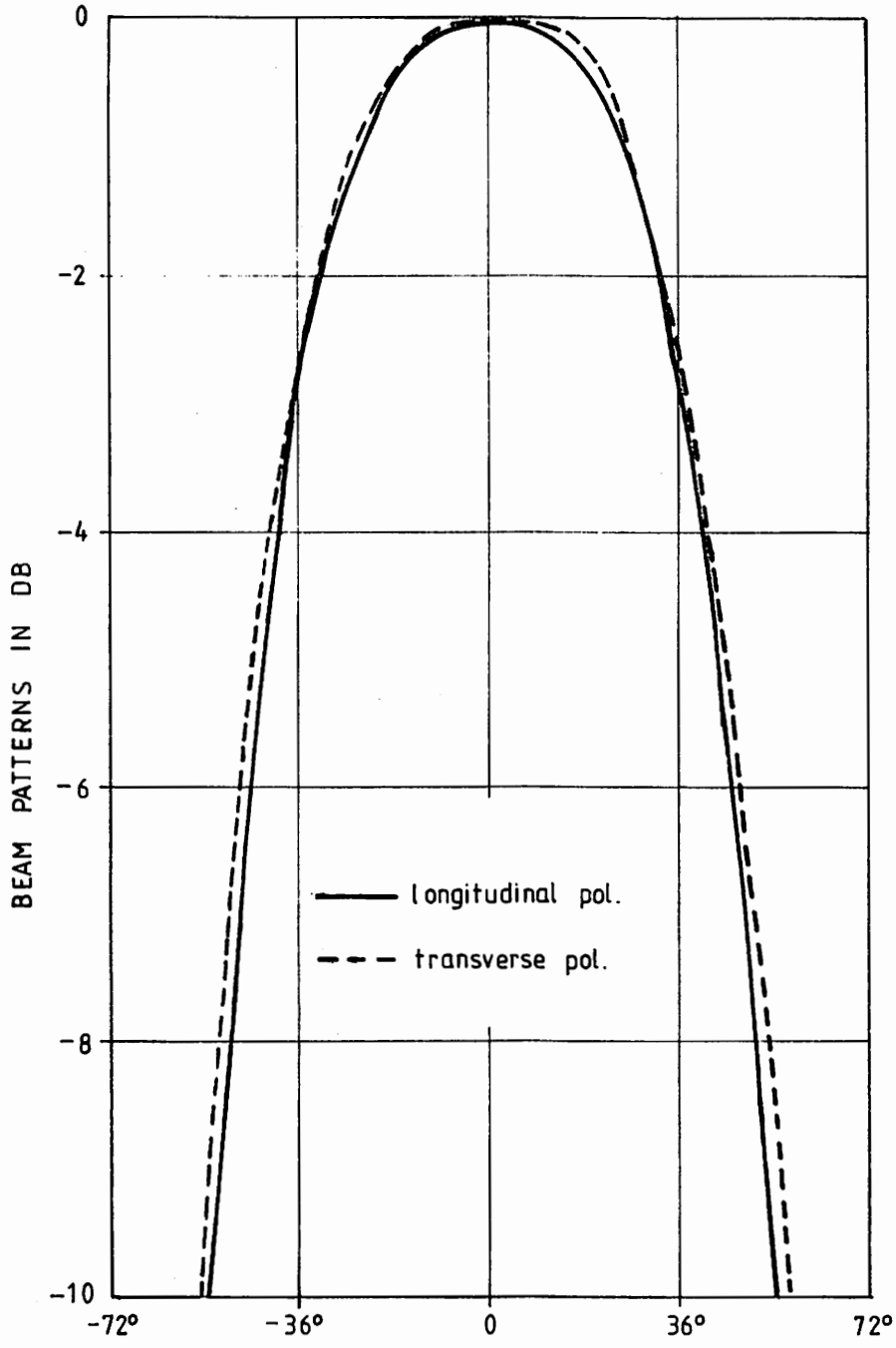

Fig. 6.11. Comparison of measured beam patterns.
Feed design with 4 rods.

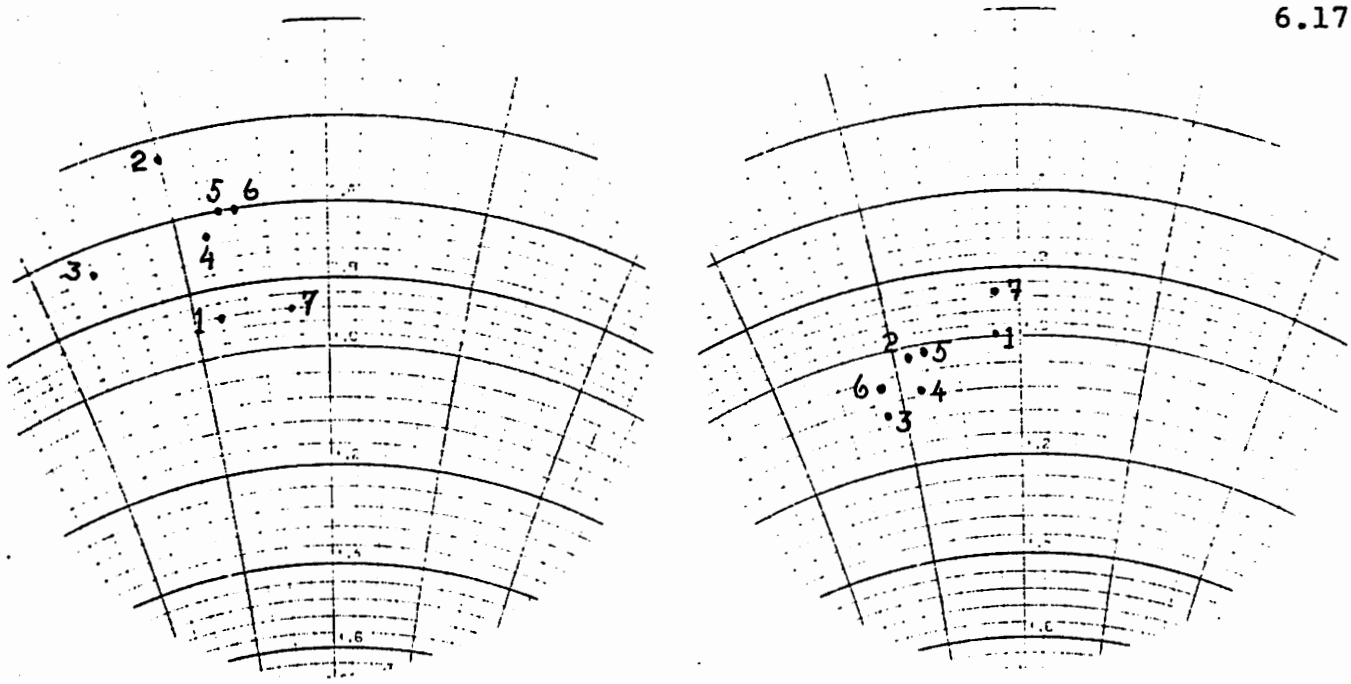

a) Transverse polarization b) Longitudinal polarization

Fig. 6.12. Measured variations in the active impedance along the linear array. The numbering of the dipoles are shown in Fig. 5.2. Feed design with 4 rods. No phase steering, e.g. scan angle θ=0 deg.

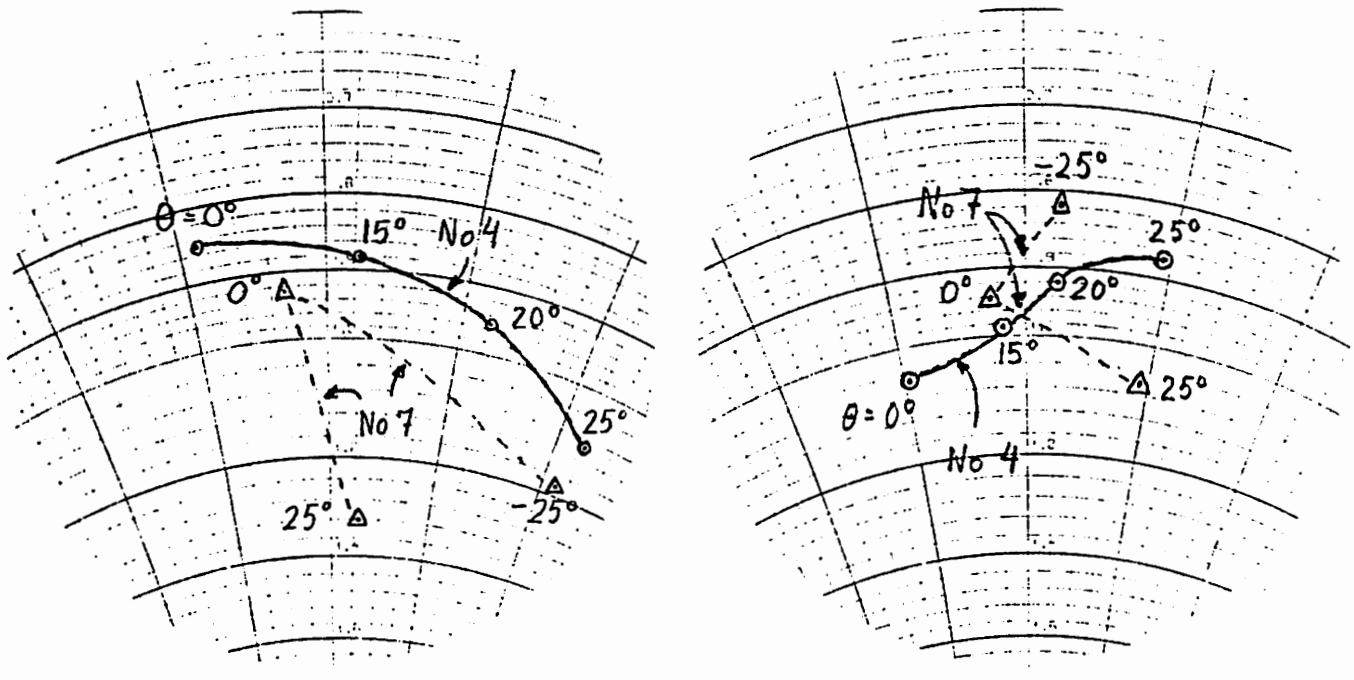

a) Transverse polarization b) Longitudinal polarization

Fig. 6.13. Measured variations in the active impedances as a function of scan angle θ on center dipole (⊙), e.g. dipole No. 4, and on end dipole (△), e.g. No. 7. Feed design with 4 rods. Dipole No. 7 is only measured for θ=0°, 25° and -25°.

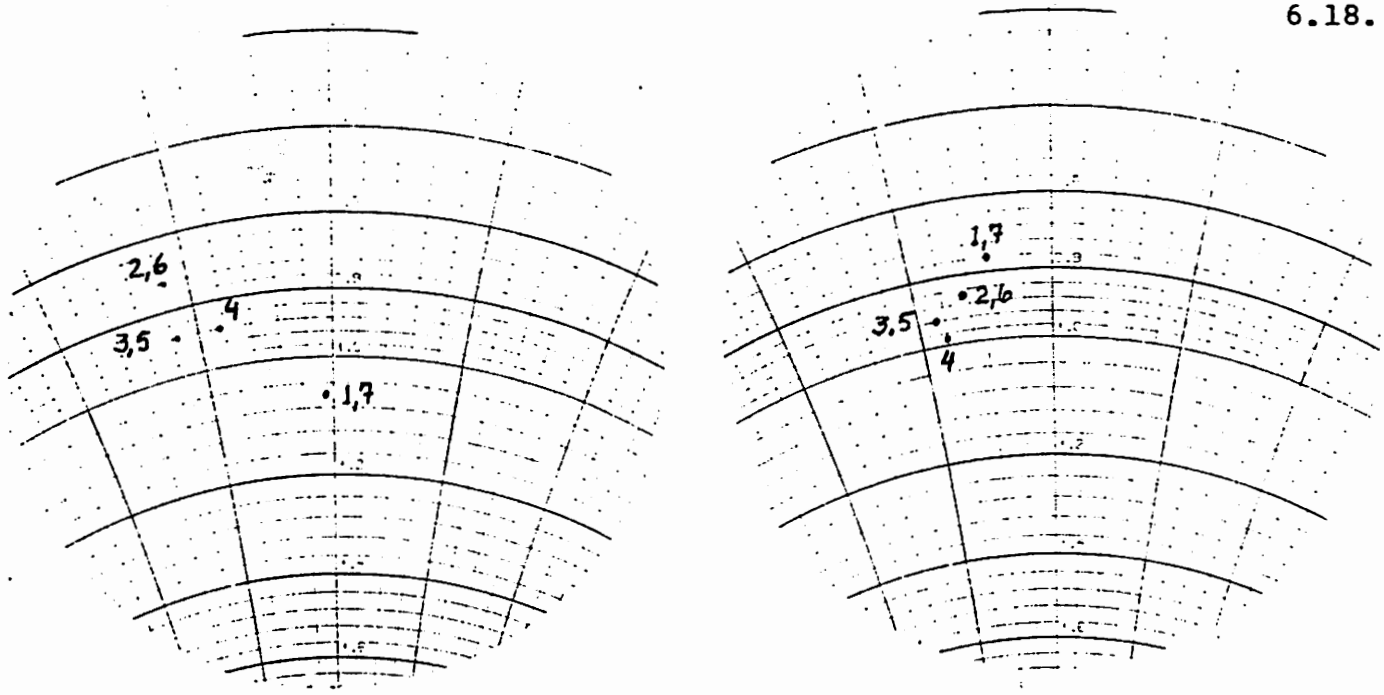

a) Transverse polarization b) Longitudinal polarization

Fig. 6.14. Computed variations in the active impedance along an array of crossed dipoles without rods. 7 elements that are numbered successively from one end to the other. Scan angle $\theta=0^{\circ}$. Program described in Chapter 3.3.

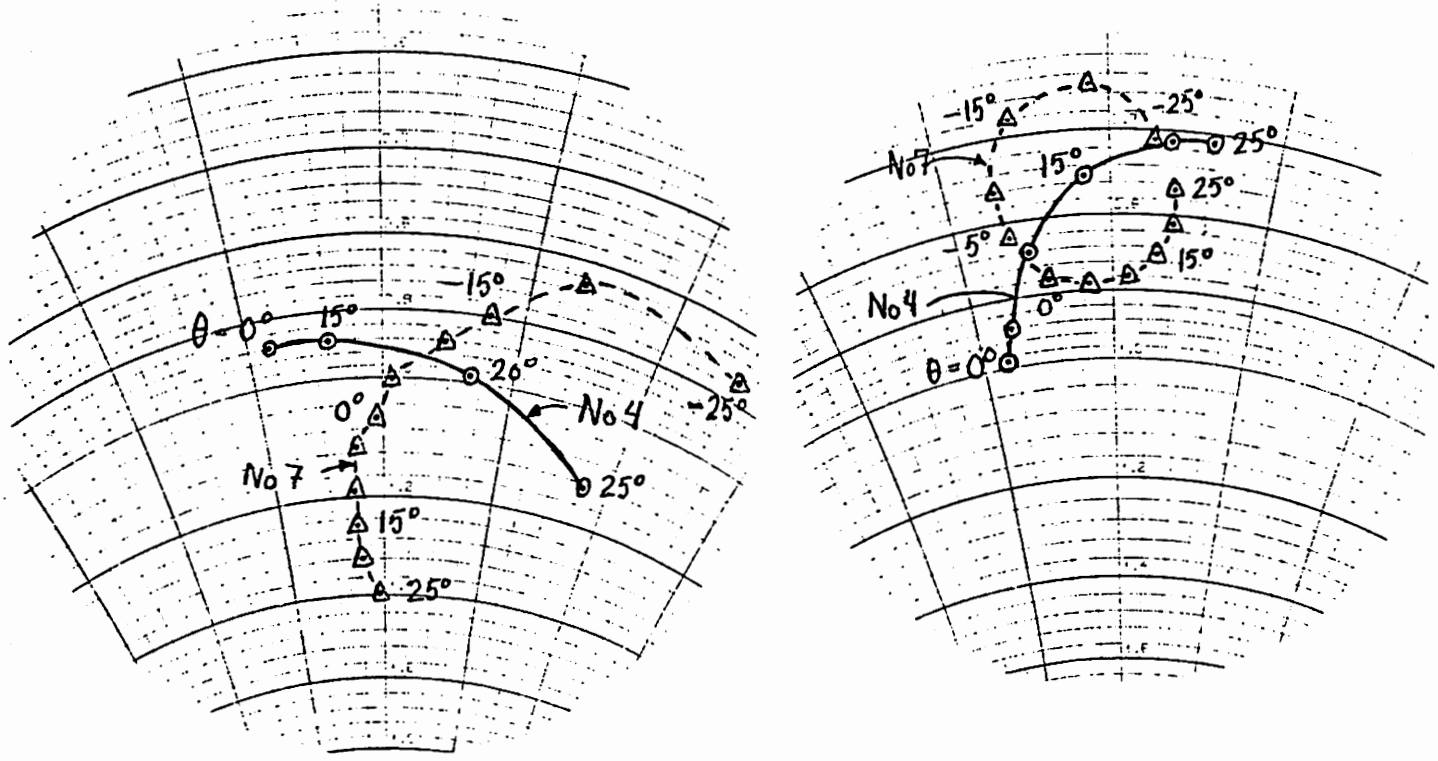

a) Transverse polarization b) Longitudinal polarization

Fig. 6.15. Computed variations in active impedance as a function of scan angle θ, on center dipole (⊙), e.g. dipole No. 4, and on end dipole (△), e.g. No. 7. Crossed dipoles without rods. Program in Chapter 3.3.

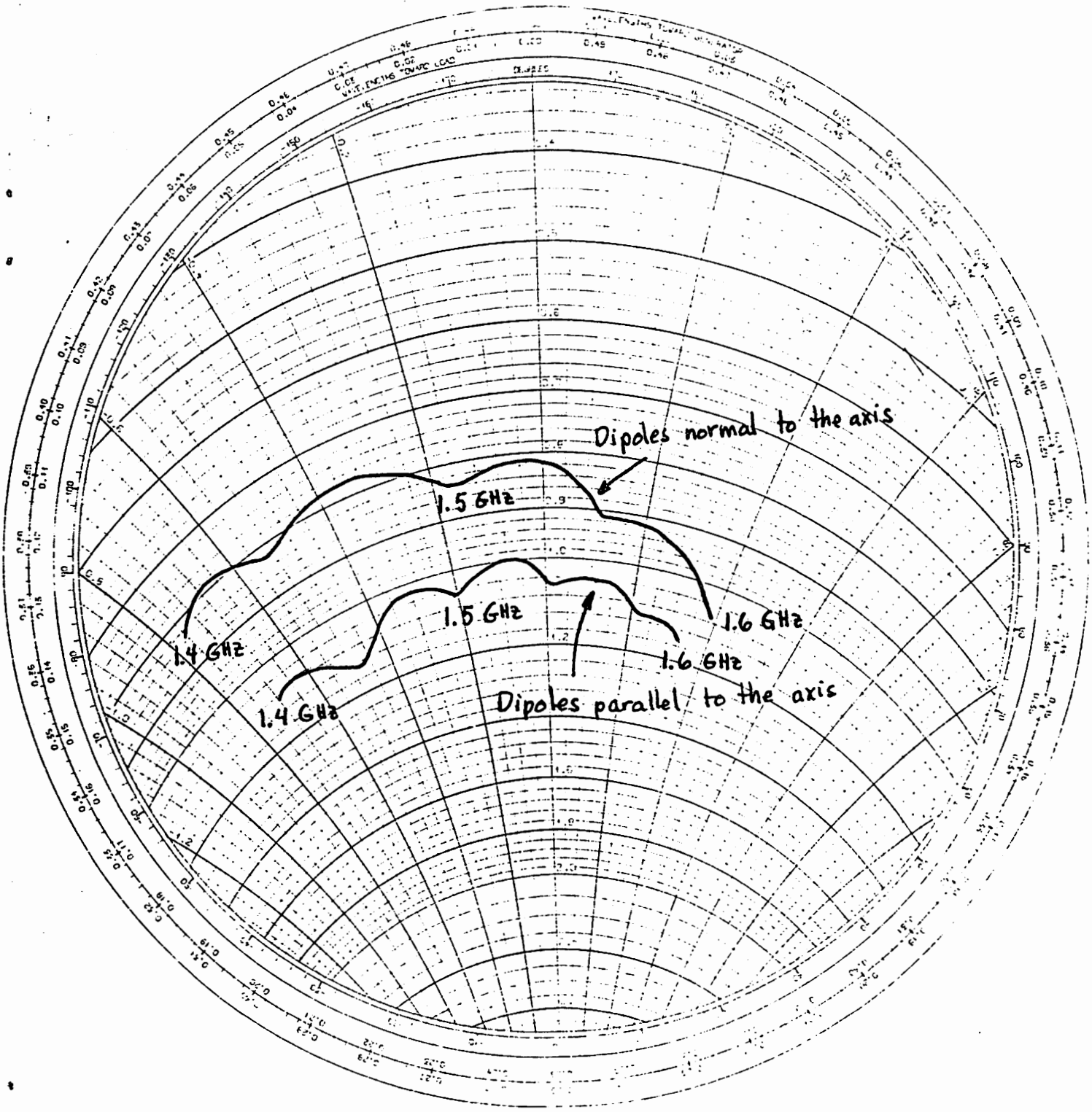

Fig. 6.16. Measured impedance variations with frequency on the scale model. Scan angle θ=0. Center dipole.

6.3. Performance of Feed.

A list of performance data is given at the end of this section. Fig. 6.17 shows the power dissipation in the dummy loads calculated from Eq. (2.36), using the measured impedances in Fig. 6.13 for the center dipole. Fig. 6.17 also shows the relative error signal caused by reflections from the dipoles, calculated from the measured impedances on the center dipole and Eq. (2.39). The error signal, e.g. the reflection coefficient referred to the input of the hybrids (see Fig. 2.3) is high for small scan angles because the reflections then add almost in phase on the input of the hybrid. It is clear from Fig. 6.17 that a better match at $\theta=0$, resulting in a higher mismatch at $\theta=25^{\circ}$, is preferred if the maximum error signal is to be reduced to less than 0.1. The power dissipation will still be less than 600W.

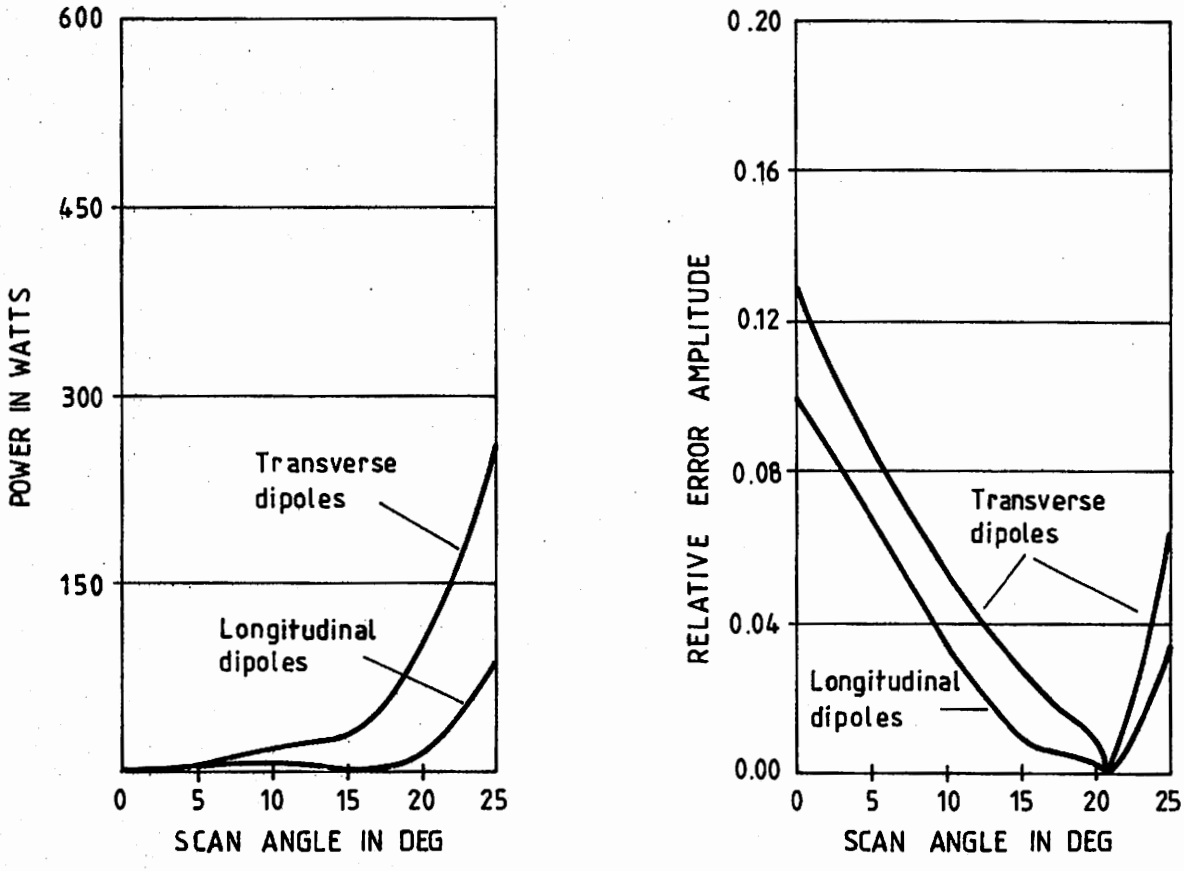

Fig. 6.17. Power dissipation in dummy loads and the reflections referred to the input of the hybrid (375 kW average power).

A study of the table on the next page makes it clear that the feed satisfies the requirements discussed in Chapter 2. There are two exceptions. The spillover lobes will be higher than the design goal. A reduction is not possible without decreasing the aperture efficiency severely. The mismatch of the dipole impedance at $\theta=0$ is slightly too high.

The power dissipation in the dummy loads, Fig. 6.17, may have been less for the transverse polarization if the impedance curve in Fig. 6.13a had passed more nearly through the center of the Smith Chart. The impedance variations may also have been less for the transverse polarization if the dipole height over ground plane were smaller, see Fig. 4.1.

Performance of proposed feed design	C=computed M=measured	Reference	Beam matching rods. Polarization Longitudinal	Beam matching rods. Polarization Transverse	Extra imp. match. rods. Longitudinal polarization
Aperture efficiency (spillover included)	C	Eq. (2.3)	0.901	0.886	0.899
Spillover efficiency	C	Eq. (2.5)	0.938	0.915	0.932
Spillover lobes at -180 deg	C	Eq. (2.21)	-22.7dB	-21.8dB	-22.4dB
Spillover lobes at + 84 deg	C		-20.2dB	-19.7dB	-20.0dB
Cross section directivity of feed	C and M	Eq. (2.22)	6.91dB	6.64dB	6.80dB
Taper at inner reflector edge (-180 deg)	C and M		-6.3 dB	-5.2 dB	-5.9 dB
Taper at outer reflector edge (84 deg)	C and M		-7.3 dB	-6.6 dB	-7.0 dB
Position of phase center over ground plane	C	Sec. 2.3	0.066λ	-0.029λ	0.090λ
R.m.s. phase errors referred to phase center	C	Sec. 2.3	1.38^{o}	1.27^{o}	1.24^{o}
Best position of focal line over ground plane	C	Sec. 2.3	0.02	0.02	0.02
R.m.s. phase errors referred to focal line above	C	Sec. 2.3	2.14^{o}	2.18^{o}	2.8^{o}
Method of computations		Sec. 2.3	MM	GTD half wave dipole	MM
VSWR at broadside, $f = f_0$	M	Fig. 6.13		1.3	1.22
VSWR at 25 deg scan angle	M	Fig. 6.13		1.56	1.28
VSWR at broadside, $f = f_0 - 0.05f_0$	M	Fig. 6.16		2.0	1.8
VSWR at broadside, $f = f_0 + 0.05f_0$	M	Fig. 6.16		1.4	1.4
Coupling between orthogonal dipoles	M			-43dB	

7. CONCLUSION WITH EXPECTED OVER ALL PERFORMANCE.

A feed design for the EISCAT VHF cylinder antenna is proposed. It consists of crossed dipoles over a finite ground plane, and uses beam matching rods to form the beam pattern of the longitudinal polarization. When F/D = 0.45, the aperture efficiency for circular polarization is 8% higher with these rods than without. The optimum dimensions of the feed and the reflector are shown in Chapter 6.

If the proposed feed design is used, the over all performance of the EISCAT VHF cylinder antenna will be as shown in the table below. The performance parameters are given at broadside, e.g. with no phase steering of the line feed, at the center frequency. The expected performance is based on expected data (E) from computations and measurements, and guaranteed data (G) from the antenna manufacturer. The blockage efficiencies are calculated using simple geometrical blockage.

Design goals at center frequency		Eff.	Loss(dB)	
Aperture efficiency (Eq. 2.1) (Spillover included)	Design 1 or 2	0.89	0.506	E
Blockage efficiency, feed	1.5m offset	1.00		E
Blockage efficiency, support towers	0.3m	0.9925	0.033	G
and diagonal beams	30cm beam	0.991	0.039	G
Opening between reflectors	10cm	0.9975	0.011	G
Random surface errors Systematic surface errors (with gravity and wind up to 12m/s)	2cm r.m.s.	0.966	0.150	G
Random dev. of feed line from focal line Systematic dev. of feed line from focal line	2cm r.m.s.	0.966	0.150	G
Random phase errors of line feed	4 deg r.m.s.	0.994	0.025	G
Amplitude balance of line feed	0.5 dB	0.995	0.020	G
Phase errors across the cross section feed pattern with focal line as ref.	3 deg r.m.s.	0.997	0.012	E
Insertion loss of power distr. system	Attenuation (with RL345)	0.85	0.700	G
	1.4VSWR	0.972	0.122	G
Insertion loss (and VSWR) of feeder elements	0.02dB loss	0.9954	0.020	E
Total	$\eta_{over\ all}$	0.66	1.79	

G = guarantees from antenna manufacturer

E = expected performance from scale model measurements and calculations.

Aperture dimensions 120 m x 40 m yields an effective aperture area referred to the TX terminal of

$$A_{eff} = \eta \cdot 4800 m^2 = \underline{\underline{3200 m^2}}$$

REFERENCES.

1. Request for Proposal. Invitation from EISCAT to bid for a VHF radar-antenna system.

2. Ruze: Antenna Tolerance Theory. A Review. Proceedings of IEEE, Vol. 54, No. 4, April 1966, pp. 633-640.

3. Rusch and Potter: Analysis of Reflector Antennas. Academic Press, 1970, New York-London.

4. Silver: Microwave Antenna Theory and Design, McGraw-Hill, 1949.

5. Hansen: Microwave Scanning Antennas. Vol. 1, Apertures. Academic Press, 1964.

6. Mittra: Numerical and Asymptotic Techniques in Electromagnetics. Springer-Verlag. 1975.

7. Bracewell: Tolerance Theory of Large Antennas. IRE trans. on AP, jan. 1961, pp. 49-56.

8. Collin: Foundations for Microwave Engineering. McGraw-Hill 1966.

9. King: The Theory of Linear Antennas. Harvard University Press 1956.

10. Hauger: Impedans for dipol i fritt rom og som element i rekkeantenne. Hovedoppgave 1977, Institutt for radioteknikk og signalteori, NTH.

11. R.F. Harrington: Time-Harmonic Electromagnetic Fields. McGraw-Hill Book Co., New York, 1961.

12. R.G. Kouyoumjian and P.H. Pathak: A Uniform Geometrical Theory of Diffraction for an Edge in a Perfectly Conducting Surface, Proc. IEEE, vol. 62, pp. 1448-1461, Nov. 1974.

13. R.F. Harrington: Field Computation by Moment Methods. Macmillian New York, 1968.

14. Hansen: Microwave Scanning Antennas. Vol. 2, Array Theory and Practice. Academic Press 1966.

15. Edelberg and Oliner: Mutual Coupling Effects in Large Antenna Arrays II: Compensation Effects. IRE Trans. on A.P., July 1960, pp. 360-367.

16. Enclosure to MBB proposal No. 77-239/05B (78) of febr. 21st, 1978.

17. IEEE Standard, Definition of Terms for Antennas. IEEE Std 145-1973.

18. Per-Simon Kildal: Discrete Phase Steering by Permuting Precut Phase Cables. EISCAT Technical Note 78/6. Sept. 1978.

APPENDIX A: MATHEMATICAL DERIVATIONS OF APERTURE EFFICIENCY INTEGRALS.

The parabolic cylinder antenna is fed from a linear array feed positioned along the x-axis (see fig. 1.1). The feed has element spacing close enough to suppress grating lobes. Phase steering is not considered. The source field is expressed in terms of x, ψ and ρ where ρ is the length of the radial line from the x-axis to the field point and ψ is the angle between this line and the negative z-axis.

$\vec{a}_x$, $\vec{a}_y$, $\vec{a}_z$, $\vec{a}_\rho$, $\vec{a}_\psi$, $\vec{a}_R$, $\vec{a}_\theta$ and $\vec{a}_\phi$ are unit vectors in the direction of increasing x, y, z, ρ, ψ, R, θ and ϕ respectively. Z_0 is the wave impedance in free space, e.g.

$$Z_0 = \sqrt{\frac{\mu_0}{\varepsilon_0}}$$

The equations in Section A.2, A.3 and A.4 in this appendix must not be confused with the equations in Chapter 2, 3 and 4, although they are numbered in the same way.

A.1. Feed Pattern Approximations.

The reflector is assumed to be in the near field region of the linear array feed antenna (Ref. 5, page 33), e.g. $F < L^2/\lambda$. The lateral extent ℓ of the radiating parts of the feed, e.g. the dimensions in the cross section plane (yz plane), must satiesfy $F > 2\frac{\ell^2}{\lambda}$ or $\ell < \sqrt{\frac{\lambda F}{2}}$ (see end of this section) so that the Fraunhofer approximation may be used for the cross section radiation pattern of the feed. With these assumptions the field from the source $\vec{E}^F(x,\psi,\rho)$ propagates in the form of a cylindrical wave with the predominant components of the field in the tangent plane of the cylindrical wavefront, as discussed in Ref. 4 page 151. Therefore, when the x-axis is taken to be the phase reference point, the source field may be written as

$$\vec{E}^F(x,\psi,\rho) = \vec{b}(x,\psi)\frac{e^{-jk\rho}}{\sqrt{\rho}} \tag{1.1}$$

$$\vec{b}(x,\psi) = \begin{cases} b_x(x,\psi)\vec{a}_x + b_\psi(x,\psi)\vec{a}_\psi & 0 < x < L \\ 0 & x < 0,\ x > L \end{cases} \tag{1.2}$$

This approximation neglects end effects at x = 0 and x = L such as the broadening of the beam and a field component in the radial direction. The overall effects are, however, small when $\rho << L^2/\lambda$. This is clear from a study of the field patterns in Ref. 5 page 4.

The analysis is restricted to cases where the x and ψ variation of the field are separable, e.g. for the x and ψ polarization successively

$$b_x(x,\psi) = K_x f_x(x) g_x(\psi) \tag{1.3a}$$

$$b_\psi(x,\psi) = K_\psi f_\psi(x) g_\psi(\psi) \tag{1.3b}$$

where K_x and K_ψ are constants, $f_x(x)$ and $f_\psi(x)$ are the field distributions along the x-axis, and $g_x(\psi)$ and $g_\psi(\psi)$ are the cross section field patterns of the line feed. The following abbreviated notation will be used

$$b_{x,\psi}(x,\psi) = K_{x,\psi} f_{x,\psi}(x) g_{x,\psi}(\psi) \tag{1.4}$$

$f_x(x)$ and $f_\psi(x)$ are functions of the excitation of the linear

array source. When phase steering is not considered, they are usually real functions. $g_x(\psi)$ and $g_\psi(\psi)$ are in general complex, but when the feed has a well defined phase center which is the same for both polarizations and coincides with the x-axis, they are real. The phase centers for the two polarizations may not coincide. If for instance the x polarization of the feed has a defined phase center that is displaced a distance Δ from the x-axis in the direction ψ_0 , the Fraunhofer approximation

($\Delta < \frac{1}{2}\sqrt{\frac{\lambda F}{2}}$) yields that (See fig. 1.3)

$$g_x(\psi) = |g_x(\psi)|\, e^{j\delta} \tag{1.5a}$$

$$\delta = k(\rho - \rho') \approx k\Delta\cos(\psi_0 - \psi) \tag{1.5b}$$

The power radiated by the feed in each of the two polarizations is

$$P^F_{x,\psi} = \frac{1}{2}\int_{-\pi}^{\pi}\int \frac{1}{Z_0}|\vec{E}^F(x,\psi,\rho)\cdot\vec{a}_{x,\psi}|^2 dx\rho d\psi \tag{1.6}$$

Substitution of Eq. (1.1) and (1.4) gives

$$P^F_{x,\psi} = \frac{1}{2Z_0}|K_{x,\psi}|^2 \int_0^L |f_{x,\psi}(x)|^2 dx \int_{-\pi}^{\pi} |g_{x,\psi}(\psi)|^2 d\psi \tag{1.7}$$

The Fraunhofer approximation was used for the cross section radiation pattern of the feed. The condition for this is discussed in more detail here. Consider Fig. 1.3. Let $\Delta = \frac{\lambda}{2}$ be a displacement of a radiating part of the feed from the x-axis. The distance ρ' to a field point on the reflector may be expressed as

$$\rho' = \sqrt{\rho^2 + \Delta^2 - 2\rho\Delta\cos(\psi_0 - \psi)} \tag{1.8}$$

The expansion

$$\sqrt{1+x} = 1 + \frac{1}{2}x - \frac{1}{8}x^2 + \ldots\ldots \tag{1.9}$$

yields

$$\rho' = \rho\sqrt{1 - 2\frac{\Delta}{\rho}\cos(\psi_0-\psi) + (\frac{\Delta}{\rho})^2}$$

$$\rho' = \rho(1 - \frac{\Delta}{\rho}\cos(\psi_0-\psi) + \frac{1}{2}(\frac{\Delta}{\rho})^2 - \frac{1}{2}(\frac{\Delta}{\rho})^2\cos^2(\psi_0-\psi) + \ldots)$$

The Fraunhofer approximation yields $\rho' \approx \rho$ in amplitude expressions and

$$\rho' = \rho - \Delta\cos(\psi_0-\psi)$$

in phase expressions. The condition for this is that the second order term in the expansion gives a negligible phase contribution, for instance less than $\frac{2\pi}{16}$. Thus

$$k\rho\frac{1}{2}(\frac{\Delta}{\rho})^2(1-\cos^2(\psi_0-\psi)) < \frac{2\pi}{16}$$

$$\Delta^2 < \frac{\rho\lambda}{8\sin^2(\psi_0-\psi)}$$

If ψ_0 is any direction, then

$$\frac{\rho}{\sin^2(\psi_0-\psi)} \geq F$$

so that

$$\Delta < \frac{1}{2}\sqrt{\frac{F\lambda}{2}} \qquad (1.10)$$

Introduction of the lateral dimension $\ell = 2\Delta$ of the feed gives

$$\boxed{F > 2\frac{\ell^2}{\lambda}} \qquad (1.11)$$

which is the most common condition for the Fraunhofer approximation.

A.2. Aperture Field Method.

The field in the main secondary beam may be calculated using the aperture formulation, see for instance Ref. 6 page 220. The reflector has a parabolic cross section so that (see Section A.4 in this appendix)

$$\rho = \frac{F}{\cos^2\frac{\psi}{2}} = \frac{2F}{1+\cos\psi} \tag{2.1}$$

$$y = 2F\,\mathrm{tg}\,\frac{\psi}{2} \tag{2.2}$$

The aperture plane is chosen to be the xy plane in Fig.1.1. Thus, the normal to the aperture is

$$\vec{n} = \vec{a}_z \tag{2.3}$$

The aperture field $\vec{E}^a$ is approximated using geometrical optics (GO). The rays diverging from the focal line (Eq. 1.1) are reflected from the reflector with reflection coefficient -1, and proceed parallel to each other so that

$$\vec{E}^a(x,y) = -\frac{e^{-j2kF}}{\sqrt{\rho}}(b_x(x,\psi)\vec{a}_x + b_\psi(x,\psi)\vec{a}_y) \tag{2.4}$$

$$\vec{H}^a(x,y) = \frac{1}{Z_0}\vec{a}_z \times \vec{E}^a(x,y) \tag{2.5}$$

where the relations between ρ, ψ and y are given by Eq. (2.1) and (2.2). The scattered far field $\vec{E}^s(\theta,\phi)$ a distance R from the aperture plane is found in Ref. 6 page 220 to be

$$E^s(\theta,\phi) = -\frac{j\omega\mu_0}{4\pi}\left(\frac{e^{-jkR}}{R}\right)\iint_{\text{aperture}}\left\{-\frac{1}{Z_0}(\vec{n}\times\vec{E}^a)\times\vec{a}_R + \left[\vec{n}\times\vec{H}^a - ((\vec{n}\times\vec{H}^a)\cdot\vec{a}_R)\vec{a}_R\right]\right\}e^{jk\vec{r}\cdot\vec{a}_R}dxdy \tag{2.6}$$

where $\vec{a}_R$ is the unit vector in the direction of the field point and $\vec{r}$ is the position vector to the aperture field point

$$\vec{r} = x\vec{a}_x + y\vec{a}_y \tag{2.7}$$

Alternative formulations are possible based on only $(\vec{n} \times \vec{E}^a)$ or only $(\vec{n} \times \vec{H}^a)$. See the principle of equivalent sources in Ref. 11 page 106. Eq. (2.6) may be written in terms of the $\vec{E}^a$ field only, because

$$\vec{n} \times \vec{H}^a = - \frac{1}{Z_0} \vec{E}^a \tag{2.8}$$

Thus

$$\left[\vec{n} \times \vec{H}^a - ((\vec{n} \times \vec{H}^a) \cdot \vec{a}_R) \vec{a}_R\right] = - \frac{1}{Z_0} \left[\vec{E}^a - (\vec{E}^a \cdot \vec{a}_R) \vec{a}_R\right] \tag{2.9}$$

The direction normal to the aperture is considered first, e.g. the on axis far field. Here

$$\vec{a}_R = \vec{a}_z \tag{2.10}$$

The vector identity

$$\vec{a} \times (\vec{b} \times \vec{c}) = (\vec{a} \cdot \vec{c}) \vec{b} - (\vec{a} \cdot \vec{b}) \vec{c} \tag{2.11}$$

yields (use also Eq. (2.3) and (2.9))

$$-(\vec{n} \times \vec{E}^a) \times \vec{a}_R = \vec{a}_R \times (\vec{a}_z \times \vec{E}^a) = - \vec{E}^a \tag{2.12}$$

Eq. (2.9) and (2.12) give for the on axis field $(\vec{r} \cdot \vec{a}_R = 0)$

$$\vec{E}^s(0, 0) = \frac{j\omega\mu}{4\pi} \left(\frac{e^{-jkR}}{R}\right) \int\int_{\text{aperture}} \frac{2}{Z_0} \vec{E}^a(x, y)\, dxdy \tag{2.13}$$

The relation

$$\frac{j\omega\mu}{2\pi Z_0} = \frac{j\omega\sqrt{\mu\epsilon}}{2\pi} = \frac{j}{\lambda} \tag{2.14}$$

and Eq. (2.4), (1.3a) and (1.3b) give

$$\vec{E}^s(0, 0) = - \frac{j}{\lambda} \left(\frac{e^{-jk(R+2F)}}{R}\right) \left\{ K_x \int_0^L f_x(x)\, dx \int_E^{E+D} \frac{g_x(\psi)}{\sqrt{\rho}} dy\, \vec{a}_x \right.$$

$$\left. + K_\psi \int_0^L f_\psi(x)\, dx \int_E^{E+D} \frac{g_\psi(\psi)}{\sqrt{\rho}} dy\, \vec{a}_y \right\} \tag{2.15}$$

Eq. (2.15) may be written with the abbreviated notation in Eq. (1.4). Thus

$$\boxed{E^s_{x,y}(0,\ 0) = -\frac{j}{\lambda}\left(\frac{e^{-jk(R+2F)}}{R}\right)K_{x,\psi}\int_0^L f_{x,\psi}(x)\,dx\int_E^{E+D}\frac{g_{x,\psi}(\psi)}{\sqrt{\rho}}dy} \tag{2.16}$$

Eq. (2.2) gives (see also Section A.4 in this appendix)

$$dy = \frac{F}{\cos^2\frac{\psi}{2}}d\psi = \rho d\psi \tag{2.17}$$

which is substituted together with Eq. (2.2) in Eq. (2.16). The on-axis far field is then

$$\boxed{E^s_{x,y}(0,\ 0) = -\frac{j}{\lambda}\left(\frac{e^{-jk(R+2F)}}{R}\right)\sqrt{F}K_{x,\psi}\int_0^L f_{x,\psi}(x)\,dx\int_{\psi_1}^{\psi_2}\frac{g_{x,\psi}(\psi)}{\cos\frac{\psi}{2}}d\psi} \tag{2.18}$$

An alternative formulation is found if ρ and ψ are expressed in terms of y, see Appendix A.

$$\psi = 2\,\mathrm{arctg}\left(\frac{y}{2F}\right) \tag{2.19}$$

$$\rho = F\left(1 + \left(\frac{y}{2F}\right)^2\right) \tag{2.20}$$

3. Aperture Efficiency Integrals.

The directive gain in a given direction is defined as 4π times the ratio of the radiation intensity in that direction to the total power radiated by the antenna. The maximum value of the directive gain is the directivity which for the parabolic cylinder in Fig. 1.1 is in the direction normal to the aperture, e.g. on axis. The directivity will be found for each of the two polarizations using the abbreviated notation introduced in Eq. (1.5). The indexes x and ψ are used for the feed polarizations while the corresponding indexes are x and y for the secondary beam polarization on axis. Thus, the directivity $G_{x,y}$ is

$$G_{x,y} = \frac{4\pi\ I^{max}_{x,y}}{P^F_{x,\psi}} \tag{3.1}$$

where $I^{max}_{x,y}$ is the radiation intensity (power per steradian) on axis. Eq. (2.16) gives

$$I^{max}_{x,y} = \frac{R^2}{2Z_0} |E^s_{x,y}(0,0)|^2$$

$$= \frac{|K_{x,\psi}|^2}{2Z_0\lambda^2} \left| \int_0^L f_{x,\psi}(x)\,dx \right|^2 \left| \int_E^{E+D} \frac{g_{x,\psi}(\psi)}{\sqrt{\rho}}\,dy \right|^2 \qquad (3.2)$$

$P^F_{x,\psi}$ is the total power radiated by the feed so that Eq. (3.1) gives the directivity with spillover included. $P^F_{x,\psi}$ given by Eq. (1.7), and Eq. (3.2) is substituted in Eq. (3.1). The result is

$$G_{x,y} = \frac{4\pi}{\lambda^2} \frac{\left| \int_0^L f_{x,\psi}(x)\,dx \right|^2}{\int_0^L |f_{x,\psi}(x)|^2 dx} \frac{\left| \int_E^{E+D} \frac{g_{x,\psi}(\psi)}{\sqrt{\rho}}\,dy \right|^2}{\int_{-\pi}^{\pi} |g_{x,\psi}(\psi)|^2 d\psi} \qquad (3.3)$$

The effective aperture is

$$A_{x,y} = \frac{\lambda^2}{4\pi} G_{x,y} \qquad (3.4)$$

It is convenient to write the aperture efficiency $\eta^a_{x,y}$ as

$$\eta^a_{x,y} = \frac{A_{x,y}}{LD} = \eta^{\ell}_{x,y}\,\eta^c_{x,y} \qquad (3.5)$$

e.g. separated into a <u>longitudinal aperture efficiency</u> $\eta^{\ell}_{x,y}$ and a <u>cross section aperture efficiency</u> $\eta^c_{x,y}$.
$\eta^c_{x,y}$ is the aperture efficiency in the plane normal to the linear array feed axis.

$$\boxed{\eta^c_{x,y} = \frac{\left| \int_E^{E+D} \frac{g_{x,\psi}(\psi)}{\sqrt{\rho}}\,dy \right|^2}{D \int_{-\pi}^{\pi} |g_{x,\psi}(\psi)|^2 d\psi}} \qquad (3.6)$$

$\eta^{\ell}_{x,y}$ is the aperture efficiency in the plane parallel to the linear array axis.

$$\eta^{\ell}_{x,y} = \frac{\left| \int_0^L f_{x,\psi}(x)\,dx \right|^2}{L \int_0^L \left| f_{x,\psi}(x) \right|^2 dx} \tag{3.7}$$

A <u>cross section directivity</u> $G^{c}_{x,y}$ may be defined. That is the directivity in the cross section plane compared with an isotropic line source, e.g. a line source with a rotationally symmetric radiation pattern in the cross section plane. $G^{c}_{x,y}$ is defined by

$$G^{c}_{x,y} = \frac{2\pi D}{\lambda}\eta^{c}_{x,y} \tag{3.8}$$

In the same way a <u>longitudinal directivity</u> $G^{\ell}_{x,y}$ is defined. That is the directivity if the antenna had an isotropic radiation pattern in the cross section plane, but the same field distribution $f_{x,\psi}(x)$ along the x-axis (see for instance page 13 in Ref. 1), e.g.

$$G^{\ell}_{x,y} = \frac{2L}{\lambda}\eta^{\ell}_{x,y} \tag{3.9}$$

Some alternative expressions to Eq. (3.6) may be used. The relation between Eq. (2.16) and (2.18) gives (ψ in radians)

$$\eta^{c}_{x,y} = \frac{F\left| \int_{\psi_1}^{\psi_a} \frac{g_{x,\psi}(\psi)}{\cos\frac{\psi}{2}} d\psi \right|^2}{D \int_{-\pi}^{\pi} \left| g_{x,\psi}(\psi) \right|^2 d\psi} \tag{3.10}$$

The aperture distribution $a_{x,y}(y)$ may also be introduced

$$a_{x,y}(y) = \frac{g_{x,\psi}(\psi)}{\sqrt{\rho}} = \frac{g_{x,\psi}(2\,\mathrm{arctg}(\frac{y}{2F}))}{\sqrt{F(1 + (\frac{y}{2F})^2)}} \tag{3.11}$$

From Eq. (2.17)

$$\int_{-\pi}^{\pi} \left| g_{x,\psi}(\psi) \right|^2 d\psi = \int_{-\pi}^{\pi} \frac{\left| g_{x,\psi}(\psi) \right|^2}{\rho} \rho d\psi = \int_{-\infty}^{\infty} \left| a_{x,y}(y) \right|^2 dy \qquad (3.12)$$

where $a_{x,y}(y)$ is extended to infinity although the boundaries of the aperture are $y = E$ and $y = D + E$. The reason is that spillover is included in the expression of $\eta_{x,y}^{c}$.

A third alternative of Eq. (3.6), the cross section aperture efficiency, is, therefore

$$\eta_{x,y}^{c} = \frac{\left| \int_{E}^{E+D} a_{x,y}(y)\, dy \right|^2}{D \int_{-\infty}^{\infty} \left| a_{x,y}(y) \right|^2 dy} \qquad (3.13)$$

A.4. Geometrical Relations.

Reference is made to Fig. 1.1 and Fig. 1.2. The parabolic cylinder surface is in the rectangular coordinate system x,y described by

$$z = -F + \frac{1}{4F}y^2 = -F(1 - (\frac{y}{2F})^2)$$

It is convenient to use cylindrical coordinates x, ρ, ψ as defined in Fig.1.2. The equation becomes

$$\rho = \frac{2F}{1+\cos\psi} = \frac{F}{\cos^2\frac{\psi}{2}}$$

Some useful relations between ρ, ψ, z and y for a point on the surface are shown below

$$y = \rho\sin\psi = \frac{2F\sin\psi}{1+\cos\psi} = 2F\,tg\frac{\psi}{2}$$

$$z = -\rho\cos\psi = -\frac{2F\cos\psi}{1+\cos\psi} = -F(1-tg^2\frac{\psi}{2})$$

$$tg\frac{\psi}{2} = \frac{y}{2F}$$

$$\sin\frac{\psi}{2} = \frac{y}{2F\sqrt{1+(\frac{y}{2F})^2}}$$

$$\cos\frac{\psi}{2} = \frac{1}{\sqrt{1+(\frac{y}{2F})^2}}$$

$$\sin\psi = \frac{y}{F(1+(\frac{y}{2F})^2)}$$

$$\cos\psi = \frac{1-(\frac{y}{2F})^2}{1+(\frac{y}{2F})^2}$$

$$dy = \frac{F}{\cos^2\frac{\psi}{2}}d\psi$$

$$\frac{dz}{d\psi} = \frac{Ftg\frac{\psi}{2}}{\cos^2\frac{\psi}{2}} = \frac{F\sin\frac{\psi}{2}}{\cos^3\frac{\psi}{2}}$$

$$d\psi = \frac{\cos^2 \frac{\psi}{2}}{F} dy = \frac{1}{F(1+(\frac{y}{2F})^2)} dy$$

$$\rho = \sqrt{y^2 + z^2} = F(1 + (\frac{y}{2F})^2)$$

The derivations of these equations are based on simple trigonometric relations like

$$\sin\psi = 2\sin\frac{\psi}{2}\cos\frac{\psi}{2}$$

$$\cos\psi = \cos^2 \frac{\psi}{2} - \sin^2 \frac{\psi}{2} = 2\cos^2 \frac{\psi}{2} - 1 = 1 - 2 \sin^2 \frac{\psi}{2}.$$

APPENDIX B. NUMERICAL RESULTS.

B.1. Longitudinal Polarization with Two Rods.

```
* * * * * * * * * * * * * * * * * * *
*   CORNER REFLECTOR WITH RODS      *
*   DIPOLE PARALELL TO CORNER       *
*   THE MOMENT METHOD               *
* * * * * * * * * * * * * * * * * * *
```

WIDTH OF WALLS : A = 1,00 LAMBDA

DIPOLE HEIGHT : H = ,25 LAMBDA

CORNER ANGLE : V = 180,00 DEG,

SUB, DIV, OF A WALL : NI = 20

NO, OF RODS, ONE SIDE : NI = 1

DIAMETER OF RODS : DS = ,02 LAMBDA

POSITION OF RODS (IN LAMBDA FROM CORNER) :

X (1) = + ,45 Y (1) = ,45

PHASE CENTER, DISTANCE OVER ORIGO .066 LAMBDA

BEAM PATTERN:

ANGLE	DB	PHASE IN DEG. FROM REF. POINT PHASE CENTER	ORIGO	DZ
.00	.00	-1.50	.74	.06
6.00	-.03	-1.15	.95	.31
12.00	-.13	-.27	1.45	.93
18.00	-.38	.79	1.86	1.53
24.00	-.87	1.58	1.76	1.71
30.00	-1.69	1.78	.84	1.12
36.00	-2.91	1.17	-1.13	-.44
42.00	-4.67	-.40	-4.27	-3.09
48.00	-6.91	-2.99	-8.61	-6.91
54.00	-9.86	-6.61	-14.17	-11.88
60.00	-13.55	-11.21	-20.85	-17.93
66.00	-18.37	-16.42	-28.28	-24.69
72.00	-25.32	-20.51	-34.69	-30.40
78.00	-39.67	3.36	-13.22	-8.19
84.00	-33.06	113.55	94.51	100.28
90.00	-28.35	107.72	86.20	92.72
96.00	-26.77	93.93	69.93	77.20
102.00	-26.36	76.60	50.13	58.15
108.00	-26.51	56.61	27.75	36.50
114.00	-27.00	34.63	3.45	12.90
120.00	-28.02	11.00	-22.40	-12.28
126.00	-29.49	-15.25	-50.73	-39.98
132.00	-31.51	-47.95	-85.37	-74.03
138.00	-32.94	-91.50	-130.68	-118.80
144.00	-32.25	-134.52	-175.26	-162.91
150.00	-31.23	195.64	153.55	166.31
156.00	-31.75	173.13	129.91	143.01
162.00	-34.47	146.35	102.24	115.61
168.00	-37.26	95.53	50.77	64.34
174.00	-34.97	51.47	6.33	20.01
180.00	-33.53	40.61	-4.66	9.06

WEIGHTED R.M.S. PHASE ERROR FOR ANGLES LESS THAN 50.0 DEG.

WITH PHASE CENTER AS REF. POINT : 1.38 DEG.

WITH ORIGO AS REF. POINT : 2.73 DEG.

WITH REF. POINT DZ= .02 LAMDA OVER ORIGO : 2.14 DEG.

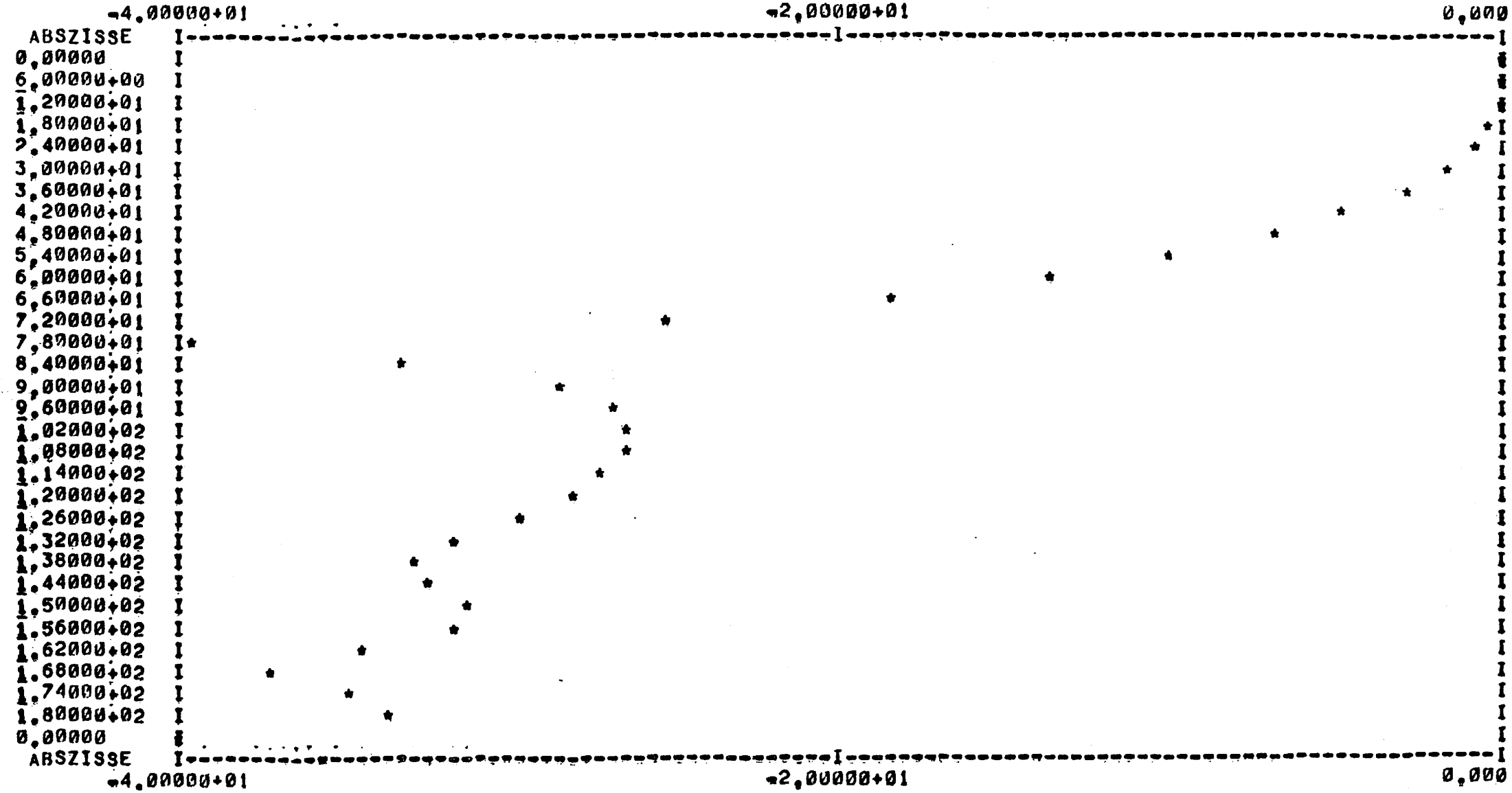
-4,00000+01
-2,00000+01
0,000
ABSZISSE
0,00000
6,00000+00
1,20000+01
1,80000+01
2,40000+01
3,00000+01
3,60000+01
4,20000+01
4,80000+01
5,40000+01
6,00000+01
6,60000+01
7,20000+01
7,80000+01
8,40000+01
9,00000+01
9,60000+01
1,02000+02
1,08000+02
1,14000+02
1,20000+02
1,26000+02
1,32000+02
1,38000+02
1,44000+02
1,50000+02
1,56000+02
1,62000+02
1,68000+02
1,74000+02
1,80000+02
0,00000
ABSZISSE
-4,00000+01
-2,00000+01
0,000

```
* * * * * * * * * * * * * * * * * * * * * * * *
*   CYLINDRICAL PARABOLIC REFLECTOR ANTENNA     *
*   WITH OFFSET FEED AND NO BLOCKAGE            *
* * * * * * * * * * * * * * * * * * * * * * * *
```

APERTURE WIDTH	: D	=	40,00 METER
EXTRA FEED OFFSET	: DOFF	=	1,50 METER
WAVELENGTH	: LAMBDA	=	1,34 METER
FEED, CROSS SECTION GAIN	: FGAIN	=	6,91 DB

NEXT PAGE:

FEED CROSS SECTION BEAM PATTERN (RELATIVE POWER)

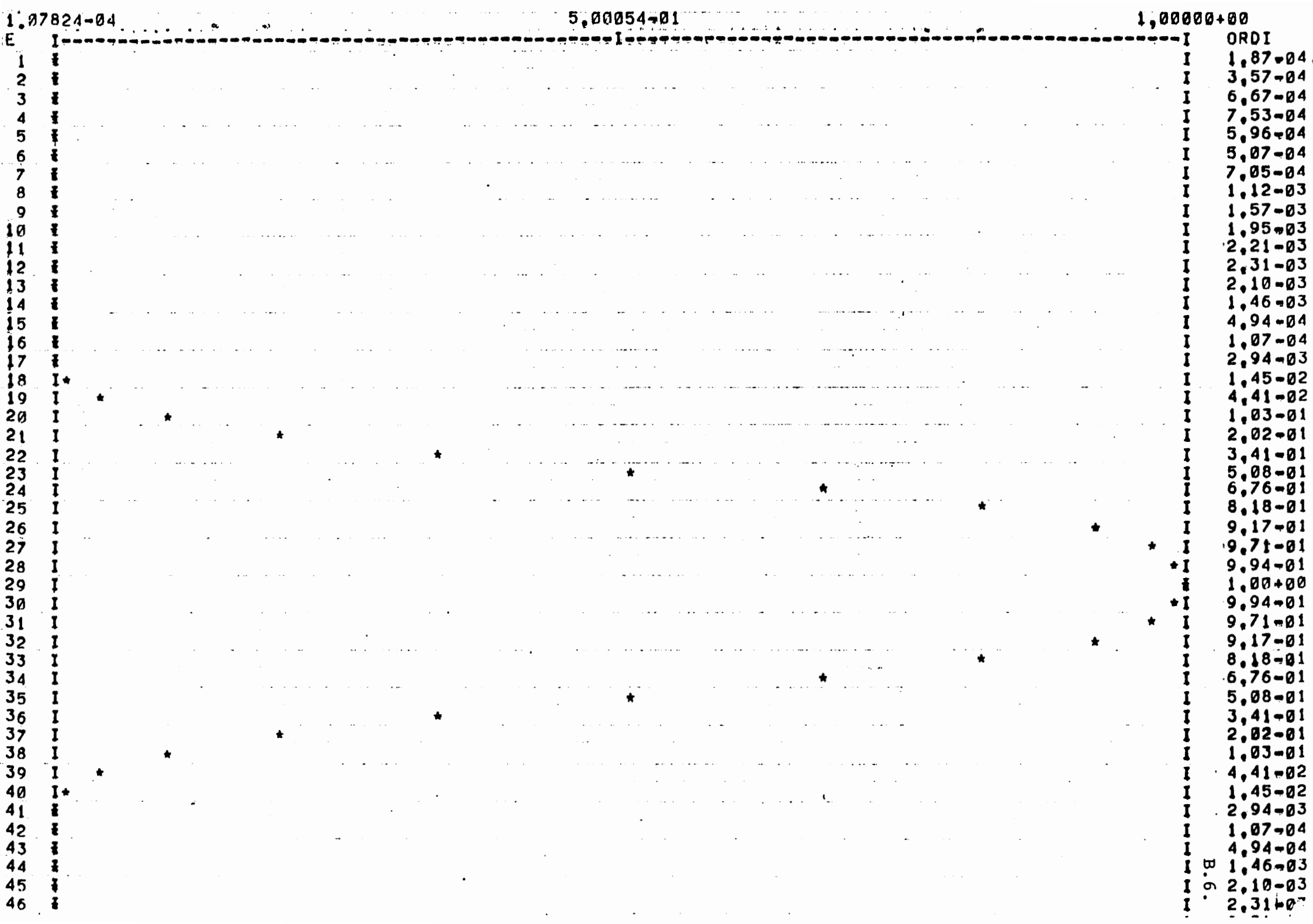
1,07824-04
5,00054-01
1,00000+00
E
ORDI
1 1,87-04
2 3,57-04
3 6,67-04
4 7,53-04
5 5,96-04
6 5,07-04
7 7,05-04
8 1,12-03
9 1,57-03
10 1,95-03
11 2,21-03
12 2,31-03
13 2,10-03
14 1,46-03
15 4,94-04
16 1,07-04
17 2,94-03
18 1,45-02
19 4,41-02
20 1,03-01
21 2,02-01
22 3,41-01
23 5,08-01
24 6,76-01
25 8,18-01
26 9,17-01
27 9,71-01
28 9,94-01
29 1,00+00
30 9,94-01
31 9,71-01
32 9,17-01
33 8,18-01
34 6,76-01
35 5,08-01
36 3,41-01
37 2,02-01
38 1,03-01
39 4,41-02
40 1,45-02
41 2,94-03
42 1,07-04
43 4,94-04
44 1,46-03
45 2,10-03
46 2,31-0

F/D = .45
S/D = 1.25
PSISUB = 91.43 DEG

PSINOT (DEG)	APERTURE TAPER LOWER (DB)	UPPER (DB)	SPILL-OVER EFF.	APER-TURE EFF.	AP. EFF./ (S/D)	SPILLOVERLOBES LOWER (DB)	UPPER (DB)
45.0	-4.8	-8.9	.941	.892	.716	-21.0	-21.6
46.0	-5.2	-8.4	.942	.896	.719	-21.4	-21.2
47.0	-5.6	-8.0	.941	.899	.721	-21.8	-20.8
48.0	-6.0	-7.7	.940	.901	.723	-22.3	-20.5
49.0	-6.3	-7.3	.938	.901	.723	-22.7	-20.2
50.0	-6.7	-6.9	.936	.901	.723	-23.1	-19.8
51.0	-7.1	-6.6	.933	.900	.722	-23.5	-19.5
52.0	-7.5	-6.2	.929	.897	.720	-24.0	-19.2
53.0	-8.1	-5.9	.925	.894	.718	-24.5	-18.9
54.0	-8.7	-5.6	.921	.890	.714	-25.2	-18.6
55.0	-9.1	-5.3	.915	.884	.710	-25.6	-18.3
56.0	-9.5	-5.0	.909	.878	.704	-26.0	-18.1
57.0	-10.0	-4.7	.903	.871	.699	-26.5	-17.8
58.0	-10.6	-4.5	.896	.863	.692	-27.1	-17.5
59.0	-11.3	-4.2	.889	.854	.685	-27.8	-17.3
60.0	-12.1	-4.0	.881	.844	.678	-28.6	-17.0

B.2. Transverse Polarization.

```
* * * * * * * * * * * * * * * * * * *
*   CORNER REFLECTOR                  *
*   DIPOLE NORMAL TO CORNER           *
*   G. T. D.                          *
* * * * * * * * * * * * * * * * * * *
```

DIPOLE LENGTH	:	L	=	,50 LAMBDA
WIDTH OF WALLS	:	A	=	1,00 LAMBDA
DIPOLE HEIGHT	:	H	=	,25 LAMBDA
CORNER ANGLE	:	V	=	179,90 DEG.
SUB. DIV. OF A DIP. ARM	:	NMAX	=	5

PHASE CENTER, DISTANCE OVER ORIGO -,029 LAMBDA

BEAM PATTERN:

ANGLE	DB	PHASE IN DEG, FROM REF, POINT PHASE CENTER	ORIGO	DZ
,00	,00	-1,34	-2,35	-3,05
6,00	-,00	-1,06	-2,01	-2,67
12,00	-,07	-,30	-1,08	-1,62
18,00	-,28	,64	,14	-,21
24,00	-,71	1,39	1,28	1,20
30,00	-1,44	1,66	2,04	2,30
36,00	-2,54	1,19	2,16	2,84
42,00	-4,02	-,20	1,45	2,60
48,00	-5,91	-2,70	-,28	1,40
54,00	-8,21	-6,49	-3,22	-,95
60,00	-10,97	-11,74	-7,56	-4,66
66,00	-14,24	-18,65	-13,60	-9,93
72,00	-18,17	-27,42	-21,26	-16,99
78,00	-23,10	-38,21	-31,00	-26,00
84,00	-30,33	-49,92	-41,64	-35,89
90,00	-36,95	-141,70	-132,33	-125,83
96,00	-33,90	94,64	105,09	112,34
102,00	-29,04	81,72	93,24	101,24
108,00	-27,00	67,97	80,54	89,26
114,00	-26,35	54,49	68,08	77,51
120,00	-27,06	41,09	55,64	65,74
126,00	-29,75	25,17	40,63	51,36
132,00	-36,21	-10,97	5,33	16,65
138,00	-34,87	-110,48	-93,41	-81,56
144,00	-28,54	-138,65	-120,90	-108,57
150,00	-26,34	-149,14	-130,79	-118,06
156,00	-27,15	-155,71	-136,87	-123,80
162,00	-32,54	-162,59	-143,36	-130,01
168,00	-43,59	45,78	65,29	78,83
174,00	-29,63	25,54	45,22	58,88
180,00	-26,70	24,86	44,60	58,30

WEIGHTED R.M.S. PHASE ERROR FOR ANGLES LESS THAN 50,0 DEG,

WITH PHASE CENTER AS REF, POINT : 1,27 DEG,

WITH ORIGO AS REF, POINT : 1,64 DEG,

WITH REF, POINT DZ= ,02 LAMDA OVER ORIGO : 2,18 DEG,

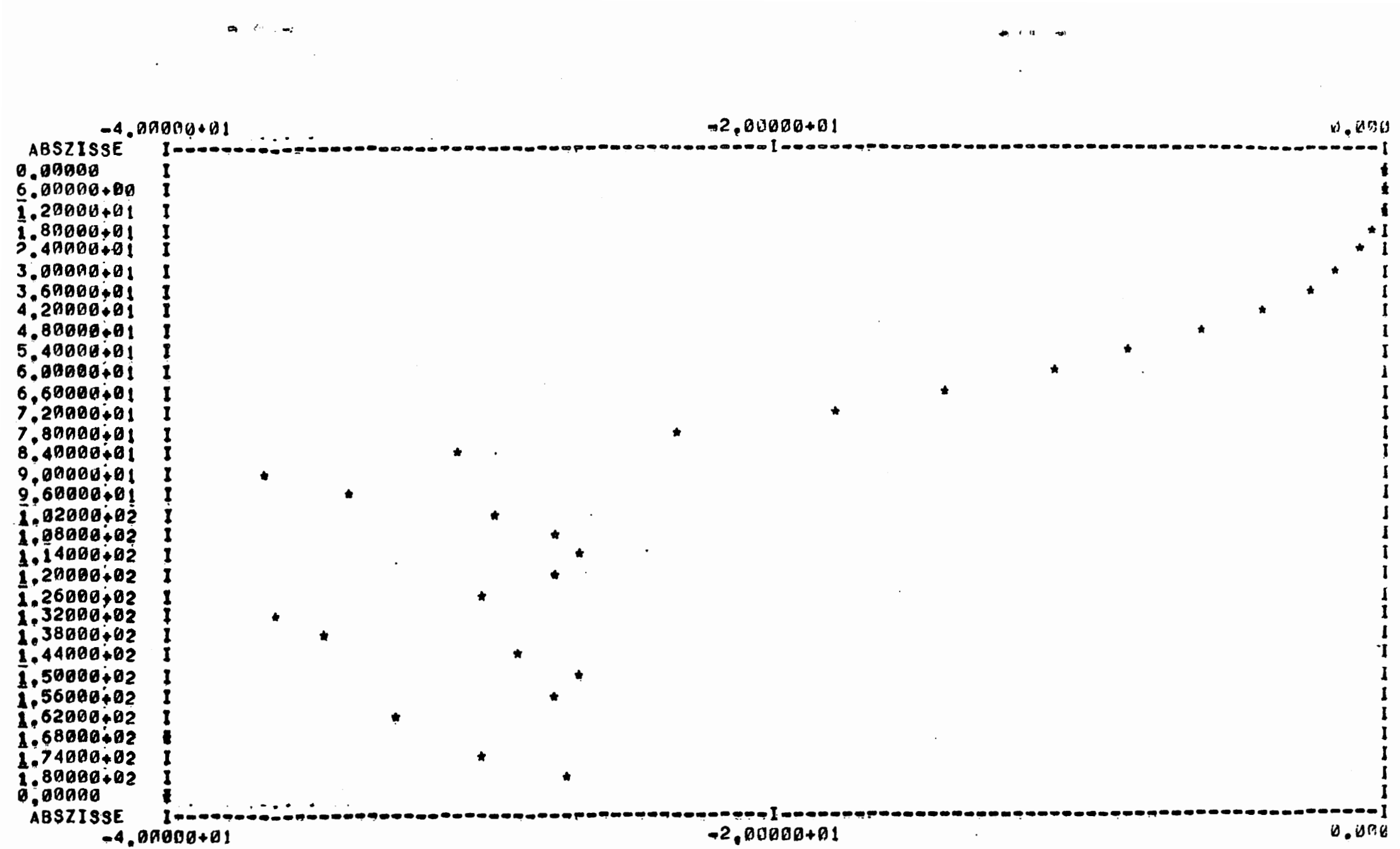
-4.00000+01
-2.00000+01
0.000
ABSZISSE
0.00000
6.00000+00
1.20000+01
1.80000+01
2.40000+01
3.00000+01
3.60000+01
4.20000+01
4.80000+01
5.40000+01
6.00000+01
6.60000+01
7.20000+01
7.80000+01
8.40000+01
9.00000+01
9.60000+01
1.02000+02
1.08000+02
1.14000+02
1.20000+02
1.26000+02
1.32000+02
1.38000+02
1.44000+02
1.50000+02
1.56000+02
1.62000+02
1.68000+02
1.74000+02
1.80000+02
0.00000
ABSZISSE
-4.00000+01
-2.00000+01
0.000

B.11.

```
* * * * * * * * * * * * * * * * * * * * * * * *
*   CYLINDRICAL PARABOLIC REFLECTOR ANTENNA     *
*   WITH OFFSET FEED AND NO BLOCKAGE            *
* * * * * * * * * * * * * * * * * * * * * * * *
```

APERTURE WIDTH	: D	=	40,00 METER
EXTRA FEED OFFSET	: DOFF	=	1,50 METER
WAVELENGTH	: LAMBDA	=	1,34 METER
FEED, CROSS SECTION GAIN	: FGAIN	=	6,64 DB

NEXT PAGE:

FEED CROSS SECTION BEAM PATTERN (RELATIVE POWER)

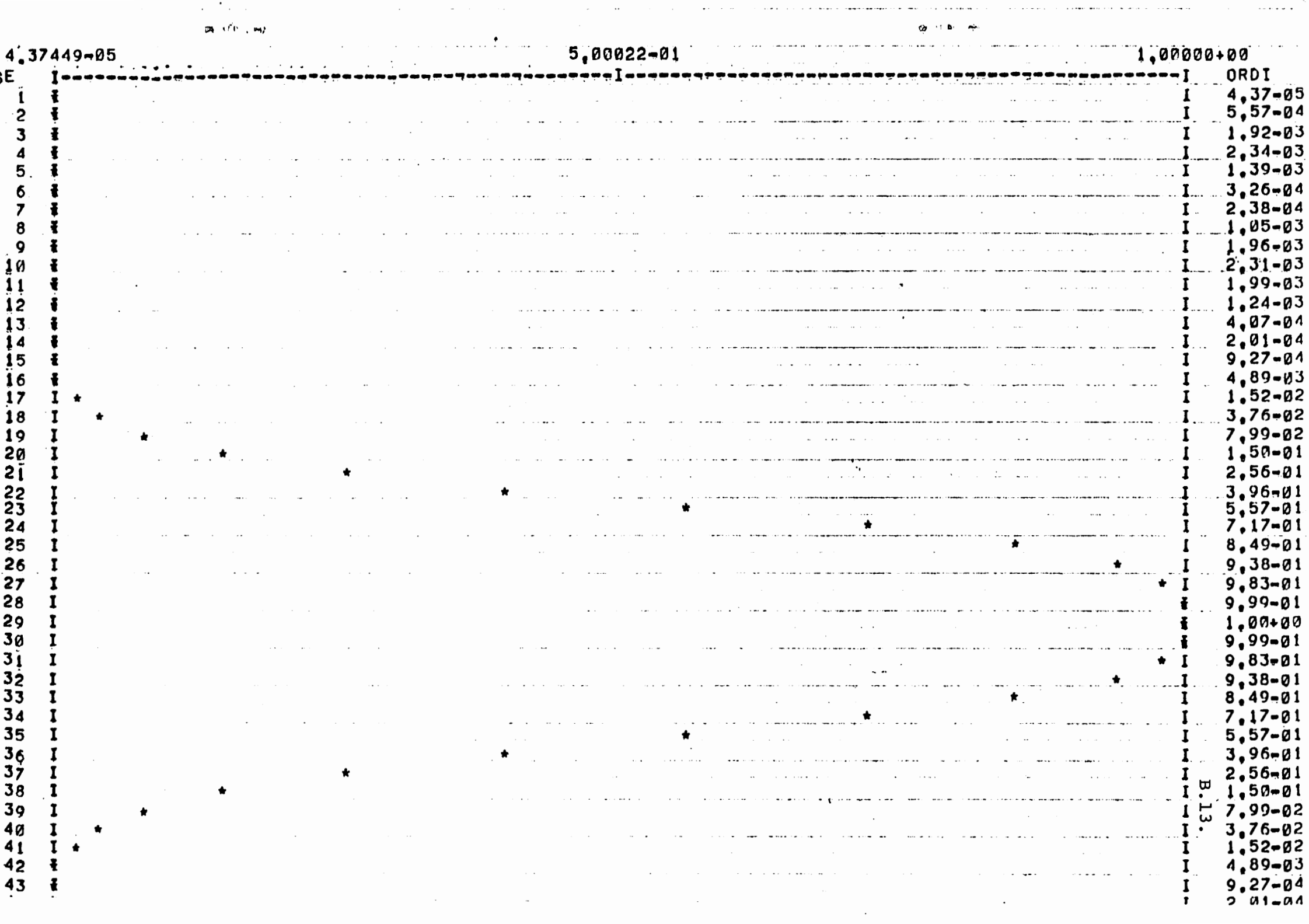
4,37449-05
5,00022-01
1,00000+00
SE
ORDI
1 4,37-05
2 5,57-04
3 1,92-03
4 2,34-03
5 1,39-03
6 3,26-04
7 2,38-04
8 1,05-03
9 1,96-03
10 2,31-03
11 1,99-03
12 1,24-03
13 4,07-04
14 2,01-04
15 9,27-04
16 4,89-03
17 1,52-02
18 3,76-02
19 7,99-02
20 1,50-01
21 2,56-01
22 3,96-01
23 5,57-01
24 7,17-01
25 8,49-01
26 9,38-01
27 9,83-01
28 9,99-01
29 1,00+00
30 9,99-01
31 9,83-01
32 9,38-01
33 8,49-01
34 7,17-01
35 5,57-01
36 3,96-01
37 2,56-01
38 1,50-01
39 7,99-02
40 3,76-02
41 1,52-02
42 4,89-03
43 9,27-04

B.13.

F/D	= .45
S/D	= 1.25
PSISUB	= 91.43 DEG

PSINOT (DEG)	APERTURE TAPER LOWER (DB)	UPPER (DB)	SPILL-OVER EFF.	APER-TURE EFF.	AP. EFF./ (S/D)	SPILLOVERLOBES LOWER (DB)	UPPER (DB)
48.0	-5.0	-6.9	.917	.886	.711	-21.5	-20.0
49.0	-5.2	-6.6	.915	.886	.711	-21.8	-19.7
50.0	-5.5	-6.3	.913	.886	.711	-22.1	-19.4
51.0	-5.8	-6.0	.911	.885	.710	-22.5	-19.1
52.0	-6.2	-5.7	.907	.883	.708	-22.9	-18.9